Understanding Genetic Factors That Modulate Hedgehog-Driven Skin Cancer

by

Kenneth Gordon Trieu

A dissertation submitted in partial fulfillment
of the requirements for the degree of
Doctor of Philosophy
(Cell and Developmental Biology)
in the University of Michigan
2022

Doctoral Committee:

Professor Andrzej A. Dlugosz, Chair
Professor Pierre A. Coulombe
Associate Professor Xing Fan
Associate Professor David B. Lombard
Associate Professor Sunny Y. Wong

Kenneth Gordon Trieu

ketrieu@umich.edu

ORCID iD: 0000-0002-4851-1876

Acknowledgments

The work in this dissertation would not have been possible without the help of many amazing individuals that I have encountered throughout my scientific journey thus far. To begin, I want to express my gratitude for my Ph.D. mentor, Dr. Sunny Wong. Thank you for teaching and developing me to become a rigorous scientist. Thank you for pushing me to critically think, ask meaningful questions, and when to take risks related to my thesis project. I appreciate that I can go to you any time to discuss about anything. I will always remember the great memories about the unexpected results that we have encountered. Finally, thank you for supporting my interests outside of lab.

Thank you to my past mentors, Drs. Alexey Veraksa and Xingbin Ai. I sincerely appreciate these two individuals and their support for preparing me for graduate school.

Thank you to my committee members, Dr. Andrzej Dlugosz, Dr. Pierre Coulombe, Dr. David Lombard, and Dr. Xing Fan. Thank you Anj for your thoughtful questions, excitement, and deep knowledge in basal cell carcinoma. Thank you to Pierre, David, and Xin for always providing critical feedback, encouragement, and pushing me to critically assess every experimental outcome. I walked away from each committee meeting knowing that I was heading in the right direction. I feel so privileged to have had the support of these outstanding scientists during my graduate career.

Thank you to all the lab members in the Wong lab, past and present. I first would like to thank Natalia, Arlee, and Jamie for integrating me into the lab when I first joined. You all helped navigate my preliminary exam process and I am thankful for the help. I also would like to thank Rachel, Sibyl, Noah, and Tom for the countless scientific discussions and random conversations in the lab. I also want to express my appreciation for Owen and Virginia. These two individuals provided critical data for my thesis project and I had a wonderful time mentoring you two. Finally, I would like to thank Monique, Dawn, LiJyun, Marina, Jacob, and Stefan for being fantastic lab neighbors.

I am so fortunate to have been a part of the Cell and Developmental Biology (CDB) community. Learning about the different research topics in the department helped me get exposed to concepts that I would not have thought about. Thank you to Dr. Pierre Coulombe and the CDB admin staff for helping me navigate each step of graduate school. I would also like to acknowledge the OGPS staff for helping graduate students in career development.

Thank you to my funding sources for supporting my thesis project and professional growth. Thank you, National Institute of Health (NIH), for awarding me an NRSA F31 fellowship (F31 CA254080). Thank you, Rackham Graduate School, for awarding me the graduate student research grant to support my thesis work. Thank you to the Endowment for Basic Science (EBS) program for awarding me the excellence in basic science award (EBSA) for additional financial support. Finally, thank you Leo Foundation, Donald & Patricia Roof Fund, NIH, and UM-SBDRC for providing financial support to the Wong lab.

I am so lucky to have crossed paths with Fatima, Cyrina, David, Derek, Thad, Siva, Ashwin, and Gabbi during graduate school. You all are such great friends and have impacted my life in so many ways. I would also like to give a shoutout to the indoor soccer squad. Thank you all and I will cherish the amazing memories!

Most importantly, I would like to thank my family for their support. I would not be where I am without you all. I am so privileged to have such understanding parents and I sincerely thank my sister for helping me start my scientific journey. Thank you all for believing in me. I am excited to see what we will do together next!

Table of Contents

List of Figures

List of Tables

Abstract

The Hedgehog (Hh) signaling pathway is essential for instructing tissues to properly develop during vertebrate embryogenesis. Perturbations that cause constitutive activation of Hh signaling, primarily through loss-of-function mutations in *PTCH1*, drive the formation of basal cell carcinoma (BCC). While mutations in the Hh pathway play a necessary role for this disease, BCCs also possess high tumor mutational burdens, suggesting that additional mutations may collaborate with Hh signaling to promote oncogenesis. My thesis therefore examines whether other genetic factors can collaborate with Hh signaling to promote the formation of macroscopic BCC-like tumors in mice.

Using BCC mouse models, I found that loss of *Ptch1* is not sufficient to promote macroscopic tumor formation. Because *NOTCH1*, *TRP53*, and *MYCN* are frequently mutated in human BCCs, I investigated if these genetic factors can collaborate with Hh signaling to drive tumor progression. Indeed, ablating either *Notch1* or *Trp53* in our BCC mouse model system caused rare "successful" macroscopic tumors to form. Upon ablating Notch signaling, I found that microscopic BCC-like tumors persist and resist tumor regression. Losing *Trp53* likely promotes tumor mutability and helps enable genomic amplification of *Gli1* or *Gli2*. Finally, I found that overexpression of *MYCN* promotes proliferation and tumor progression. Collectively, these data suggest acquired secondary mutations that upregulate *Gli1*, *Gli2* and/or Mycn levels enable tumors to expand indefinitely. Losing Notch1 and p53 also facilitates tumor progression.

I also determined whether immune privilege extends to BCC and addressed if inhibiting CD200 suppresses tumor initiation. CD200 is thought to be a potential immunosuppressive molecule in the hair follicle and is expressed in BCC. I found that suppression of CD200 did not affect nascent tumor size during tumor initiation. Furthermore, suppression of CD200 did not affect immune cell numbers in tumor-containing skin.

Finally, gene amplification is a common genetic alteration in cancer, and some amplified genes may cause cells to divide or become resistant to therapy. However, there are limited *in situ* hybridization approaches to detect and visualize copy number changes. I therefore

optimized the new DNAscope® duplex assay to examine *GLI1, GLI2,* and *MYCN* copy number in human BCC samples.

In summary, my findings expand our understanding of key aspects of BCC biology and define genetic factors that drive BCC progression. Furthermore, the tools and assays I have optimized can be leveraged in futures studies in skin cancer biology.

Chapter 1: Introduction

1.1 Summary

Constitutive Hedgehog (Hh) signaling is the main driver for basal cell carcinoma (BCC), the most common form of skin cancer. This chapter introduces the Hh signaling pathway and its importance in development, homeostasis, and disease. I also focus on BCC mouse models generated over the past 30 years and explain how these tools helped advanced our knowledge for BCC. I further describe in detail how various non-canonical signaling pathways collaborate with Hh signaling in BCCs and their relevance to combinatorial therapies. Finally, I will briefly introduce CD200 signaling in BCC and pose key questions that I will address in subsequent chapters.

1.2 Hedgehog signaling drives basal cell carcinoma

1.2.1 Introduction

In this section, I introduce an overview of the core components of Hh signaling in the context of development, homeostasis, and disease. I further describe how the Hh pathway plays a causative role in BCC. In addition, I will describe the initial discovery of BCCs and the key pathological clinical features. Because BCC is a Hh-driven disease, I will also describe the advantages and disadvantages of the FDA approved anti-Hh therapeutic drug vismodegib.

1.2.2 Hedgehog

Hh proteins are secreted lipoproteins that specify cell patterning [1-3]. The Hh gene was first discovered in *Drosophila melanogaster* screens for defects in segment patterning [4]. Drosophila have a single Hh gene and larvae with defects in *Hh* displayed segment defects resembling hedgehog spines. In mammals, the HH gene has three homologs, *Sonic Hedgehog* (*Shh*), *Indian Hedgehog* (*Ihh*) and *Desert Hedgehog* (*Dhh*) [5-11]. All three homologs display unique expression patterning and *Shh* is typically studied the most. Mutant *Shh* knockout mice display absence of cell types within the neural tube, distal limb structures, spinal column, ribs, and develop cyclopia [12]. Furthermore, *Shh* knockout mice display significant defects in the lung, heart, and foregut [13-16]. Additionally, the skin epidermis in *Shh* knockout mice appear

normal during development; however, hair follicles fail to form a mature follicle [17, 18]. Thus, Hh signaling is critical for proper tissue formation during embryogenesis.

In the absence of Hh ligand, the 12-transmembrane protein Patched1 (Ptch1) localizes to the primary cilium and blocks the function of the 7-transmembrane protein Smoothened (Smo). It is well documented that Smo is a positive mediator of Hh signaling [19-21]. Without Smo activation, downstream GLI family transcription factors are degraded or processed into repressor forms. The function of GLI repressor forms inhibits the transcription of Hh target gene expression (described in more detail below). When Hh is present, Hh binds to Ptch1 and internalizes Ptch1 for degradation, which then allows Smo to move to the cilium to induce the activation of GLI transcription factors (**Figure 1-1**). Indeed, *Ptch1* mutant embryos display increased Hh activity and develop expansion of ventral neural cell types and polydactyly [22-24].

Core elements of the Hh pathway were originally identified from genetic approaches performed in *Drosophila*. Activated Smo signals through Cubitus interruptus (Ci), a zinc finger transcription factor that serves as a downstream activator or repressor for the Hh pathway. When Hh is absent, Ci is processed into a repressor form (CiR), which inhibits the expression of Hh target genes [25]. The processing of active or repressive Ci is mediated by the kinesin-related protein Costal2 (Cos2, mammalian homolog is Kif7). It has been demonstrated that Ci and Cos2 physically interact and are also bound by additional proteins including unphosphorylated Smo, the serine/threonine kinase Fu, and Sufu [26-29]. Furthermore, loss of Cos2 or one of the kinases that phosphorylate Ci can lead to higher Hh pathway activity [30, 31]. Additionally, Cos2 can recruit additional kinases such as, protein kinase A (PKA), casein kinase I (CKI), and glycogen synthase kinase 3 (GSK3), to phosphorylate full-length Ci [32, 33].

While the activation and repression functions are largely driven by Ci in flies, mammals have three GLI proteins that play different roles in Hh signaling. Gli1 plays an activating role and is a well-established downstream Hh target gene; however, Gli1 is dispensable for development [34, 35]. Hh transcriptional activation is normally executed by full-length Gli2 [36], and overexpression of a truncated form of Gli2 lacking its N-terminal repressor domain drives constitutive Hh signaling both *in vitro* and *in vivo* [37, 38]. On the other hand, a proteolytically processed form of Gli3 missing the activator domain transcriptionally represses pathway activity [39-41]. Furthermore, overexpression of a truncated Gli3 lacking its carboxy-terminal activator

domain causes constitutive repression of Hh signaling [42]. Similar to the Cos2-Fu-Sufu complex in flies, Gli proteins are positively and negatively regulated by Kif7 and Sufu [43, 44].

Many mouse studies have highlighted specific roles and functional redundancies of *Gli1*, *Gli2*, and *Gli3*. Although it is suggested that Gli1 is dispensable during development [35], ectopic expression of *Gli1* controls multiple ventral cell fate in the central nervous system during development [45, 46]. *Gli2* seems to play a greater role in neural tube development because *Gli2* mutant mice fail to develop floor plate throughout the midbrain, hindbrain, and spinal cord [47, 48]. *Gli3* mutant mice appear to have a subtle expansion of neural subtypes [49]. These data likely suggest neural tube cells predominantly require *Gli2*, while *Gli1* and *Gli3* play supporting roles. In addition, *Gli1;Gli2* deficient mice display more severe phenotypes in the neural tube compared to single mutant mice [35]. This suggest that *Gli1* and *Gli2* have more overlapping functions in the Hh pathway. To further highlight the importance of *Gli2*, activation of Gli2 is essential for the formation of hair follicles [50]. Finally, the loss of *Gli3* leads to polydactyly [51]. Litingtung et al. and te Welscher et al. observed loss of *Gli3* in *Shh* knockout background restores digit formation [52, 53]. This suggest that Shh may suppress Gli3 repressor formation in the limb bud. In addition, *Gli2;Gli3* knockout mice have defects in the development of the neural arches and display bilateral pair of extra ribs [54]. Collectively, tissues can respond to Hh signaling in various ways where Shh can either activate the function of *Gli2* or inhibit the formation of *Gli3* repressor.

Given the importance of Hh signaling in development, aberrant Hh signaling can result in a wide variety of birth defects and diseases. Aberrant Hh signaling has been implicated in many cancers through ligand-independent, ligand-dependent autocrine/juxtracrine signaling, and ligand-dependent paracrine signaling or reverse paracrine signaling (**Figure 1-2**) [55]. Ligand-independent activation of Hh signaling is caused either by activating mutations in *Smo*, inactivating mutations either in *Ptch1* or *Sufu*, or amplification in downstream *GLI* activity. These mutations result in the formation of basal cell carcinoma, medulloblastoma, or rhabdomyosarcoma [24, 56-59]. For Hh autocrine/juxtracrine constitutive signaling, Hh ligand is produced and taken up by the same or surrounding cells. Indeed, it is proposed that tumor cells respond to Hh in an autocrine manner and reported in tumors arising in the brain, ovary, liver, breast, prostate, colorectal, and digestive tract [60-66]. Finally, the role of Hh signaling in stromal cells has also been shown in several cancers already mentioned above (reviewed in [67]). As an

example, Fan et al. demonstrated the role of ligand-dependent paracrine signaling in prostate tumor cells [68]. *Kras*-driven pancreatic cancer is another well studied example for ligand-dependent paracrine signaling [69-71]. Indeed, Tian et al. observed surrounding myofibroblast receive Hh activity from pancreatic tumor cells [72]. Collectively, these examples suggest the various mechanisms of aberrant Hh signaling during tumorigenesis.

1.2.3 Molecular genetics of BCC

For the focus of this section, I will describe the molecular genetics of BCCs. In 1827, Arthur Jacob observed a "destructive ulceration of peculiar character" around the eyelids that we now call BCC [73]. Follow up medical reports in the 1900s further originated the term Basalzellenkrebs as a locally invasive and malignant tumor that develop from the basal layer of the epidermis or hair follicle [74, 75]. In 1974, the World Health Organization classified and ultimately retained the name "BCC". BCC is the most common skin cancer with >5 million new cases diagnosed each year [76].

The development of BCC is associated with genetic predisposition or exposure to ultraviolet (UV) radiation and is typically more common in the elderly population [77]. Due to UV light sunbeds, however, younger people may be susceptible to develop BCCs earlier in their lifetime [78]. Although BCCs is the most common skin cancer, BCCs rarely metastasize and most can be cured by surgical excision. In more advanced lesions, BCCs can be removed by Mohs micrograph surgery [79]. Clinically, BCC appears as translucent papules or nodules that slowly grows, and in some cases, may be pigmented. BCCs are grouped together with skin squamous cell carcinomas (SCC) and other less common non-melanoma skin cancers. Histologically, BCC are keratinocyte epithelial tumors that resemble the basal layer of the epidermis. These basal (or basaloid) cells are arranged in palisades at the tumor periphery and are distinct from the surrounding stroma. BCCs can display varying morphological tumor architecture and growth patterns. The major subtypes of human BCCs include, superficial, nodular, micronodular, infiltrating, and sclerosing [80].

Initially reported in 1894 and later described in detail by Gorlin et al., the understanding of Hh signaling in BCC came from studying patients who are genetically prone to develop BCC throughout their lifetime [81, 82]. Using family-based linkage studies, it was demonstrated that patients with Gorlin syndrome patients (also known as basal cell nevus syndrome) are more susceptible to develop multiple BCCs and medulloblastoma starting at a young age [83]. Gorlin

syndrome patients harbor a causative loss-of-function mutation in *PTCH1* (chromosome 9q22) [56, 84-86]. It later became clear that the majority of sporadic BCCs have mutations in *PTCH1* (~70%), whereas the remaining have oncogenic activating mutations in *SMO* (~10-20%) [59, 87].

1.2.4 Anti-hedgehog therapeutic treatments

The very first discovery that the Hh pathway is sensitive to small molecules originated from sheep ingesting corn lilies (*Veratrum californicum*). Maternal sheep that ingested this plant gave birth to single eyed (cyclopic) lambs [88]. The analogous human developmental condition holoprosencephaly is linked to *SHH* mutations [89, 90]. It was later identified that the alkaloid compound, cyclopamine, can be isolated from *Veratrum californicum* [91, 92]. Indeed, it was initially demonstrated by Chen et al. that cyclopamine binds to SMO and suppresses Hh pathway activity, highlighting its therapeutic potential [93]. Athar et al. later demonstrated oral administration of cyclopamine can reduce BCC growth in UV-irradiated *Ptch1*$^{+/-}$ mice [94]. These data ultimately supported the concept that cyclopamine and other SMO antagonists may be a useful treatment for BCC.

In 2012, the FDA approved the therapeutic drug vismodegib (vismo, GDC-0449), a compound that selectively inhibits SMO, and is prescribed for Gorlin patients or patients with advanced BCC [95, 96]. Clinical trials have demonstrated patients responding well to treatment (>50%) with some patients having a complete response. However, the remaining 50% of patients develop a partial response to drug treatment. A strong reason why tumors resist vismo is because of acquired SMO mutations that limit drug binding (SMO inhibitor resistance). Two complementary studies by Atwood et al. and Sharpe et al. identified mutations in SMO that confer resistance to vismo [97, 98]. Interestingly, resistance-associated mutations classified into two groups. Group one mutations occurred within or adjacent to the drug binding pocket, whereas group two mutations occurred at distant sites. Furthermore, Sharpe et al. sequenced BCCs and identified copy number alterations in *SUFU* and *GLI2*, suggesting other potential alternative resistance mechanisms.

Because BCCs can acquire mutations to resist drug binding, this opened many questions to identify alternative mechanisms to inhibit SMO or downstream components of the Hh pathway. Kim et al. demonstrated the FDA-approved antifungal agent, itraconazole, as a potential alternative to inhibit SMO-resistant tumors [99]. An alternative therapeutic approach to consider is to inactivate downstream GLI activity. Indeed, atypical protein kinase C ι/λ

inhibition suppresses Gli activation in BCCs (discussed more in **section 1.4.7**) [97, 100]. In addition, arsenic trioxide may be an alternative inhibitor for GLI; however, clinical trials have proven to be ineffective [99, 101]. Altogether, understanding additional mechanisms in drug resistant BCC may potentially open alternative therapeutic strategies.

Distinct from BCC drug resistance, BCCs can undergo tumor regression but a subset of cells can persist during vismo treatment (tumor persistence). Persisting tumors display suppressed Hh activity and are dormant with the potential to reactivate growth upon drug withdrawal. It has been demonstrated that patients on vismo stop drug treatment because of on-target side effects such as, muscle cramps, weight loss, hair loss, fatigue, and loss of taste [96, 102]. To understand the mechanisms how BCC tumors persist, the initial observation of persisting tumor cells originated from Hutchin et al [103]. Eberl et al. later observed peripheral basal tumor cells persist throughout treatment and this population likely drives recurrent tumor formation [104]. Sanchez-Danes et al. further observed persisting $LGR5^+$ cells and Wnt pathway activation promotes recurrent tumor formation upon drug withdrawal [105]. Similar observations were observed from Biehs et al. [106]. Collectively, these data highlight the need to identify strategies to eliminate persistent tumor cells during vismo treatment.

1.3 BCC mouse models

1.3.1 Introduction

In this section, I describe an overview of genetically engineered BCC mouse models. Most of these models target deletion or overexpression of the different components of the Hh pathway (e.g., Shh, GLI transcription factors, Sufu, oncogenic SMO, and Ptch1). I will describe each model below and describe how the generation of these models helped identify the stem cell origin of BCC.

1.3.2 Shh & GLI overexpression models

The generation of the first BCC mouse model was reported by Oro et al., where *Shh* was driven by the Keratin 14 (K14) promoter (*K14;Shh* mice) [107]. Although *K14;Shh* mice developed BCC-like epidermal proliferative lesions around ~E17.5, these mice were embryonic lethal. To circumvent this issue, *K14;Shh* cells were then grafted into SCID mice, which developed microscopic BCC-like tumors that transformed into aberrant hair follicle structures with sebaceous glands ~3-10 weeks post-engraftment. Building upon these findings, Fan et al. performed retroviral transduction to overexpress SHH in human keratinocytes [108]. Long

terminal repeat driven SHH keratinocytes were grafted into immune deficient mice and displayed similar histological features seen in BCCs. Thus, these studies showed that SHH overexpression can induce BCC-like tumor formation.

As mentioned already, GLI1 and GLI2 transcription factors are key downstream activators of the Hh pathway [109]. Nilsson et al., Grachtchouk et al., and Hutchin et al. each provided evidence either GLI1, GLI2 (or Gli2) overexpression, or mutant forms of Gli2 is sufficient to promote BCC-like tumors in mice [103, 110, 111]. Nilsson et al. generated mice expressing human *GLI1* under the control of the bovine Keratin 5 (K5) promoter (*BK5;GLI1* mice), and observed the formation of BCCs, trichoepitheliomas, cylindromas, and trichoblastomas ~1-13 weeks post-birth [110]. Grachtchouk et al. generated mice expressing mouse *Gli2* under the control of the bovine K5 promoter (*BK5;Gli2* mice) [111]. Indeed, *BK5;Gli2* mice developed multiple BCC-like tumors on the ears, tail, trunk, and the dorsal aspects of paws ~3 months of age. *BK5;Gli2* tumors also exhibited elevated Hh activity and displayed palisading periphery.

Gli proteins all contain a C-terminal transactivation domain, but Gli2 and Gli3 also have an N-terminal repression domain [38]. Indeed, it was demonstrated that removal of the N-terminal repression domain (GLI2ΔN) promotes nodular BCC-like tumors in mice [112]. Sheng et al. also addressed the tumorigenic potential of the Gli2 N-terminal repression domain (Gli2ΔN2) [37]. Interestingly, mice expressing mouse *Gli2ΔN2* under the control of the bovine K5 promoter (*BK5;Gli2ΔN2* mice) rarely developed classic BCCs, and developed skin tumors that resemble trichoblastomas, cylindromas, and basaloid follicular hamartomas [37]. Together, these data support the concept that Gli2ΔN2, GLI2ΔN, and full length Gli2 may have different oncogenic potential for the formation of various skin-derived tumors. In support of this idea, *ΔK5;SMOM2* mice (truncated *Keratin 5* promoter), which exhibit low-level Hh signaling, develop basaloid follicular hamartomas [113]. This finding suggests that varying levels of Hh signaling activity can result in formation of distinct tumor types

Finally, Hutchin et al. generated a tetracycline response element (TRE) *Gli2* allele (*TRE-Gli2*), with the tetracycline-regulated transcriptional transactivator (tTA) fused to the bovine K5 promoter (*BK5-tTA;TRE-Gli2* mice) [103]. The generation of this mouse model allows temporal *Gli2* inactivation in the presence of doxycycline. It was demonstrated upon doxycycline

administration, fully developed BCC-like tumors regress. Collectively, these studies demonstrate that overexpression of GLI activity drives BCC-like tumors in mice.

1.3.3 Ptch inactivation & oncogenic Smo models

As mentioned previously, it is well established that the primary genetic aberration seen in ~70% of human BCCs, is the loss of the tumor suppressor PTCH1. The remaining ~10-20% is through a mutated oncogenic form of SMO. To mimic *Ptch1* loss-of-function, Aszterbaum et al. generated *Ptch1*-heterozygous mice (*Ptch1*^{Neo12} mice, one copy of *Ptch1* & one copy of *lacZ*), and observed microscopic BCC-like tumors develop after >9 months of age [114]. Interestingly, exposing *Ptch1*^{Neo12} mice to UV radiation dramatically enhanced the formation of microscopic BCC- and SCC-like tumors in ~4 months. These tumors possessed elevated β-gal expression, confirming that these tumors possess elevated Hh activity. Similar observations were also noted by Mancuso et al. [115]. Finally, it is important to note that loss of p53 in *Ptch1*-heterozygous models accelerates tumor formation.

Because conventional whole-body constitutive approaches typically limit studies due to embryonic lethality, the Cre-*loxP* system significantly advanced BCC mouse model engineering. Early work using the *Ptch1* conditional knock out technology originated from Uhmann et al. and Zibat et al. [116, 117]. To restrict *Ptch1* conditional knockout to the skin and stem cell compartment of the hair follicle, Adolphe et al. utilized mice expressing a retinoic acid-inducible Keratin 6 (K6) promoter-driven *Cre* to target deletion of *Ptch1* (*K6a-Cre;Ptch1* mice) [118]. Upon retinoic acid administration, microscopic BCC-like tumors developed ~16 weeks later. These microscopic BCC-like tumors also expressed elevated levels of cyclin D1 and cyclin B1, two established Hh target genes. These initial early studies therefore demonstrated the specificity of the Cre-*loxP* system in an adult setting.

To mimic SMO gain-of-function, Xie et al. generated mice expressing human *SMOM2* under the *K5* promoter (*K5;SMOM2* mice) [59]. Indeed, they observed microscopic BCC-like tumors with elevated Hh activity at ~E18. *K5;SMOM2* mice also developed fused digits and spina bifida. The very first conditional *SmoM2* mouse model utilized mice expressing a tamoxifen-inducible CAGGS ubiquitous promoter-driven *Cre*^{ER} to target activation of Cre-inducible *SmoM2* knocked into the ROSA26 locus (*CAGGS-Cre*^{ER}*;SmoM2* mice) [119]. All mice ~6-10 weeks post-tamoxifen developed microscopic BCC-like tumors, rhabdomyosarcoma, medulloblastoma, and pancreatic lesions.

1.3.4 Sufu mutant models

Suppressor of fused (Sufu) is known to negatively regulate Gli activity. Svärd et al. confirmed elevated Hh activity in heterozygous mutant *Sufu* embryos (*Sufu*$^{+/-}$ mice) and in a mouse embryonic fibroblast cell line [44]. However, *Sufu*$^{+/-}$ mice aged up to two years developed basaloid follicular hamartomas and aberrant sebaceous glands, and rarely any BCCs. This suggest mutations in *Sufu* and additional mutations in the Hh pathway are needed for sustained tumor progression. To circumvent this issue, Li et al. generated a tamoxifen-inducible K14 promoter-driven *Cre*^{ESR1} to target inactivation of *Sufu* and *Kif7* (*K14-Cre*^{ESR1}*;Sufu;Kif7*-heterozygous mice) [120]. Kif7 is suggested to positively and negatively regulate Hh activity [43, 121]. Indeed, *K14-Cre*^{ESR1}*;Sufu;Kif7*-heterozygous mice developed microscopic BCC-like tumors and basaloid follicular hamartomas ~7-12 weeks post-tamoxifen. Collectively, these results build upon the understanding that manipulations in downstream Hh regulators is an important collaborator to drive the formation of BCC-like tumors in mice.

1.3.5 p53 mutant models

TP53 is a well-known tumor suppressor and is commonly mutated in a wide variety of human cancers [122]. Not surprisingly, *TP53* is commonly mutated in BCC (>50%) and has been demonstrated that losing *Trp53* promotes BCC tumorigenesis [123-125]. Most BCC mouse models mimic loss-of-function mutations; however, *TP53* missense mutations are the most common mutations observed in human cancers (reviewed in [126]). As an example, Boettcher et al. demonstrated missense variants in the DNA-binding domain results in a dominant-negative effect in hematopoietic cells. This suggests dominant-negative activity of p53 may drive clonal selection. Indeed, Bonilla et al. identified three missense germline *TP53* variants in human sporadic BCCs [127]. While it remains to be determined, incorporation of these missense variants into mouse models may yield new insights into BCC biology.

1.3.6 Cellular origin of BCC

Over the past 30 years, many research groups have generated multiple mouse models that either conditionally inactivate *Ptch1* or activate *SmoM2* in skin epidermal stem cells or hair follicle stem cells [104-106, 112, 128-136]. These results have reported discrepancies for the cellular origin of BCCs; however, it is probable that there could be multiple cellular origins for BCC tumor development. For example, Youssef et al. induced BCC-like tumors using *SmoM2* and demonstrated that tumors primarily arise from the interfollicular epidermis [134]. In contrast,

Grachtchouk et al. demonstrated that BCC-like tumors can arise from hair follicle stem cells using a truncated activated form of GLI2 (GLI2ΔN) [112]. Conclusions from Peterson et al. and others have observed hair follicle stem cells and mechanosensory touch dome epithelia give rise to BCC-like tumors upon deletion of *Ptch1* [104, 130, 135, 137]. Interestingly, hair follicle derived tumors develop nodular tumors and share similar stem cell markers in the hair follicle, whereas epidermal derived tumors resemble more superficial-like [135]. Altogether, these data could explain the various subtypes observed in humans.

As summarized in **Table 1-1**, mouse models have provided critical understanding into the genetics and cellular origin of BCC. As mentioned already in this section, perturbations in Shh, GLI transcription factors, Ptch1, SMO, and Sufu all play critical roles in BCC development. As time continues and additional models become more refined, ongoing studies have already started to model how various mutations beyond Hh play a causative role in BCC tumorigenesis. Indeed, recent exome sequencing studies have revealed that BCCs possess the highest mutational burden of all cancers, with 50-75 mutations/MB in sporadic BCCs and 21-33 mutations/MB in Gorlin BCCs [97, 138-140]. The immense mutational burden seen in BCC suggests there are multiple opportunities for other genetic factors to collaborate with Hh signaling to promote BCC progression. As I describe in the next section and in chapter 2, many reports have suggested additional crosstalk / non-canonical signaling pathways collaborating with Hh signaling in BCC.

1.4 Crosstalk / Non-canonical pathways in BCC

1.4.1 Introduction

Previous and recent studies have identified additional crosstalk / non-canonical pathways that synergize with the Hh pathway in BCCs. Our growing knowledge of these pathways in BCC include Notch, Wnt / β-catenin, Hippo, receptor tyrosine kinases (RTKs), G protein-coupled receptor (GPCRs), atypical protein kinase c (aPKC), mammalian target of rapamycin (mTOR), transforming growth factor-β (TGF-β), and serum response factor (SRF) (**Figure 1-3**). In this section, I will briefly describe how each pathway modulates BCC tumorigenesis, drug response and resistance.

1.4.2 Notch

The Notch signaling pathway is a conserved cell-cell signaling cascade that regulates a wide range of tissues. In mammals, there are four notch receptors (Notch1-4) and five Notch ligands (delta-like 1-3, jagged1-2) [141]. This pathway is activated by cell-cell contact between

these receptors and ligands. The receptor-ligand binding results in downstream cleavage of the Notch receptor, which releases an activated Notch intracellular activated domain (NICD). NICD is then able to enter the nucleus and bind with RBPJ, allowing co-activators like mastermind-like (MAML1), to drive Notch target gene expression. Canonical Notch target genes include *Hes* and *Hey* family members. In the skin epidermis, Notch is an established modulator of terminal differentiation [141]. Notch receptors are expressed in the differentiating layers of the epidermis, hair follicles, and activated cells primed for differentiation. When Notch signaling is ablated by deleting *Rbpj* in the epidermis, this results in impaired epidermal and hair follicle differentiation [142]. Furthermore, Moriyama et al. demonstrated Hes1 modulates cell specification of spinous and granular cell differentiation during epidermal development [143].

Notch is a well-established tumor suppressor in the skin. Early evidence by Nicholas et al. and Demehri et al. defined the tumor suppressive role for Notch signaling in the skin [144, 145]. Nicholas et al. reported *Notch1*-deficient mice develop occasional BCCs late in life and these tumors display increased expression of *Gli1*, *Gli2*, *Ptch1*, and *Shh*. Demerhi et al. generated mice expressing the *Msx2* promoter-driven *Cre* to target deletion of *Notch1* (*Msx2-Cre;Notch1* mice) and observed occasional BCC-like tumors develop around 20 months of age. *Msx2-Cre;Notch1* mice also exhibited significant stromal hyperplasia and increased infiltration of immune cells.

To evaluate how *Notch1*-deficient BCCs respond to vismo drug treatment, Eberl et al. addressed this question [104]. This study demonstrated that inhibiting *Notch1* enables tumors to persist upon drug treatment but does not cause drug resistance. Interestingly, activating Notch activity promotes tumor regression. In addition, Shi et al. determined Notch signaling is significantly downregulated in human BCCs and treatment of JAG1 induces cell apoptosis *in vitro* [146]. Collectively, these data suggest a potential combinatorial treatment strategy to activate Notch and suppress Hh signaling in BCCs.

1.4.3 Wnt / β-Catenin

Wnt / β-Catenin pathway is a critical regulator of cell fate determination, motility, polarity, and stem cell biology. Initial discovery of Wnt was reported in the early 1970's in the Drosophila gene *Wingless* (*Wg*). The mammalian gene, *int-1*, was later discovered in studies with oncogenic retroviruses in breast cancer [147]. The resulting fusion name Wnt, a combination of both *Wg* and *int-1*, was therefore established [148]. The major hallmark of Wnt pathway

activation is the translocation of β-Catenin into the nucleus. When Wnt signaling is off, cytoplasmic β-Catenin is degraded by the Axin, adenomatosis polyposis coli (APC), protein phosphatase 2A (PP2A), glycogen synthase kinase 3 (GSK3β) and casein kinase 1α (CK1α) destruction complex [149, 150]. When this pathway is activated, Wnt binds to the Frizzled and Lrp5/6 co-receptor complex, which subsequently leads to cytoplasmic phosphorylation of Lrp5/6 by GSK3β and CK1α [151]. This results in the recruitment of Dishevelled (DSH) to inactivate the degradation complex to allow β-Catenin to enter the nucleus. β-Catenin then binds with LEF / TCF co-activators to drive target gene expression [152]. Canonical Wnt target genes include *Lgr5* and *Axin2* family members.

Early discovery of activated Wnt / β-Catenin in BCC originated from Yang et al. [153]. Human superficial BCC buds and mouse M2SMO microscopic tumors displayed increased cytoplasmic and nuclear β-Catenin signaling. Interestingly, these bud-like tumors closely resembled the embryonic hair germ, reiterating the concept that BCCs share similar properties to hair follicles. Finally, by incorporating a Wnt pathway antagonist (Dkk1) into SMOM2-expressing mice, BCC-like buds were inhibited. Similar observations of elevated β-Catenin in BCCs were also observed by Salto-Tellez et al. [154].

Expanding on the importance of Wnt pathway activation in BCC, Larsimont et al. determined that Sox9 is required for BCC formation in a Wnt / β-Catenin manner [133]. It was determined that Sox9 is upregulated during early BCC initiation, which promotes self-renewing division, suppresses normal differentiation program, and regulates extracellular matrix and cytoskeleton remodeling. As mentioned previously in **section 1.2.4**, two recent studies suggest Wnt^+ tumor cells persist during vismo treatment, and this population likely drives recurrent tumor formation upon drug withdrawal. Using either LGK-974 or anti-LRP6 treatment with vismo partially suppresses BCC regrowth [105, 106]. Collectively, these data all demonstrate how Wnt signaling modulates BCC and suppression of this pathway may partially reduce tumor recurrence.

1.4.4 Hippo

Hippo signaling is a critical regulator of tissue growth and organ size [155, 156]. This pathway was originally identified in genetic studies of *Drosophila melanogaster* as a suppressor of tissue growth [157, 158]. The major core components of Hippo pathway comprise of two kinases Mst1/2 and Lats1/2, their adaptor proteins Mob1A/B and Sav1, and the transcriptional co-

activators Yap/Taz. When the core Hippo kinases are inactive, Yap/Taz then localize into the nucleus where they canonically interact with TEA domain transcription factor family members (TEAD1-4) to drive target gene expression. Canonical Hippo target genes include *Cyr61* and *Ctgf* [159]. Hippo pathway activity is inactive when Lats1/2 is phosphorylated and retains phosphorylated Yap/Taz in the cytoplasm for degradation.

Studies in mice have demonstrated that YAP is required for skin development and maintenance of stem cell fate in the epidermis [160-162]. Loss of YAP reduces proliferation in the epidermis, whereas *Sav1*$^{-/-}$ mice display thickened epidermis [161, 163]. Mechanistically, Silvis et al. demonstrated deletion of the tumor suppressor α-catenin regulates the localization and activity of Yap1, highlighting the role of adherent junction proteins in Hippo signaling [164]. Furthermore, extracellular matrix (ECM) stiffness regulates YAP/TAZ activity and suggests Hippo activity can be regulated by external mechanical cues [162, 165].

Recent findings have suggested a role for Hippo activity in BCCs [166-168]. Akladios et al. reported increased nuclear YAP levels in tamoxifen-inducible *K14-Cre*^{ER}*;SmoM2* mice. It was also demonstrated that YAP activity drives GLI2 nuclear accumulation through β-catenin activation. Using an alternative model, similar results were observed when using an active mutant form of YAP (YAP2-5SA-ΔC). These data suggest a positive reciprocal signaling network consisting of Hippo, Hh, and Wnt / β-Catenin signaling in BCC. Two follow up studies later determined that active Hippo signaling is required for BCC initiation as well as SCC tumorigenesis [167, 168]. Debaugnies et al. and Maglic et al. showed the requirement of Yap/Taz in the pathogenesis of BCC using *K14-Cre*^{ER}*;SmoM2* mice. Mechanistically, Maglic et al. demonstrated that Yap regulates JNK/JUN stability to modulate BCC progression.

Finally, it is well-established that the non-receptor tyrosine phosphatase, PTPN14, serves as a negative regulator of YAP activity through direct interaction [169-173]. Indeed, Bonilla et al. identified loss-of-function *PTPN14* mutations in human BCCs [127]. Yurchenko et al. further observed significant increase in nuclear YAP1 localization in human intrinsically resistant BCC [174]. It was revealed by RNA-seq that *TEAD2–SLC6A16*, *YAP1–CWF19L2*, and/or *C11orf70–YAP1* putative fusions could be an explanation for hyperactivation of Hippo pathway activity. Collectively, these studies highlight the need to identify targeted therapeutics for Hippo signaling in BCC.

1.4.5 Receptor Tyrosine Kinases (RTKs)

Receptor tyrosine kinases are key cell-surface receptors that regulate cell proliferation, differentiation, migration, survival, and metabolism [175, 176]. In humans, there are fifty-eight known RTK, which are classified into twenty subfamilies. In the presence of signaling molecules (e.g., growth factors) binding to RTKs, neighboring RTKs will associate together and crosslink. Crosslinking of RTKs results in phosphorylation and induces various downstream signal transduction. One of the most studied intracellular signaling cascade triggered by RTKs is the mitogen-activated protein kinase (MAPK) cascade [177]. MAPK is initiated with the activation of Ras, a G protein anchored on the plasma membrane. Activated Ras then phosphorylates the first serine-threonine kinase in the MAPK cascade, followed by subsequent phosphorylation in the two-remaining serine-threonine kinases. Phosphorylation of these kinases ultimately drives changes in gene transcription.

The observation of activated RAS/MAPK in BCC originated from Zhao et al. [178]. In this study, BCC tumors that develop resistance to vismo display high levels of phospo-ERK. Interestingly, BCC resistant tumors may exhibit characteristics of SCC and this study identified 91% genetic similarity between pretreatment BCC and posttreatment SCC. These data may suggest that Hh-driven BCC tumors may evolve into RAS/MAPK-driven SCCs and may be one potential mechanism to evade Smo inhibitor treatment. Kuonen et al. followed up with this concept and observed an inverse correlation between primary cilia and RAS/MAPK activation in human resistant BCCs [179]. Another follow up study by Kuonen et al. further elucidated how cFOS mediates BCC to SCC tumor evolution [180]. It was identified that c-FOS concomitantly activates EGFR/Ras/MAPK signaling and suppression of this signaling pathway reverts SCC back to BCC. Altogether, these findings may suggest the potential use of MAPK inhibitors when BCCs “evolve” into SCC.

Epidermal growth factor receptor (EGFR), a prototypical RTK, has also been suggested in BCC tumorigenesis. Kasper et al. first demonstrated EGFR signaling synergizes with GLI1 and GLI2 via stimulation of RAS/RAF/MEK/ERK signaling pathway in human keratinocytes [181]. Using mouse BCC cell lines, Schnidar et al. observed elevated EGFR mRNA and significant levels of total and activated tyrosine–p-EGFR protein expression [182]. To determine the *in vivo* relevance of Hh-EGFR interaction, Eberl et al. generated tamoxifen-inducible *K5-Cre^{ER};SmoM2;EGFR*-knockout mice [132]. Indeed, deletion of *EGFR* in this system reduced microscopic BCC-like tumors in the ear.

Finally, anaplastic lymphoma kinase (ALK) is a transmembrane RTK and is a member of the insulin receptor superfamily. ALK is known to regulate brain and neuronal development [183]. The initial observation of ALK's synergistic role in BCCs originated from Ning et al. [184]. This study demonstrated ALK activates GLI1 in parallel with the Hh pathway. Altogether, RTKs is reported to modulate tumor progression and may be involved in the transition of BCC to SCC.

1.4.6 G protein-coupled receptors (GPCRs)

G-protein coupled receptors (GPCRs) are seven-transmembrane proteins that serve numerous roles in physiological processes, cancer, as well as coordinating cues with stem cell behavior [185-187]. Not surprisingly, RNA-seq datasets in mice have identified numerous GPCRs in various skin keratinocytes and hair follicle compartments [188]. In the presence of ligand binding, GPCRs undergo conformational changes which activate heterotrimeric G proteins. Activation of heterotrimeric G proteins induces a GDP to GTP exchange in Gα subunits, which subsequently dissociates from the Gαβγ complexes, followed by activation of downstream effectors.

In the skin, well known GPCRs are leucine-rich repeat-containing G protein coupled receptors (LGRs) and the smoothened frizzled class receptor (SMO). Early studies identified an upregulation of GPR49 (also known as LGR5/HG38/FEX) in certain cases of BCC and can modulate tumor formation and proliferation [189]. Another G protein expressed in skin is the stimulatory alpha subunit Gαs (*Gnas*). Iglesias-Bartholome et al. generated tamoxifen-inducible *K14-Cre^{ER};Gnas*-knockout mice and determined deletion of Gαs is sufficient to drive stem cell expansion resulting in BCC-like tumor formation [190]. Disruption of Gαs or protein kinase A (PKA) promotes cell autonomous Hh and Hippo pathway stimulation, suggesting Gαs–PKA signaling as a non-canonical tumor suppressor.

1.4.7 Atypical Protein Kinase C (aPKC)

Protein kinases are enzymes that catalyze protein phosphorylation and protein kinase C (PKC) is a well-studied protein kinase [191-193]. PKC contains unique cysteine-rich Zn-finger motifs that can be further classified into different isozymes. Atypical PKC (aPKC) represents one of these subgroups and has two isoforms, ι/λ and ζ. All PKC family members usually require calcium signaling, diacylglycerol, and phosphatidylserine for their activation. However, it is demonstrated that phosphatidylserine is sufficient for aPKC maximal activity and aPKCs do

not require calcium [194]. Many studies have also demonstrated aPKCs can be activated through the phosphatidylinositol 3-kinase (PI3K) pathway, mitogenic, insulin, or apoptotic signaling pathway [195-199].

The first observation of aPKC's role in BCC was determined in a proteomic screen by Atwood et al. [100]. It was demonstrated that atypical protein kinase C iota/lambda (aPKC ι/λ), a centrosome-associated protein involved in cell polarity and ciliogenesis, can phosphorylate GLI1. It was further determined that *PRKCI*, the gene encoding aPKC ι/λ, was overexpressed in human primary and resistant BCC. Furthermore, topically treated allografted BCC-like tumors with an aPKC inhibitor reduced *Gli1* mRNA levels and tumor area. To better understand the role of aPKC ι/λ in BCC, Mirza et al. demonstrated the mechanism in which aPKC ι/λ recruits histone deacetylase 1/2 (HDAC1/2) to GLI1 to form a positive feed forward loop in the Hh pathway [200]. It is suggested that aPKC acts as a priming kinase for the deacetylation of GLI1 by HDAC1. Consistent with this result, an additional follow up study by Mirza et al. defined the role of LAP2 proteins in modulating GLI1 acetylation or deacetylation in BCCs [201]. LAP2α forms an activating complex with HDAC1 and competes to deacetylate or activate GLI1. Collectively, these data suggest disrupting the LAP2 chaperoning system, HDAC, and aPKC may be promising therapeutic targets in BCC.

1.4.8 Mammalian Target of Rapamycin (mTOR)

The mammalian Target of Rapamycin (mTOR) is a critical regulator of cell growth and metabolism [202, 203]. mTOR is a serine/threonine protein kinase in the PI3K-related kinase (PIKK) family. mTOR comprises the catalytic subunit of the two known multi-subunit mTOR complexes known as mTOR complex 1 and 2 (mTORC1 / mTORC2). These two complexes have unique signaling roles in which mTORC1 regulates cell growth and metabolism, whereas mTORC2 controls proliferation and survival. Specifically, mTORC2 phosphorylates and activates downstream Akt (also known as protein kinase B) [204]. Indeed, there are reports suggesting synergistic mTOR/PI3K/Akt pathway and Hh signaling in the regulation of neuronal precursor cell cycle progression and murine medulloblastoma tumors [205-207].

The initial observation of increased Akt in murine BCCs originated from Kim et al. [208]. AKT S473 phosphorylation in BCC-like tumors was observed in hairless SKH1-*Ptch1*$^{+/-}$ mice. It was further demonstrated that either genetic or pharmacological inhibition of AKT inhibits BCC growth. A follow up study by Kim et al. further identified mTOR is a direct transcriptional

target of SOX9, suggesting that the SOX9-mTOR axis acts downstream of Hh signaling [209]. As mentioned previously, SOX9 is reported to be a critical mediator in BCC growth [132, 133]. Consistent with these initial observations, two recent studies by Chow et al. also suggest the role of mTOR and PI3K in BCCs [210, 211]. It was demonstrated that mTOR promotes aPKC activation but is likely promoting tumor growth independent of Gli1. These data suggest mTOR acts downstream of the Hh pathway. The second study by Chow et al. further determined PI3K promotes aPKC- and AKT1-dependent degradation of the cyclin-dependent kinase inhibitor p21. Altogether, these data suggest a convergence between Hh and mTOR signaling in BCCs.

1.4.9 Transforming growth factor-β (TGFβ)

Transforming growth factor-β (TGFβ) signaling, which includes three isoforms (TGF-β1/2/3), are critical mediators of cell proliferation, differentiation, morphogenesis, tissue homeostasis and regeneration [212, 213]. The effects of TGFβ can be positive or negative and depends on the cellular context. Activation of TGFβ signaling initiates with binding of the specific dual cell-surface receptors type I and II (TGFBR1 and TGFBR2). Type I receptors can be subdivided into two subgroups. Group one can activate Smad2/3 by TGFβ proteins, and group two activate Smad1/5/8 by bone morphogenetic proteins (BMPs). Smads are the first responders to pathway activation and serve as transcriptional activators of cell differentiation. Smads consist of three types, receptor-regulated (R-Smads), common mediator (Co-Smads), and inhibitory (I-Smads). Upon ligand binding, type II TGFβ receptors phosphorylates type 1 TGFβ, which phosphorylates and activates R-Smads (e.g., Smad3). R-Smads bind with Co-Smads (also known as Smad4) and translocate into the nucleus, where this complex regulates transcription of TGFβ responsive genes. I-Smads (Smad7) associates with type I TGFβ receptor and suppresses phosphorylation of R-Smads.

The initial observations of TGFβ activity in BCC originated from Stamp et al. and Schmid et al. [214, 215]. It was determined that increased TGFβ activity is largely expressed in the stroma and BCCs display weaker expression of TGFβ1. This suggests increased TGFβ in the stroma may induce fibrotic alterations in the tumor microenvironment. In contrast, Gambichler et al. observed high mRNA expression of TGFβ1, Smad3, and Smad7 in BCCs [216]. In addition, a report by Fan et al. observed high TGFβ2 and concomitant phosphorylation of Smad2/3 in *K14-Cre;SmoM2* tumors and surrounding stroma [217]. Although these reported data suggest

discrepancies for TGFβ1 or TGFβ2 expression in BCC, it likely suggests TGFβ/Smad signaling plays both autocrine and paracrine roles in BCCs and in the stroma.

Finally, a recent study by Kuonen et al. demonstrated a role for TGFβ, fibronectin, and integrin α5β1 in the pathogenesis of aggressive infiltrative BCC [218]. Mechanistically, fibronectin promotes BCC migration through integrin α5β1 and drives downstream phosphorylation of focal adhesion kinase (FAK). It was further demonstrated that inhibition of phosphorylated FAK (PF-562271) or inhibition of α5β1 (K34C) suppressed TGFβ activity. Altogether, these data define the significance of TGFβ and Hh signaling in BCC.

1.4.10 Serum response factors (SRF)

Serum response factors (SRF) are transcription factors known to associate with the cofactors ELK1 or MKL1 and 2 (MKL1/2, also known as MRTF-A/B and MAL). This association then drives transactivation in a cell- and context-specific manner [219-222]. A secondary pathway that converges upon SRF occurs through Rho-dependent changes in actin dynamics [223, 224]. RhoA subsequently activates downstream Rho-associated protein kinase (ROCK) and mammalian homolog of Drosophila diaphanous (mDIA) to cause restructuring of globular actin to filamentous actin. The restructuring to filamentous actin therefore allows the translocation of MKL1/2 into the nucleus to drive target gene expression.

The first observation for SRF-MKL activity in BCC originated from Whitson et al. [225]. Using the Feature Overlapper for Chromosomal Interval Subsets (FOCIS) and Gene Set Enrichment Analysis (GSEA) algorithms, SRF was the top hit candidate as a putative GLI1 cofactor in resistant BCCs. It was further determined that SRF-MKL complex is required for maintained elevated expression of Hh target genes. Treatment with the MKL1 inhibitor (CCG-203971) suppressed resistant tumor growth. To further define active nuclear MKL in resistant BCCs, Yao et al. identified three prognostic surface markers using single-cell RNA sequencing [226]. By separating MKL-active BCC cells by fluorescence-activated cell sorting, the top three enriched surface markers for this resistant cell population included, LYPD3, TACSTD2 (also known as TROP-2), and LY6D. Yao et al. further showed AP-1 mediates chromatin accessibility and drives nuclear MKL activity. This study provides the rationale to explore AP-1 inhibitors to target resistant BCCs. Altogether, these data highlight how SRF-MKL activity modulates BCC resistance and therapy.

1.5 CD200 signaling and BCC

In this short section, I will briefly introduce the cell surface glycoprotein CD200. CD200 is highly expressed in the hair follicle and is thought to suppress inflammation and confer immune privilege [227, 228]. CD200 is broadly expressed in both hemopoietic and non-hemopoietic cells, thymocytes, neurons, some T cells, and dendritic cells [229, 230]. CD200 is a ligand and binds to immune cells that express the receptor for CD200 (CD200R) to induce intracellular signaling. In mice, there are three related CD200R-like homologues, whereas humans consist of CD200R and hCD200La [229, 231]. In murine epidermis, Rosenblum et al. demonstrated CD200R is expressed on Langerhans cells and activated dendritic epidermal T cells [232]. Furthermore, Cherwinski et al. identified CD200R on mast cells, macrophages, dendritic cells and T cells in murine and human skin [233]. Finally, CD200 is preferentially expressed in the outer root sheath of the hair follicle and suggest the communication between hair follicles and immune cells is regulated by the interaction of CD200-CD200R [234]. Collectively, the CD200-CD200R interaction is thought to reduce inflammation, prevent hair follicle-specific autoimmunity and may protect epidermal stem cells from autoimmune destruction (reviewed in [228]).

The initial observation for CD200 expression and its role in BCC tumorigenesis originated from Colmont et al. [235]. Peterson et al. later observed murine BCC tumors express CD200 and *Ptch1*-deficient keratinocytes express high *CD200* expression [135]. Altogether, these data raise some immediate questions. Does suppression of CD200 affect hair regeneration, BCC initiation, or pre-existing advanced BCC? In chapter 4, I address if inhibiting CD200 suppresses tumor initiation and describe preliminary experimental results in more detail.

1.6 Dissertation summary

A combination of mouse models, molecular biology tools, and genomic sequencing approaches has significantly advanced our knowledge for BCC in the past 30 years. Much of this work focused on identifying how each component of the Hh pathway contributes to BCC development. My thesis aims to shed light on other aspects of BCC biology that are less understood, including the specific genetic factors that allow dormant BCC-like tumors to progress into macroscopic disease. Recent deep sequencing studies have revealed sun-exposed skin can tolerate high rates of mutations [139, 140]. In chapter 2, I evaluate what acquired secondary mutations allow tumor cells to escape tumor dormancy [236]. In chapter 3, I developed a BCC mouse model where *Trp53* and *Notch1* are simultaneously deleted. The use for this

model is to understand if concomitant deletion of these genetic factors provides a greater advantage for tumor cells to progress. I also developed a BCC mouse model where *MYCN* is overexpressed in *Gli1;Ptch1;Notch1*-deficient (GPN1) tumors. Additionally, I developed a BCC mouse model where *Mycn* is deleted to determine if eliminating a well-established oncogene provides a disadvantage for tumor cells. In chapter 4, I shift my focus on the role of CD200 in BCCs. I characterized tumor size and immune markers upon anti-CD200 treatment in tumor-containing skin. In chapter 5, I optimized the new DNAscope® duplex assay to detect and visualize *GLI1*, *GLI2*, and *MYCN* copy number in human BCC samples. In chapter 6, I reflect on key lessons I have learned from my thesis and propose future experiments.

1.7 Figures

Figure 1-1: Schematic of mammalian hedgehog signaling

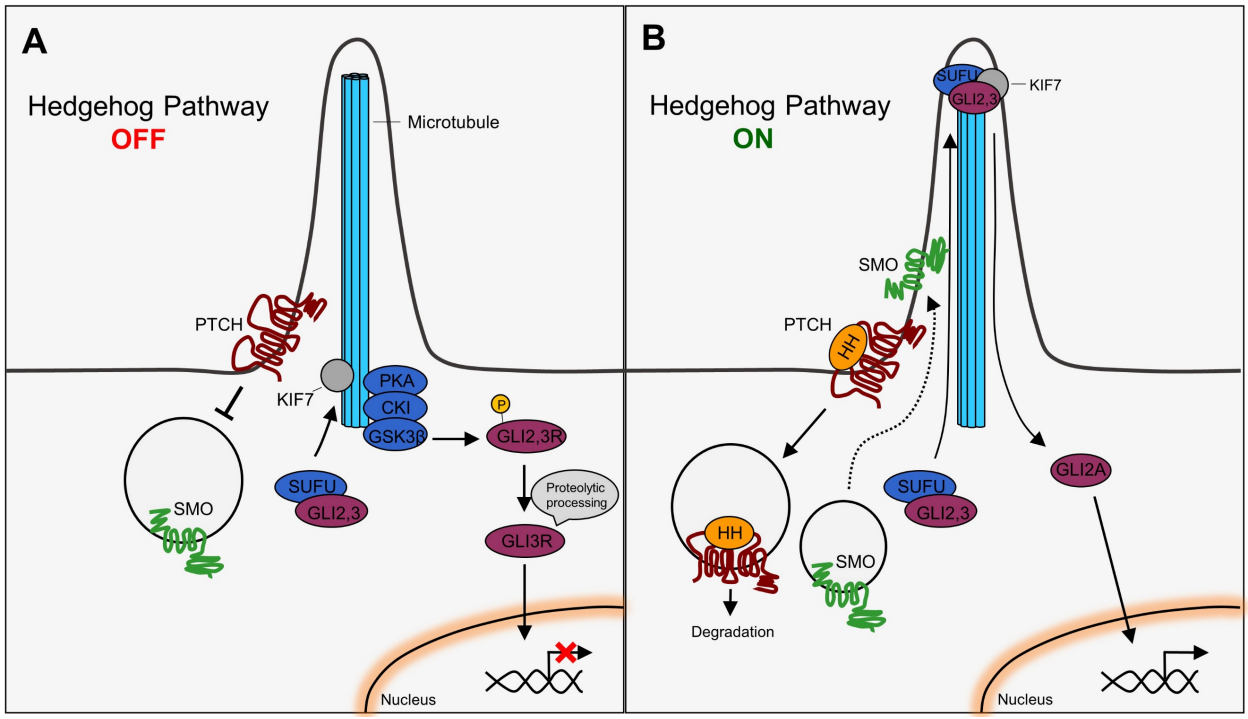

A. In the absence of Hedgehog (HH) ligand, PTCH localizes to the primary cilium and prevents SMO from entering the cilium. GLI2 and GLI3 are phosphorylated by PKA, CKI, and GSK3β. Proteolytic cleavage processes GLI3 into a carboxy terminal truncated repressor form (GLI3R) and degrades GLI2. GLI3R subsequently enters the nucleus and inhibits transcription of downstream Hedgehog target genes, such as *Ptch2*, *Gli1*, and *Mycn*.

B. In the presence of HH ligand, PTCH is internalized for degradation and allows SMO to traffic into the primary cilium. At the cilium, SMO activation results in the dissociation of the GLI-SUFU-KIF7 complex, inhibits the formation of GLI3 repressor, and activates GLI2 (GLI2A). GLI2A enters the nucleus to promote transcription of Hedgehog target genes, whose protein products negatively and positively feedback on this pathway.

Figure 1-2: Mechanisms for aberrant hedgehog pathway activation

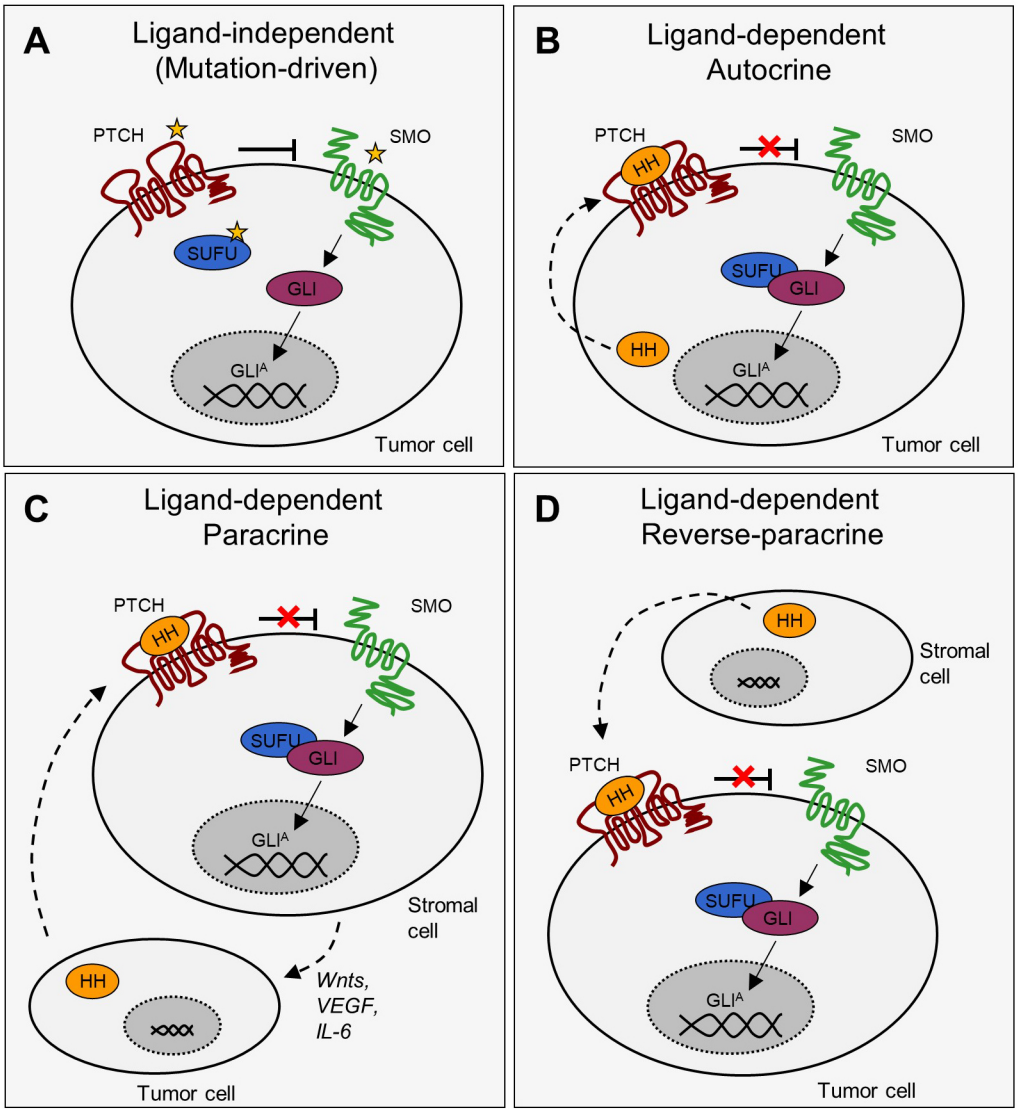

A. Ligand-independent HH activation is due to inactivating mutations in PTCH1 or SUFU; activating mutations in SMO; or amplification of GLI activity.

B. In autocrine signaling, tumor cells secrete HH and respond to HH ligands.

C. In paracrine signaling, tumor cells produce HH ligands and activate HH pathway in stroma cells (e.g., Wingless/Wnt, Vascular endothelial growth factor, and interleukin 6). For example, Vascular endothelial growth factor is a mediator of angiogenesis and is important for tumor growth (reviewed in [237]).

D. In reverse paracrine signaling, stromal cells produce HH ligands which activate HH pathway in tumor cells. An example of this mechanism has been demonstrated in malignant lymphoma [238].

Figure 1-3: Crosstalk signaling pathways in BCC

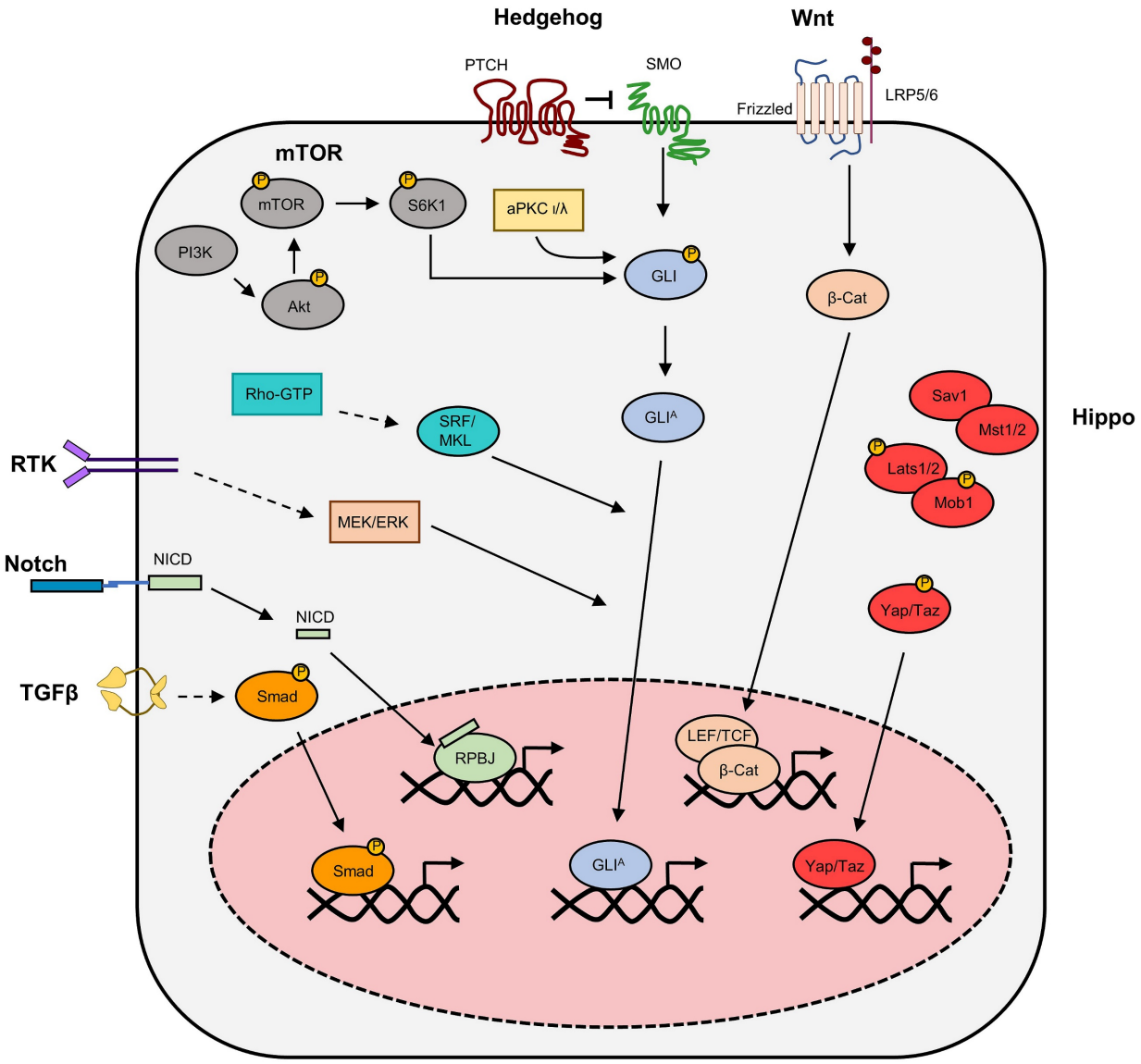

Schematic of the crosstalk signaling pathways in BCC described in **section 1.4**.

Table 1-1: Summary of engineered BCC mouse models

BCC Tumor Mouse Model	Time of Hh activation	Microscopic lesions advance to macroscopic disease?	Reference
K14;Shh	Embryonic	No	(107)
K5;SMOM2 (Human)	Embryonic	No	(59)
Ptch+/-	Embryonic	Yes* (UVR exposure accelerates tumor progression)	(114, 115)
Bovine K5;GLI1 (Human)	Embryonic	Yes	(110)
Bovine K5;Gli2	Embryonic	Yes	(111)
Bovine K5;Gli2ΔN2 (deleted form of "Gli2")	Embryonic	No	(37)
K5-tTA;TRE-Gli2	Embryonic or postnatal	Yes	(103)
Sufu+/-	Embryonic	No	(44)
CAGGS-CreER;SmoM2	P10	No	(119)
ΔK5;SmoM2	Embryonic	No	(113)
K6a-Cre;Ptch1fl/fl	Embryonic	No	(118)
K14-CreERT;SmoM2-YFP	P30-35	No	(128)
K14-CreERT;CLEG	P30-35	No	
K14-CreERT;SmoM2-YFP;Kif3afl/-	P30-35	No	
K14-CreERT;CLEG;Kif3afl/-	P30-35	No	
K15-CrePR1;Ptch+/-;p53fl/fl	7.5 weeks	Yes	(129)
K14-CreER2;Ptch+/-;p53fl/fl	7.5 weeks	Yes	
Bovine K5rtTA;TRE-GLI1 (Human)	P16	No	(130)
Bovine K5-CrePR;Ptchfl/fl	P18-24	No	
Lgr5-EGFP-CreERT2;Ptchfl/fl	P14-20	No	
K15-CrePR;SmoM2-YFP	7.5 weeks	No	(131)
K15-CrePR1;rtTA;tetO-GLI2ΔN (human)	7-8 weeks	Yes	(112)
Lgr5-EGFP-CreERT2;rtTA;tetO-GLI2ΔN (human)	7-8 weeks	Yes	
K14-rtTA;tetO-GLI2ΔN (human)	7-8 weeks	Yes?*	
K5-CreER;rtTA;tetO-GLI2ΔN (human)	7-8 weeks	Yes	
K5-CreER;SmoM2	P28	No	(132)
K14-CreESR1;Sufufl/fl;Kif7fl/fl	8 weeks	No	(120)
K5-Cre;Ptch1fl/fl	Embryonic	No	
K14-CreER;Ptch1fl/fl	P28	No	(134)
K14-CreER;SmoM2-YFP	P23-28	No	
K14-CreER;SmoM2-YFP	6 weeks	No	(133)
K14-CreER;SmoM2-YFP;Sox9fl/fl	6 weeks	No	
K14-CreERT;Ptch1fl/fl	8 weeks	No	(135)
Gli1-CreERT2;Ptch1fl/fl	8 weeks	No	
Hes1-CreERT2;Ptch1fl/fl	8 weeks	No	
Lrig1-CreERT2;Ptch1fl/fl	8 weeks	No	
K14-CreERT;Ptch1fl/fl;p53fl/fl	8 weeks	Yes?* (study only looked at microscopic tumors)	
Gli1-CreERT2;Ptch1fl/fl;Notch1fl/fl	4.5 weeks	Yes* (study only looked at microscopic tumors)	(104)
Gli1-CreERT2;Ptch1fl/fl;p53fl/fl	4.5 weeks	Yes* (study only looked at microscopic tumors)	
Gli1-CreERT2;SmoM2-YFP	4.5 weeks	No	

K14-CreER;SmoM2-YFP;Lgr5-DTR-GFP	7 weeks	No	[105]
K14-CreER;Ptch1fl/fl;Lgr5-DTR-GFP	7 weeks	No	
K14-CreER;Ptch1fl/fl;p53fl/fl	Unknown (Reported Cre leakiness)	Yes?* (study only looked at microscopic tumors)	[106]
Ptch+/- (SKH-1 mice)	Embryonic	Yes?*	[209]
K14-CreER;SmoM2-YFP;Yapfl/fl	P24	No	[168]
K14-CreER;SmoM2-YFP;Yapfl/f;Tazfl/fl	Unknown	No	[167]
Gli1-CreERT2;Ptch1fl/fl;TRE-MYCN	8 weeks	Yes	In this thesis (Chapter 2)
Gli1-CreERT2;Ptch1fl/fl;Mycnfl/fl	8 weeks	No	In this thesis (Chapter 3)
Gli1-CreERT2;Ptch1fl/fl;Notch1;p53fl/fl	8 weeks	Yes	In this thesis (Chapter 3)
Gli1-CreERT2;Ptch1fl/fl;Notch1;TRE-MYCN	8 weeks	Yes	In this thesis (Chapter 3)

1.8 References

1. Lum, L. and P.A. Beachy, *The Hedgehog response network: sensors, switches, and routers.* Science, 2004. **304**: p. 1755-1759.

2. Huangfu, D. and K.V. Anderson, *Signaling from Smo to Ci/Gli: conservation and divergence of Hedgehog pathways from Drosophila to vertebrates.* Development, 2006. **133**(1): p. 3-14.

3. Briscoe, J. and P.P. Therond, *The mechanisms of Hedgehog signalling and its roles in development and disease.* Nat Rev Mol Cell Biol, 2013. **14**(7): p. 416-29.

4. Nüsslein-Volhard, C. and E. Wieschaus, *Mutations affecting segment number and polarity in Drosophila.* Nature, 1980. **287**(5785): p. 795-801.

5. Echelard, Y., et al., *Sonic hedgehog, a member of a family of putative signaling molecules, is implicated in the regulation of CNS polarity.* Cell, 1993. **75**(7): p. 1417-30.

6. Krauss, S., J.P. Concordet, and P.W. Ingham, *A functionally conserved homolog of the Drosophila segment polarity gene hh is expressed in tissues with polarizing activity in zebrafish embryos.* Cell, 1993. **75**(7): p. 1431-44.

7. Riddle, R.D., et al., *Sonic hedgehog mediates the polarizing activity of the ZPA.* Cell, 1993. **75**(7): p. 1401-16.

8. Chung, U.I., et al., *Indian hedgehog couples chondrogenesis to osteogenesis in endochondral bone development.* J Clin Invest, 2001. **107**(3): p. 295-304.

9. Vortkamp, A., et al., *Regulation of rate of cartilage differentiation by Indian hedgehog and PTH-related protein.* Science, 1996. **273**(5275): p. 613-22.

10. Bitgood, M.J., L. Shen, and A.P. McMahon, *Sertoli cell signaling by Desert hedgehog regulates the male germline.* Current Biology, 1996. **6**(3): p. 298-304.

11. St-Jacques, B., M. Hammerschmidt, and A.P. McMahon, *Indian hedgehog signaling regulates proliferation and differentiation of chondrocytes and is essential for bone formation.* Genes Dev, 1999. **13**(16): p. 2072-86.

12. Chiang, C., et al., *Cyclopia and defective axial patterning in mice lacking Sonic hedgehog gene function.* Nature, 1996. **383**(6599): p. 407-13.

13. Bellusci, S., et al., *Involvement of Sonic hedgehog (Shh) in mouse embryonic lung growth and morphogenesis.* Development, 1997. **124**(1): p. 53-63.

14. Pepicelli, C.V., P.M. Lewis, and A.P. McMahon, *Sonic hedgehog regulates branching morphogenesis in the mammalian lung.* Curr Biol, 1998. **8**(19): p. 1083-6.

15. Washington Smoak, I., et al., *Sonic hedgehog is required for cardiac outflow tract and neural crest cell development.* Dev Biol, 2005. **283**(2): p. 357-72.

16. Litingtung, Y., et al., *Sonic hedgehog is essential to foregut development.* Nat Genet, 1998. **20**(1): p. 58-61.

17. Chiang, C., et al., *Essential role for Sonic hedgehog during hair follicle morphogenesis.* Dev Biol, 1999. **205**(1): p. 1-9.

18. St-Jacques, B., et al., *Sonic hedgehog signaling is essential for hair development.* Curr Biol, 1998. **8**(19): p. 1058-68.

19. Singla, V. and J.F. Reiter, *The primary cilium as the cell's antenna: signaling at a sensory organelle.* Science, 2006. **313**(5787): p. 629-33.

20. Wong, S.Y. and J.F. Reiter, *The primary cilium at the crossroads of mammalian hedgehog signaling.* Curr Top Dev Biol, 2008. **85**: p. 225-60.

21. Murone, M., A. Rosenthal, and F.J. de Sauvage, *Sonic hedgehog signaling by the Patched–Smoothened receptor complex.* Current Biology, 1999. **9**(2): p. 76-84.

22. Milenkovic, L., et al., *Mouse patched1 controls body size determination and limb patterning.* Development, 1999. **126**(20): p. 4431-40.

23. Motoyama, J., et al., *Differential requirement for Gli2 and Gli3 in ventral neural cell fate specification.* Dev Biol, 2003. **259**(1): p. 150-61.

24. Goodrich, L.V., et al., *Altered neural cell fates and medulloblastoma in mouse patched mutants.* Science, 1997. **277**(5329): p. 1109-13.

25. Aza-Blanc, P., et al., *Proteolysis that is inhibited by hedgehog targets Cubitus interruptus protein to the nucleus and converts it to a repressor.* Cell, 1997. **89**(7): p. 1043-53.

26. Chen, C.H., et al., *Nuclear trafficking of Cubitus interruptus in the transcriptional regulation of Hedgehog target gene expression.* Cell, 1999. **98**(3): p. 305-16.

27. Wang, G., et al., *Interactions with Costal2 and suppressor of fused regulate nuclear translocation and activity of cubitus interruptus.* Genes Dev, 2000. **14**(22): p. 2893-905.

28. Préat, T., et al., *A putative serine/threonine protein kinase encoded by the segment-polarity fused gene of Drosophila.* Nature, 1990. **347**(6288): p. 87-9.

29. Lum, L., et al., *Hedgehog signal transduction via Smoothened association with a cytoplasmic complex scaffolded by the atypical kinesin, Costal-2.* Mol Cell, 2003. **12**(5): p. 1261-74.

30. Wang, Q.T. and R.A. Holmgren, *The subcellular localization and activity of Drosophila cubitus interruptus are regulated at multiple levels.* Development, 1999. **126**(22): p. 5097-106.

31. Zhang, W., et al., *Hedgehog-regulated Costal2-kinase complexes control phosphorylation and proteolytic processing of Cubitus interruptus.* Dev Cell, 2005. **8**(2): p. 267-78.

32. Price, M.A. and D. Kalderon, *Proteolysis of the Hedgehog signaling effector Cubitus interruptus requires phosphorylation by Glycogen Synthase Kinase 3 and Casein Kinase 1.* Cell, 2002. **108**(6): p. 823-35.

33. Price, M.A. and D. Kalderon, *Proteolysis of cubitus interruptus in Drosophila requires phosphorylation by protein kinase A.* Development, 1999. **126**(19): p. 4331-9.

34. Bai, C.B. and A.L. Joyner, *Gli1 can rescue the in vivo function of Gli2.* Development, 2001. **128**(24): p. 5161-72.

35. Park, H.L., et al., *Mouse Gli1 mutants are viable but have defects in SHH signaling in combination with a Gli2 mutation.* Development, 2000. **127**(8): p. 1593-605.

36. Pan, Y., et al., *Sonic hedgehog signaling regulates Gli2 transcriptional activity by suppressing its processing and degradation.* Mol Cell Biol, 2006. **26**(9): p. 3365-77.

37. Sheng, H., et al., *Dissecting the oncogenic potential of Gli2: deletion of an NH(2)-terminal fragment alters skin tumor phenotype.* Cancer Res, 2002. **62**(18): p. 5308-16.

38. Sasaki, H., et al., *Regulation of Gli2 and Gli3 activities by an amino-terminal repression domain: implication of Gli2 and Gli3 as primary mediators of Shh signaling.* Development, 1999. **126**(17): p. 3915-24.

39. Tempé, D., et al., *Multisite protein kinase A and glycogen synthase kinase 3beta phosphorylation leads to Gli3 ubiquitination by SCFbetaTrCP.* Mol Cell Biol, 2006. **26**(11): p. 4316-26.

40. Wang, B., J.F. Fallon, and P.A. Beachy, *Hedgehog-regulated processing of Gli3 produces an anterior/posterior repressor gradient in the developing vertebrate limb.* Cell, 2000. **100**(4): p. 423-34.

41. Wang, B. and Y. Li, *Evidence for the direct involvement of {beta}TrCP in Gli3 protein processing.* Proc Natl Acad Sci U S A, 2006. **103**(1): p. 33-8.

42. Meyer, N.P. and H. Roelink, *The amino-terminal region of Gli3 antagonizes the Shh response and acts in dorsoventral fate specification in the developing spinal cord.* Dev Biol, 2003. **257**(2): p. 343-55.

43. Cheung, H.O., et al., *The kinesin protein Kif7 is a critical regulator of Gli transcription factors in mammalian hedgehog signaling.* Sci Signal, 2009. **2**(76): p. ra29.

44. Svärd, J., et al., *Genetic elimination of Suppressor of fused reveals an essential repressor function in the mammalian Hedgehog signaling pathway.* Dev Cell, 2006. **10**(2): p. 187-97.

45. Hynes, M., et al., *Control of cell pattern in the neural tube by the zinc finger transcription factor and oncogene Gli-1.* Neuron, 1997. **19**(1): p. 15-26.

46. Lee, J., et al., *Gli1 is a target of Sonic hedgehog that induces ventral neural tube development.* Development, 1997. **124**(13): p. 2537-52.

47. Ding, Q., et al., *Diminished Sonic hedgehog signaling and lack of floor plate differentiation in Gli2 mutant mice.* Development, 1998. **125**(14): p. 2533-43.

48. Matise, M.P., et al., *Gli2 is required for induction of floor plate and adjacent cells, but not most ventral neurons in the mouse central nervous system.* Development, 1998. **125**(15): p. 2759-70.

49. Persson, M., et al., *Dorsal-ventral patterning of the spinal cord requires Gli3 transcriptional repressor activity.* Genes Dev, 2002. **16**(22): p. 2865-78.

50. Mill, P., et al., *Sonic hedgehog-dependent activation of Gli2 is essential for embryonic hair follicle development.* Genes Dev, 2003. **17**(2): p. 282-94.

51. Hui, C.C. and A.L. Joyner, *A mouse model of greig cephalopolysyndactyly syndrome: the extra-toesJ mutation contains an intragenic deletion of the Gli3 gene.* Nat Genet, 1993. **3**(3): p. 241-6.

52. te Welscher, P., et al., *Progression of vertebrate limb development through SHH-mediated counteraction of GLI3.* Science, 2002. **298**(5594): p. 827-30.

53. Litingtung, Y., et al., *Shh and Gli3 are dispensable for limb skeleton formation but regulate digit number and identity.* Nature, 2002. **418**(6901): p. 979-83.

54. Mo, R., et al., *Specific and redundant functions of Gli2 and Gli3 zinc finger genes in skeletal patterning and development.* Development, 1997. **124**(1): p. 113-23.

55. Scales, S.J. and F.J. de Sauvage, *Mechanisms of Hedgehog pathway activation in cancer and implications for therapy.* Trends Pharmacol Sci, 2009. **30**(6): p. 303-12.

56. Johnson, R.L., et al., *Human homolog of patched, a candidate gene for the basal cell nevus syndrome.* Science, 1996. **272**(5268): p. 1668-71.

57. Raffel, C., et al., *Sporadic medulloblastomas contain PTCH mutations.* Cancer Res, 1997. **57**(5): p. 842-5.

58. Tostar, U., et al., *Deregulation of the hedgehog signalling pathway: a possible role for the PTCH and SUFU genes in human rhabdomyoma and rhabdomyosarcoma development.* J Pathol, 2006. **208**(1): p. 17-25.

59. Xie, J., et al., *Activating Smoothened mutations in sporadic basal-cell carcinoma.* Nature, 1998. **391**(6662): p. 90-2.

60. Dahmane, N., et al., *The Sonic Hedgehog-Gli pathway regulates dorsal brain growth and tumorigenesis.* Development, 2001. **128**(24): p. 5201-12.

61. Szkandera, J., et al., *Hedgehog signaling pathway in ovarian cancer.* Int J Mol Sci, 2013. **14**(1): p. 1179-96.

62. Huang, S., et al., *Activation of the hedgehog pathway in human hepatocellular carcinomas.* Carcinogenesis, 2006. **27**(7): p. 1334-40.

63. Datta, S. and M.W. Datta, *Sonic Hedgehog signaling in advanced prostate cancer.* Cell Mol Life Sci, 2006. **63**(4): p. 435-48.

64. Kubo, M., et al., *Hedgehog signaling pathway is a new therapeutic target for patients with breast cancer.* Cancer Res, 2004. **64**(17): p. 6071-4.

65. Varnat, F., et al., *Human colon cancer epithelial cells harbour active HEDGEHOG-GLI signalling that is essential for tumour growth, recurrence, metastasis and stem cell survival and expansion.* EMBO Mol Med, 2009. **1**(6-7): p. 338-51.

66. Berman, D.M., et al., *Widespread requirement for Hedgehog ligand stimulation in growth of digestive tract tumours.* Nature, 2003. **425**(6960): p. 846-51.

67. Theunissen, J.-W. and F.J. de Sauvage, *Paracrine Hedgehog Signaling in Cancer.* Cancer Research, 2009. **69**(15): p. 6007-6010.

68. Fan, L., et al., *Hedgehog signaling promotes prostate xenograft tumor growth.* Endocrinology, 2004. **145**(8): p. 3961-70.

69. Thayer, S.P., et al., *Hedgehog is an early and late mediator of pancreatic cancer tumorigenesis.* Nature, 2003. **425**(6960): p. 851-856.

70. Pasca di Magliano, M., et al., *Hedgehog/Ras interactions regulate early stages of pancreatic cancer.* Genes Dev, 2006. **20**(22): p. 3161-73.

71. Morton, J.P., et al., *Sonic hedgehog acts at multiple stages during pancreatic tumorigenesis.* Proceedings of the National Academy of Sciences, 2007. **104**(12): p. 5103-5108.

72. Tian, H., et al., *Hedgehog signaling is restricted to the stromal compartment during pancreatic carcinogenesis.* Proceedings of the National Academy of Sciences, 2009. **106**(11): p. 4254-4259.

73. Jacob, A., *Observations respecting an ulcer of peculiar character, which attacks the eyelids and other parts of the face.* Dublin Hospital Rep Commun Med Surg, 1827. **4**: p. 232-239.

74. Krompecher, E., *Der Basalzellenkrebs.* Jena: Gustav Fischer, 1903.

75. Mallory, F.B., *Recent progress in the microscopic anatomy and differentiation of cancer.* JAMA, 1910. **55**(18): p. 1513-1516.

76. *Cancer Facts & Figures 2022*. 2022; Available from: https://www.cancer.org/research/cancer-facts-statistics/all-cancer-facts-figures/cancer-facts-figures-2022.html.

77. Rubin, A.I., E.H. Chen, and D. Ratner, *Basal-cell carcinoma.* N Engl J Med, 2005. **353**(21): p. 2262-9.

78. Karagas, M.R., et al., *Use of tanning devices and risk of basal cell and squamous cell skin cancers.* J Natl Cancer Inst, 2002. **94**(3): p. 224-6.

79. Bowen, G.M., G.L. White, Jr., and J.W. Gerwels, *Mohs micrographic surgery.* Am Fam Physician, 2005. **72**(5): p. 845-8.

80. Kasper, M., et al., *Basal cell carcinoma - molecular biology and potential new therapies.* J Clin Invest, 2012. **122**(2): p. 455-63.

81. Jarisch, W., *Zur Lehre von den Hautgesschwulsten.* Arch Dermatol Syphilol (Berl). 1894. **28**: p. 162-222.

82. Gorlin, R.J. and R.W. Goltz, *Multiple nevoid basal-cell epithelioma, jaw cysts and bifid rib. A syndrome.* N Engl J Med, 1960. **262**: p. 908-12.

83. Gailani, M.R., et al., *Developmental defects in Gorlin syndrome related to a putative tumor suppressor gene on chromosome 9.* Cell, 1992. **69**(1): p. 111-7.

84. Hahn, H., et al., *Mutations of the human homolog of Drosophila patched in the nevoid basal cell carcinoma syndrome.* Cell, 1996. **85**(6): p. 841-51.

85. Klein, R.D., D.J. Dykas, and A.E. Bale, *Clinical testing for the nevoid basal cell carcinoma syndrome in a DNA diagnostic laboratory.* Genet Med, 2005. **7**(9): p. 611-9.

86. Bonifas, J.M., et al., *Parental origin of chromosome 9q22.3-q31 lost in basal cell carcinomas from basal cell nevus syndrome patients.* Hum Mol Genet, 1994. **3**(3): p. 447-8.

87. Reifenberger, J., et al., *Missense mutations in SMOH in sporadic basal cell carcinomas of the skin and primitive neuroectodermal tumors of the central nervous system.* Cancer Res, 1998. **58**(9): p. 1798-803.

88. Binns, W., et al., *A Congenital Cyclopian-Type Malformation in Lambs Induced by Maternal Ingestion of a Range Plant, Veratrum Californicum.* Am J Vet Res, 1963. **24**: p. 1164-75.

89. Nanni, L., et al., *The mutational spectrum of the sonic hedgehog gene in holoprosencephaly: SHH mutations cause a significant proportion of autosomal dominant holoprosencephaly.* Hum Mol Genet, 1999. **8**(13): p. 2479-88.

90. Wallis, D. and M. Muenke, *Mutations in holoprosencephaly.* Hum Mutat, 2000. **16**(2): p. 99-108.

91. Keeler, R.F., *Teratogenic compounds of Veratrum californicum (Durand) X. Cyclopia in rabbits produced by cyclopamine.* Teratology, 1970. **3**(2): p. 175-80.

92. Cooper, M.K., et al., *Teratogen-mediated inhibition of target tissue response to Shh signaling.* Science, 1998. **280**(5369): p. 1603-7.

93. Chen, J.K., et al., *Inhibition of Hedgehog signaling by direct binding of cyclopamine to Smoothened.* Genes Dev, 2002. **16**(21): p. 2743-8.

94. Athar, M., et al., *Inhibition of smoothened signaling prevents ultraviolet B-induced basal cell carcinomas through regulation of Fas expression and apoptosis.* Cancer Res, 2004. **64**(20): p. 7545-52.

95. Sekulic, A., et al., *Efficacy and Safety of Vismodegib in Advanced Basal-Cell Carcinoma.* New England Journal of Medicine, 2012. **366**(23): p. 2171-2179.

96. Tang, J.Y., et al., *Inhibiting the Hedgehog Pathway in Patients with the Basal-Cell Nevus Syndrome.* New England Journal of Medicine, 2012. **366**(23): p. 2180-2188.

97. Atwood, S.X., et al., *Smoothened variants explain the majority of drug resistance in basal cell carcinoma.* Cancer Cell, 2015. **27**(3): p. 342-53.

98. Sharpe, H.J., et al., *Genomic analysis of smoothened inhibitor resistance in basal cell carcinoma.* Cancer Cell, 2015. **27**(3): p. 327-41.

99. Kim, J., et al., *Itraconazole and arsenic trioxide inhibit Hedgehog pathway activation and tumor growth associated with acquired resistance to smoothened antagonists.* Cancer Cell, 2013. **23**(1): p. 23-34.

100. Atwood, S.X., et al., *GLI activation by atypical protein kinase C ι/λ regulates the growth of basal cell carcinomas.* Nature, 2013. **494**(7438): p. 484-8.

101. Ally, M.S., et al., *Effects of Combined Treatment With Arsenic Trioxide and Itraconazole in Patients With Refractory Metastatic Basal Cell Carcinoma.* JAMA Dermatol, 2016. **152**(4): p. 452-6.

102. Kumari, A., et al., *Recovery of taste organs and sensory function after severe loss from Hedgehog/Smoothened inhibition with cancer drug sonidegib.* Proc Natl Acad Sci U S A, 2017. **114**(48): p. E10369-e10378.

103. Hutchin, M.E., et al., *Sustained Hedgehog signaling is required for basal cell carcinoma proliferation and survival: conditional skin tumorigenesis recapitulates the hair growth cycle.* Genes Dev, 2005. **19**(2): p. 214-23.

104. Eberl, M., et al., *Tumor Architecture and Notch Signaling Modulate Drug Response in Basal Cell Carcinoma.* Cancer Cell, 2018. **33**(2): p. 229-243 e4.

105. Sánchez-Danés, A., et al., *A slow-cycling LGR5 tumour population mediates basal cell carcinoma relapse after therapy.* Nature, 2018.

106. Biehs, B., et al., *A cell identity switch allows residual BCC to survive Hedgehog pathway inhibition.* Nature, 2018.

107. Oro, A.E., et al., *Basal Cell Carcinoma in Mice Overexpressing Sonic Hedgehog.* Science, 1997. **276**(5313): p. 817-21.

108. Fan, H., et al., *Induction of basal cell carcinoma features in transgenic human skin expressing Sonic Hedgehog.* Nature Medicine, 1997. **3**(7): p. 788-792.

109. Kasper, M., et al., *GLI transcription factors: mediators of oncogenic Hedgehog signalling.* Eur J Cancer, 2006. **42**(4): p. 437-45.

110. Nilsson, M., et al., *Induction of basal cell carcinomas and trichoepitheliomas in mice overexpressing GLI-1.* Proc Natl Acad Sci U S A, 2000. **97**(7): p. 3438-43.

111. Grachtchouk, M., et al., *Basal cell carcinomas in mice overexpressing Gli2 in skin.* Nature Genetics, 2000. **24**(3): p. 216-217.

112. Grachtchouk, M., et al., *Basal cell carcinomas in mice arise from hair follicle stem cells and multiple epithelial progenitor populations.* J Clin Invest, 2011. **121**(5): p. 1768-81.

113. Grachtchouk, V., et al., *The magnitude of hedgehog signaling activity defines skin tumor phenotype.* Embo j, 2003. **22**(11): p. 2741-51.

114. Aszterbaum, M., et al., *Ultraviolet and ionizing radiation enhance the growth of BCCs and trichoblastomas in patched heterozygous knockout mice.* Nat Med, 1999. **5**(11): p. 1285-91.

115. Mancuso, M., et al., *Basal cell carcinoma and its development: insights from radiation-induced tumors in Ptch1-deficient mice.* Cancer Res, 2004. **64**(3): p. 934-41.

116. Uhmann, A., et al., *The Hedgehog receptor Patched controls lymphoid lineage commitment.* Blood, 2007. **110**(6): p. 1814-1823.

117. Zibat, A., et al., *Time-point and dosage of gene inactivation determine the tumor spectrum in conditional Ptch knockouts.* Carcinogenesis, 2009. **30**(6): p. 918-926.

118. Adolphe, C., et al., *Patched1 functions as a gatekeeper by promoting cell cycle progression.* Cancer Res, 2006. **66**(4): p. 2081-8.

119. Mao, J., et al., *A novel somatic mouse model to survey tumorigenic potential applied to the Hedgehog pathway.* Cancer Res, 2006. **66**(20): p. 10171-8.

120. Li, Z.J., et al., *Kif7 regulates Gli2 through Sufu-dependent and -independent functions during skin development and tumorigenesis.* Development, 2012. **139**(22): p. 4152-61.

121. Liem, K.F., Jr., et al., *Mouse Kif7/Costal2 is a cilia-associated protein that regulates Sonic hedgehog signaling.* Proc Natl Acad Sci U S A, 2009. **106**(32): p. 13377-82.

122. Hainaut, P. and G.P. Pfeifer, *Somatic TP53 Mutations in the Era of Genome Sequencing.* Cold Spring Harb Perspect Med, 2016. **6**(11).

123. Ponten, F., et al., *Molecular pathology in basal cell cancer with p53 as a genetic marker.* Oncogene, 1997. **15**: p. 1059-1067.

124. Wang, G.Y., et al., *Basal cell carcinomas arise from hair follicle stem cells in Ptch1+/- mice.* Cancer Cell, 2011. **19**: p. 1-11.

125. Wang, G.Y., et al., *Differing tumor-suppressor functions of Arf and p53 in murine basal cell carcinoma initiation and progression.* Oncogene, 2017. **36**(26): p. 3772-3780.

126. Baugh, E.H., et al., *Why are there hotspot mutations in the TP53 gene in human cancers?* Cell Death & Differentiation, 2018. **25**(1): p. 154-160.

127. Bonilla, X., et al., *Genomic analysis identifies new drivers and progression pathways in skin basal cell carcinoma.* Nat Genet, 2016. **48**(4): p. 398-406.

128. Wong, S.Y., et al., *Primary cilia can both mediate and suppress Hedgehog pathway-dependent tumorigenesis.* Nature medicine, 2009. **15**(9): p. 1055-1061.

129. Wang, G.Y., et al., *Basal cell carcinomas arise from hair follicle stem cells in Ptch1(+/-) mice.* Cancer Cell, 2011. **19**(1): p. 114-24.

130. Kasper, M., et al., *Wounding enhances epidermal tumorigenesis by recruiting hair follicle keratinocytes.* Proc Natl Acad Sci U S A, 2011. **108**(10): p. 4099-104.

131. Wong, S.Y. and J.F. Reiter, *Wounding mobilizes hair follicle stem cells to form tumors.* Proc Natl Acad Sci U S A, 2011. **108**(10): p. 4093-8.

132. Eberl, M., et al., *Hedgehog-EGFR cooperation response genes determine the oncogenic phenotype of basal cell carcinoma and tumour-initiating pancreatic cancer cells.* EMBO Mol Med, 2012. **4**(3): p. 218-33.

133. Larsimont, J.C., et al., *Sox9 Controls Self-Renewal of Oncogene Targeted Cells and Links Tumor Initiation and Invasion.* Cell Stem Cell, 2015. **17**(1): p. 60-73.

134. Youssef, K.K., et al., *Identification of the cell lineage at the origin of basal cell carcinoma.* Nat Cell Biol, 2010. **12**(3): p. 299-305.

135. Peterson, S.C., et al., *Basal cell carcinoma preferentially arises from stem cells within hair follicle and mechanosensory niches.* Cell Stem Cell, 2015. **16**(4): p. 400-12.

136. Kim, A.L., et al., *SOX9 Transcriptionally Regulates mTOR-Induced Proliferation of Basal Cell Carcinomas.* J Invest Dermatol, 2018. **138**(8): p. 1716-1725.

137. Sun, X., et al., *Coordinated hedgehog signaling induces new hair follicles in adult skin.* Elife, 2020. **9**.

138. Jayaraman, S.S., et al., *Mutational landscape of basal cell carcinomas by whole-exome sequencing.* J Invest Dermatol, 2014. **134**(1): p. 213-220.

139. Martincorena, I., et al., *Somatic mutant clones colonize the human esophagus with age.* Science, 2018. **362**(6417): p. 911-917.

140. Martincorena, I., et al., *Tumor evolution. High burden and pervasive positive selection of somatic mutations in normal human skin.* Science, 2015. **348**(6237): p. 880-6.

141. Nowell, C. and F. Radtke, *Cutaneous Notch signaling in health and disease.* Cold Spring Harb Perspect Med, 2013. **3**(12): p. a017772.

142. Blanpain, C., et al., *Canonical notch signaling functions as a commitment switch in the epidermal lineage.* Genes Dev, 2006. **20**(21): p. 3022-35.

143. Moriyama, M., et al., *Multiple roles of Notch signaling in the regulation of epidermal development.* Dev Cell, 2008. **14**(4): p. 594-604.

144. Demehri, S., A. Turkoz, and R. Kopan, *Epidermal Notch1 loss promotes skin tumorigenesis by impacting the stromal microenvironment.* Cancer Cell, 2009. **16**(1): p. 55-66.

145. Nicolas, M., et al., *Notch1 functions as a tumor suppressor in mouse skin.* Nature Genetics, 2003. **33**(3): p. 416-421.

146. Shi, F.T., et al., *Notch signaling is significantly suppressed in basal cell carcinomas and activation induces basal cell carcinoma cell apoptosis.* Mol Med Rep, 2017. **15**(4): p. 1441-1454.

147. Nusse, R., et al., *Mode of proviral activation of a putative mammary oncogene (int-1) on mouse chromosome 15.* Nature, 1984. **307**(5947): p. 131-6.

148. Nusse, R., et al., *A new nomenclature for int-1 and related genes: the Wnt gene family.* Cell, 1991. **64**(2): p. 231.

149. Logan, C.Y. and R. Nusse, *The Wnt signaling pathway in development and disease.* Annu Rev Cell Dev Biol, 2004. **20**: p. 781-810.

150. Wodarz, A. and R. Nusse, *Mechanisms of Wnt signaling in development.* Annu Rev Cell Dev Biol, 1998. **14**: p. 59-88.

151. Zeng, X., et al., *A dual-kinase mechanism for Wnt co-receptor phosphorylation and activation.* Nature, 2005. **438**(7069): p. 873-877.

152. van de Wetering, M., et al., *The beta-catenin/TCF-4 complex imposes a crypt progenitor phenotype on colorectal cancer cells.* Cell, 2002. **111**(2): p. 241-50.

153. Yang, S.H., et al., *Pathological responses to oncogenic Hedgehog signaling in skin are dependent on canonical Wnt/beta3-catenin signaling.* Nat Genet, 2008. **40**(9): p. 1130-5.

154. Salto-Tellez, M., et al., *RUNX3 protein is overexpressed in human basal cell carcinomas.* Oncogene, 2006. **25**(58): p. 7646-7649.

155. Varelas, X., *The Hippo pathway effectors TAZ and YAP in development, homeostasis and disease.* Development, 2014. **141**(8): p. 1614-26.

156. van Soldt, B.J. and W.V. Cardoso, *Hippo-Yap/Taz signaling: Complex network interactions and impact in epithelial cell behavior.* Wiley Interdiscip Rev Dev Biol, 2020. **9**(3): p. e371.

157. Huang, J., et al., *The Hippo signaling pathway coordinately regulates cell proliferation and apoptosis by inactivating Yorkie, the Drosophila Homolog of YAP.* Cell, 2005. **122**(3): p. 421-34.

158. Jia, J., et al., *The Drosophila Ste20 family kinase dMST functions as a tumor suppressor by restricting cell proliferation and promoting apoptosis.* Genes Dev, 2003. **17**(20): p. 2514-9.

159. Zhao, B., et al., *TEAD mediates YAP-dependent gene induction and growth control.* Genes Dev, 2008. **22**(14): p. 1962-71.

160. Zhang, H., H.A. Pasolli, and E. Fuchs, *Yes-associated protein (YAP) transcriptional coactivator functions in balancing growth and differentiation in skin.* Proc Natl Acad Sci U S A, 2011. **108**(6): p. 2270-5.

161. Schlegelmilch, K., et al., *Yap1 acts downstream of α-catenin to control epidermal proliferation.* Cell, 2011. **144**(5): p. 782-95.

162. Elbediwy, A., et al., *Integrin signalling regulates YAP and TAZ to control skin homeostasis.* Development, 2016. **143**(10): p. 1674-87.

163. Lee, J.H., et al., *A crucial role of WW45 in developing epithelial tissues in the mouse.* Embo j, 2008. **27**(8): p. 1231-42.

164. Silvis, M.R., et al., *α-catenin is a tumor suppressor that controls cell accumulation by regulating the localization and activity of the transcriptional coactivator Yap1.* Sci Signal, 2011. **4**(174): p. ra33.

165. Dupont, S., et al., *Role of YAP/TAZ in mechanotransduction.* Nature, 2011. **474**(7350): p. 179-183.

166. Akladios, B., et al., *Positive regulatory interactions between YAP and Hedgehog signalling in skin homeostasis and BCC development in mouse skin in vivo.* PLoS One, 2017. **12**(8): p. e0183178.

167. Debaugnies, M., et al., *YAP and TAZ are essential for basal and squamous cell carcinoma initiation.* EMBO Rep, 2018. **19**(7).

168. Maglic, D., et al., *YAP-TEAD signaling promotes basal cell carcinoma development via a c-JUN/AP1 axis.* EMBO J, 2018. **37**(17).

169. Huang, J.M., et al., *YAP modifies cancer cell sensitivity to EGFR and survivin inhibitors and is negatively regulated by the non-receptor type protein tyrosine phosphatase 14.* Oncogene, 2013. **32**(17): p. 2220-2229.

170. Liu, X., et al., *PTPN14 interacts with and negatively regulates the oncogenic function of YAP.* Oncogene, 2013. **32**(10): p. 1266-1273.

171. Michaloglou, C., et al., *The tyrosine phosphatase PTPN14 is a negative regulator of YAP activity.* PLoS One, 2013. **8**(4): p. e61916.

172. Wang, W., et al., *PTPN14 is required for the density-dependent control of YAP1.* Genes Dev, 2012. **26**(17): p. 1959-71.

173. Wilson, K.E., et al., *PTPN14 forms a complex with Kibra and LATS1 proteins and negatively regulates the YAP oncogenic function.* J Biol Chem, 2014. **289**(34): p. 23693-700.

174. Yurchenko, A.A., et al., *Frequency and Genomic Aspects of Intrinsic Resistance to Vismodegib in Locally Advanced Basal Cell Carcinoma.* Clinical Cancer Research, 2022. **28**(7): p. 1422-1432.

175. Blume-Jensen, P. and T. Hunter, *Oncogenic kinase signalling.* Nature, 2001. **411**(6835): p. 355-65.

176. Ullrich, A. and J. Schlessinger, *Signal transduction by receptors with tyrosine kinase activity.* Cell, 1990. **61**(2): p. 203-12.

177. Seger, R. and E.G. Krebs, *The MAPK signaling cascade.* The FASEB Journal, 1995. **9**(9): p. 726-735.

178. Zhao, X., et al., *RAS/MAPK Activation Drives Resistance to Smo Inhibition, Metastasis, and Tumor Evolution in Shh Pathway-Dependent Tumors.* Cancer Res, 2015. **75**(17): p. 3623-35.

179. Kuonen, F., et al., *Loss of Primary Cilia Drives Switching from Hedgehog to Ras/MAPK Pathway in Resistant Basal Cell Carcinoma.* J Invest Dermatol, 2019. **139**(7): p. 1439-1448.

180. Kuonen, F., et al., *c-FOS drives reversible basal to squamous cell carcinoma transition.* Cell Reports, 2021. **37**(1): p. 109774.

181. Kasper, M., et al., *Selective modulation of Hedgehog/GLI target gene expression by epidermal growth factor signaling in human keratinocytes.* Mol Cell Biol, 2006. **26**(16): p. 6283-98.

182. Schnidar, H., et al., *Epidermal growth factor receptor signaling synergizes with Hedgehog/GLI in oncogenic transformation via activation of the MEK/ERK/JUN pathway.* Cancer Res, 2009. **69**(4): p. 1284-92.

183. Iwahara, T., et al., *Molecular characterization of ALK, a receptor tyrosine kinase expressed specifically in the nervous system.* Oncogene, 1997. **14**(4): p. 439-49.

184. Ning, H., et al., *Identification of anaplastic lymphoma kinase as a potential therapeutic target in Basal Cell Carcinoma.* Oncotarget, 2013. **4**(12): p. 2237-48.

185. Pierce, K.L., R.T. Premont, and R.J. Lefkowitz, *Seven-transmembrane receptors.* Nature Reviews Molecular Cell Biology, 2002. **3**(9): p. 639-650.

186. Dorsam, R.T. and J.S. Gutkind, *G-protein-coupled receptors and cancer.* Nature Reviews Cancer, 2007. **7**(2): p. 79-94.

187. O'Hayre, M., et al., *The emerging mutational landscape of G proteins and G-protein-coupled receptors in cancer.* Nature Reviews Cancer, 2013. **13**(6): p. 412-424.

188. Rezza, A., et al., *Signaling Networks among Stem Cell Precursors, Transit-Amplifying Progenitors, and their Niche in Developing Hair Follicles.* Cell Reports, 2016. **14**(12): p. 3001-3018.

189. Tanese, K., et al., *G-protein-coupled receptor GPR49 is up-regulated in basal cell carcinoma and promotes cell proliferation and tumor formation.* Am J Pathol, 2008. **173**(3): p. 835-43.

190. Iglesias-Bartolome, R., et al., *Inactivation of a Gα(s)-PKA tumour suppressor pathway in skin stem cells initiates basal-cell carcinogenesis.* Nat Cell Biol, 2015. **17**(6): p. 793-803.

191. Breitkreutz, D., et al., *Protein kinase C family: on the crossroads of cell signaling in skin and tumor epithelium.* J Cancer Res Clin Oncol, 2007. **133**(11): p. 793-808.

192. Hug, H. and T.F. Sarre, *Protein kinase C isoenzymes: divergence in signal transduction?* Biochem J, 1993. **291 (Pt 2)**(Pt 2): p. 329-43.

193. Barford, D., A.K. Das, and M.P. Egloff, *The structure and mechanism of protein phosphatases: insights into catalysis and regulation.* Annu Rev Biophys Biomol Struct, 1998. **27**: p. 133-64.

194. Chauhan, V.P., et al., *Lipid activators of protein kinase C.* Life Sci, 1990. **47**(12): p. 981-6.

195. Toker, A. and L.C. Cantley, *Signalling through the lipid products of phosphoinositide-3-OH kinase.* Nature, 1997. **387**(6634): p. 673-6.

196. Berra, E., et al., *Protein kinase C zeta isoform is critical for mitogenic signal transduction.* Cell, 1993. **74**(3): p. 555-63.

197. Akimoto, K., et al., *EGF or PDGF receptors activate atypical PKClambda through phosphatidylinositol 3-kinase.* Embo j, 1996. **15**(4): p. 788-98.

198. Kotani, K., et al., *Requirement of atypical protein kinase clambda for insulin stimulation of glucose uptake but not for Akt activation in 3T3-L1 adipocytes.* Mol Cell Biol, 1998. **18**(12): p. 6971-82.

199. Díaz-Meco, M.T., et al., *The product of par-4, a gene induced during apoptosis, interacts selectively with the atypical isoforms of protein kinase C.* Cell, 1996. **86**(5): p. 777-86.

200. Mirza, A.N., et al., *Combined inhibition of atypical PKC and histone deacetylase 1 is cooperative in basal cell carcinoma treatment.* JCI Insight, 2017. **2**(21).

201. Mirza, A.N., et al., *LAP2 Proteins Chaperone GLI1 Movement between the Lamina and Chromatin to Regulate Transcription.* Cell, 2019. **176**(1-2): p. 198-212.e15.

202. Saxton, R.A. and D.M. Sabatini, *mTOR Signaling in Growth, Metabolism, and Disease.* Cell, 2017. **168**(6): p. 960-976.

203. Kim, J. and K.-L. Guan, *mTOR as a central hub of nutrient signalling and cell growth.* Nature Cell Biology, 2019. **21**(1): p. 63-71.

204. Sarbassov, D.D., et al., *Phosphorylation and regulation of Akt/PKB by the rictor-mTOR complex.* Science, 2005. **307**(5712): p. 1098-101.

205. Kenney, A.M., H.R. Widlund, and D.H. Rowitch, *Hedgehog and PI-3 kinase signaling converge on Nmyc1 to promote cell cycle progression in cerebellar neuronal precursors.* Development, 2004. **131**(1): p. 217-28.

206. Rao, G., et al., *Sonic hedgehog and insulin-like growth factor signaling synergize to induce medulloblastoma formation from nestin-expressing neural progenitors in mice.* Oncogene, 2004. **23**(36): p. 6156-62.

207. Wang, Y., et al., *The crosstalk of mTOR/S6K1 and Hedgehog pathways.* Cancer Cell, 2012. **21**(3): p. 374-87.

208. Kim, A.L., et al., *AKT1 Activation is Obligatory for Spontaneous BCC Tumor Growth in a Murine Model that Mimics Some Features of Basal Cell Nevus Syndrome.* Cancer Prev Res (Phila), 2016. **9**(10): p. 794-802.

209. Kim, A.L., et al., *SOX9 Transcriptionally Regulates mTOR-Induced Proliferation of Basal Cell Carcinomas.* Journal of Investigative Dermatology, 2018. **138**(8): p. 1716-1725.

210. Chow, R.Y., et al., *PI3K Promotes Basal Cell Carcinoma Growth Through Kinase-Induced p21 Degradation.* Frontiers in Oncology, 2021. **11**(2504).

211. Chow, R.Y., et al., *MTOR promotes basal cell carcinoma growth through atypical PKC.* Exp Dermatol, 2021. **30**(3): p. 358-366.

212. Massagué, J., *TGFβ signalling in context.* Nature Reviews Molecular Cell Biology, 2012. **13**(10): p. 616-630.

213. Hata, A. and Y.G. Chen, *TGF-β Signaling from Receptors to Smads.* Cold Spring Harb Perspect Biol, 2016. **8**(9).

214. Stamp, G.W., et al., *Transforming growth factor-beta distribution in basal cell carcinomas: relationship to proliferation index.* Br J Dermatol, 1993. **129**(1): p. 57-64.

215. Schmid, P., P. Itin, and T. Rufli, *In situ analysis of transforming growth factors-beta (TGF-beta 1, TGF-beta 2, TGF-beta 3) and TGF-beta type II receptor expression in basal cell carcinomas.* Br J Dermatol, 1996. **134**(6): p. 1044-51.

216. Gambichler, T., et al., *Increased expression of TGF-beta/Smad proteins in basal cell carcinoma.* Eur J Med Res, 2007. **12**(10): p. 509-14.

217. Fan, Q., et al., *Requirement of TGFbeta signaling for SMO-mediated carcinogenesis.* J Biol Chem, 2010. **285**(47): p. 36570-6.

218. Kuonen, F., et al., *TGFβ, Fibronectin and Integrin α5β1 Promote Invasion in Basal Cell Carcinoma.* J Invest Dermatol, 2018. **138**(11): p. 2432-2442.

219. Zaromytidou, A.I., F. Miralles, and R. Treisman, *MAL and ternary complex factor use different mechanisms to contact a common surface on the serum response factor DNA-binding domain.* Mol Cell Biol, 2006. **26**(11): p. 4134-48.

220. Wang, Z., et al., *Myocardin and ternary complex factors compete for SRF to control smooth muscle gene expression.* Nature, 2004. **428**(6979): p. 185-9.

221. Marais, R., J. Wynne, and R. Treisman, *The SRF accessory protein Elk-1 contains a growth factor-regulated transcriptional activation domain.* Cell, 1993. **73**(2): p. 381-93.

222. Janknecht, R. and A. Nordheim, *Elk-1 protein domains required for direct and SRF-assisted DNA-binding.* Nucleic Acids Res, 1992. **20**(13): p. 3317-24.

223. Sotiropoulos, A., et al., *Signal-regulated activation of serum response factor is mediated by changes in actin dynamics.* Cell, 1999. **98**(2): p. 159-69.

224. Miralles, F., et al., *Actin dynamics control SRF activity by regulation of its coactivator MAL.* Cell, 2003. **113**(3): p. 329-42.

225. Whitson, R.J., et al., *Noncanonical hedgehog pathway activation through SRF-MKL1 promotes drug resistance in basal cell carcinomas.* Nat Med, 2018. **24**(3): p. 271-281.

226. Yao, C.D., et al., *AP-1 and TGFβ cooperativity drives non-canonical Hedgehog signaling in resistant basal cell carcinoma.* Nature Communications, 2020. **11**(1): p. 5079.

227. Garza, L.A., et al., *Bald scalp in men with androgenetic alopecia retains hair follicle stem cells but lacks CD200-rich and CD34-positive hair follicle progenitor cells.* J Clin Invest, 2011. **121**(2): p. 613-22.

228. Rosenblum, M.D., et al., *CD200, a "no danger" signal for hair follicles.* J Dermatol Sci, 2006. **41**(3): p. 165-74.

229. Wright, G.J., et al., *The unusual distribution of the neuronal/lymphoid cell surface CD200 (OX2) glycoprotein is conserved in humans.* Immunology, 2001. **102**(2): p. 173-9.

230. Clark, M.J., et al., *MRC OX-2 antigen: a lymphoid/neuronal membrane glycoprotein with a structure like a single immunoglobulin light chain.* Embo j, 1985. **4**(1): p. 113-8.

231. Gorczynski, R., et al., *CD200 is a ligand for all members of the CD200R family of immunoregulatory molecules.* J Immunol, 2004. **172**(12): p. 7744-9.

232. Rosenblum, M.D., et al., *Characterization of CD200-Receptor Expression in the Murine Epidermis.* Journal of Investigative Dermatology, 2005. **125**(6): p. 1130-1138.

233. Cherwinski, H.M., et al., *The CD200 Receptor Is a Novel and Potent Regulator of Murine and Human Mast Cell Function.* The Journal of Immunology, 2005. **174**(3): p. 1348.

234. Rosenblum, M.D., et al., *Expression of CD200 on Epithelial Cells of the Murine Hair Follicle: A Role in Tissue-Specific Immune Tolerance?* Journal of Investigative Dermatology, 2004. **123**(5): p. 880-887.

235. Colmont, C.S., et al., *CD200-expressing human basal cell carcinoma cells initiate tumor growth.* Proceedings of the National Academy of Sciences, 2013. **110**(4): p. 1434.

236. Trieu, K.G., et al., *Basal cell carcinomas acquire secondary mutations to overcome dormancy and progress from microscopic to macroscopic disease.* Cell Rep, 2022. **39**(5): p. 110779.

237. Carmeliet, P., *VEGF as a key mediator of angiogenesis in cancer.* Oncology, 2005. **69 Suppl 3**: p. 4-10.

238. Dierks, C., et al., *Essential role of stromally induced hedgehog signaling in B-cell malignancies.* Nat Med, 2007. **13**(8): p. 944-51.

Chapter 2: Basal Cell Carcinomas Acquire Secondary Mutations to Overcome Dormancy and Progress From Microscopic to Macroscopic Disease[1]

2.1 Summary

Basal cell carcinomas (BCCs) frequently possess immense mutational burdens; however, the functional significance of most of these mutations remains unclear. Here, we report that loss of *Ptch1*, the most common mutation that activates upstream Hedgehog (Hh) signaling, initiates the formation of nascent BCC-like tumors that eventually enter into a dormant state. However, rare tumors that overcome dormancy acquire the ability to hyperactivate downstream Hh signaling through a variety of mechanisms, including amplification of *Gli1/2* and upregulation of Mycn. Furthermore, we demonstrate that *MYCN* overexpression promotes the progression of tumors induced by loss of *Ptch1*. These findings suggest that canonical mutations that activate upstream Hh signaling are necessary, but not sufficient, for BCC to fully progress. Rather, tumors likely acquire secondary mutations that further hyperactivate downstream Hh signaling in order to escape dormancy and enter a trajectory of uncontrolled expansion.

2.2 Introduction

Our skin is exposed to the mutagenic effects of ultraviolet (UV) radiation on a daily basis. While UV exposure is a major risk factor for skin cancer, recent deep sequencing studies have revealed that clinically normal, sun-exposed skin can tolerate surprisingly high rates of mutation without forming tumors [1-3]. Indeed, previous studies have suggested that keratinocytes that acquire cancer-associated mutations may be actively eliminated from the skin, or may persist and carry out normal physiological functions [4-7]. Why certain tumor-initiated cells fail to maintain dysmorphic growth, whereas others display unbridled proliferation, currently remains unclear.

A tumor that arises more frequently than any other is basal cell carcinoma (BCC), the world's most common cancer [8, 9]. Consistent with the high mutational rates caused by UV exposure, most BCCs arise sporadically in sun-exposed skin; however, Gorlin syndrome patients

[1] Originally published as: Trieu et al., *Basal Cell Carcinomas Acquire Secondary Mutations to Overcome Dormancy and Progress From Microscopic to Macroscopic Disease*, Cell Reports (2022), https://doi.org/10.1016/j.celrep.2022.110779. This chapter has been revised to follow thesis formatting.

who inherit one defective copy of *PTCH1* are predisposed to forming numerous BCCs [10-12]. Although rarely lethal, the ubiquity of BCC, which is diagnosed in over 5 million patients annually, represents a quality of life issue for many patients and poses a major burden on our healthcare system (American Cancer Society statistics, 2021).

Dysregulated Hedgehog (Hh) signaling is the key feature that drives all BCCs [13]. Normally, Hh signaling is suppressed by PTCH1, whose main function is to inhibit SMO, an upstream activator of the pathway. Upon binding to Hh ligands, PTCH1 is itself inactivated, allowing SMO to signal through GLI transcription factors to induce target gene expression. These targets include those that encode cell cycle regulators, such as *MYCN* and *CCND1*, as well as core components of the Hh pathway, such as *GLI1*, *PTCH1* and *PTCH2*, which provide both positive and negative feedback [14-17].

BCCs are classically driven by mutations that activate upstream Hh signaling, either through loss-of-function mutations in *PTCH1* (~70% of tumors) or gain-of-function mutations in *SMO* (~10-20% of tumors). However, BCC is also the most highly mutated cancer, with 50-75 mutations/Mb in sporadic tumors, and 21-33 mutations/Mb in Gorlin tumors [18-21]. Not surprisingly, mutations in the Hh pathway (*PTCH1*, *SMO*, *SUFU*, *GLI1/GLI2*, *MYCN*) arise frequently, as do mutations in *TP53*, Notch signaling (*NOTCH1*, *NOTCH2*) and Hippo signaling (*YAP1*, *PTPN14*, *LATS1*/*LATS2*) [20, 22, 23]. These recurrent mutations suggest that tumors initiated by loss of *PTCH1* or oncogenic *SMO* may require additional genetic changes to override tumor suppressive controls in the skin; however, this remains to be proven.

BCC is among the most highly mutated cancers [1], but this immense mutational burden also complicates the ability to distinguish functional mutations from random passenger mutations. To circumvent this problem, we generated simpler BCC mouse models that allow rare macroscopic tumors to form alongside numerous failed microscopic lesions. By comparing tumors that succeed against those which fail, we identify secondary changes that enable nascent tumors to progress to macroscopic disease.

2.3 Methods

2.3.1 Animal Models

Unless otherwise indicated, 8 week-old mice were induced with a single intraperitoneal injection of tamoxifen (TAM) at 5 mg/40 grams body weight. GPT mice were induced with TAM and later transferred to 200 mg/kg doxycycline-containing chow for 12 weeks. For animal

strain information, please see the Key Resources Table (**Table 2-1**). All studies were performed on mice of both genders in a mixed genetic background, using littermate animals for comparisons whenever possible. All mice were maintained in specific pathogen free housing and were used in accordance with regulations established by the University of Michigan Unit for Laboratory Animal Medicine.

2.3.2 Human Studies

De-identified human BCC samples embedded in paraffin were obtained through study protocol HUM00042233, HUM00075822 and HUM00051875, in accordance with procedures approved by the Institutional Review Board at the UM Medical School.

2.3.3 Immunofluorescence

Skin biopsies were fixed in 3.7% formalin overnight for paraffin embedding. For frozen sections, samples were fixed in 3.7% paraformaldehyde at 4°C for 1 hour, rinsed in PBS, sunk in 30% sucrose overnight and embedded into OCT. Frozen sections were probed with antibodies against the following antigens: p21 (1:100, Cell Signaling) and p16 (1:100, Invitrogen). Paraffin sections were antigen-retrieved by boiling slides in 1 mM EDTA, pH 8.0, for 10 minutes, and probed with antibodies against the following antigens: K14 (1:1,000, Biolegend), Ki67 (1:100, Cell Signaling and BD Biosciences), α smooth muscle actin (1:500, Cell Signaling), cleaved caspase-3 (1:100, Cell Signaling) and luciferase (1:1000, Novus). Staining was amplified using the TSA Fluorescein Plus kit for antibodies against the following targets: p53 (1:5000, Novocastra), NICD (1:500, Cell Signaling) and Mycn (1:500, Cell Signaling). Amplification was performed for 2 minutes, 4 minutes and 10 minutes, respectively, following manufacturer's instructions. Image processing was performed using Adobe Photoshop with the Auto-Blend feature applied to maximize image sharpness across focal planes.

2.3.4 RNA in situ Hybridization

RNA *in situ* staining was performed using the RNAscope 2.5 brown kit (ACD). Paraffin slides were antigen-retrieved by boiling in RNAscope retrieval buffer for 15 minutes, treated with protease for 30 minutes and incubated with target probes at 40°C for 2 hours. Probe detection was performed according to manufacturer's instructions. Paraffin slides were counterstained with hematoxylin. Please see the Key Resources Table (**Table 2-1**) for information on RNAscope probes.

2.3.5 LacZ Visualization

Frozen sections were incubated at 37° C in 1 mg/ml X-gal dissolved in 5 mM potassium ferrocyanide and 5 mM potassium ferricyanide for 30 minutes, and counterstained with nuclear fast red.

2.3.6 Phorbol ester treatment

100 µL of 12-O-Tetradecanoylphorbol-13-acetate (TPA, Sigma) dissolved at a concentration of 0.25 mg/mL in ethanol was topically applied onto shaved GP and GPN1 mice for 2 consecutive days. Two days after treatment, dorsal skin was collected.

2.3.7 DNA extraction

DNA was harvested using the DNeasy Blood & Tissue kit (Qiagen). Tumor and paired liver samples (15-25 mg) were minced in ATL buffer containing proteinase K and incubated overnight at 56°C. The next day, digested tumor and liver samples were processed according to the manufacturer's instructions.

2.3.8 Whole Exome Sequencing (WES)

WES was performed on macroscopic GPP53 and GPN1 tumors, and on matched liver samples. All sequencing and analyses were performed by Novogene. Briefly, 1 µg of DNA was used for library preparation using the Agilent SureSelectXT Mouse All Exon kit. Fragmentation was performed to generate 180-280 bp fragments and assessed on the Agilent Bioanalyzer 2100 system for quality control. Captured libraries were sequenced using Illumina NovaSeq 6000. Reads were aligned with Burrows-Wheeler Aligner (BWA; v0.7.17) using the mm10 reference genome. Conversion to BAM files was performed using Picard (v2.18.9). Single-nucleotide variants (SNVs) and InDels were identified by GATK (v4.0), followed by ANNOVAR to annotate variants. Somatic SNVs and InDels were identified by MuTect and Strelka, respectively. Somatic copy number variants (CNVs) were called by Control-FREEC (v11.4), using the setting minCNAlength parameter = 2. Low confidence CNV changes annotated as "genomic superduplications" with CNV = 1 or 3 were omitted from analyses. CNV plots were generated using CNVkit with default settings.

2.3.9 Tumor measurements

Tumor area was quantitated from 3 representative fields per sample, and an overall average was calculated for each animal and timepoint. Final values were normalized relative to that of tumors, 5 weeks post-TAM. TD tumors were quantitated by inspecting ~1 cm of skin

H&E histology, and normalizing to the length of the section. Cell proliferation was quantitated from 3 representative fields per sample and expressed as the percentage of Ki67+ tumor cells / K14+ total tumor cells. p53+ tumor cells were counted at the tumor periphery (basal) or interior (suprabasal) compartments. Three random fields were assessed for each sample, and a single average was calculated for each animal and compartment. Similar methods were used to quantitate Mycn and Ki67 overlap.

2.3.10 Quantifying in situ intensity

The Color Threshold function in ImageJ was used to highlight areas of staining and to filter out background. The total signal area was then measured using the Analyze Particles function. For *Ptch2*, the total signal area was divided by the total number of tumor cells to obtain the average signal per cell. For *Mycn*, *Mycl* and *Myc*, the signal area was quantitated separately for the basal and suprabasal compartments.

2.3.11 Statistics

For comparisons between two groups, an unpaired t-test was performed to calculate statistical significance. A Wilcoxon rank sum test with continuity correction was used to calculate p values for non-parametric data depicted by box and whisker plot. For comparisons with greater than two groups, one-way ANOVA with posthoc test (Tukey's method) was performed. For beeswarm plots, statistical significance was calculated using a linear mixed model using the lme4, lmerTest and emmeans packages on R.

2.3.12 Data and Code Availability

WES data generated for this study are available through the NCBI Sequence Read Archive (BioProject: PRJNA782990).

Table 2-1: Key Resources Table for Chapter 2

REAGENTS or RESCOURCES	SOURCE	IDENTIFIER
Antibodies		
Rabbit anti-cleaved caspase-3	Cell Signaling	Cat # 9661
Chicken anti-K14	Biolegend	Cat # 906004
Mouse anti-Ki67	BD Biosciences	Cat # 550609
Rabbit anti-Ki67	Cell Signaling	Cat # 12202S
Goat anti-luciferase	Novus	Cat # NB100-1677SS
Rabbit anti-NICD	Cell Signaling	Cat # 4147P
Rabbit anti-N-Myc	Cell Signaling	Cat # D4B2Y
Mouse anti-p16	Invitrogen	Cat # 1E12E10
Rabbit anti-p21	Cell Signaling	Cat # 2947T
Rabbit anti-p53	Novocastra	Cat # NCL-p53-CM5p
Rabbit anti-smooth muscle actin	Cell Signaling	Cat # 19245T
Biological Samples		
Mouse tissue samples, obtained in accordance with guidelines established by the University of Michigan Unit for Laboratory Animal Medicine	This manuscript	Study protocol # PRO00010041
Human BCC samples, obtained with informed consent and approved by the Institutional Review Board at the University of Michigan Medical School	This manuscript, University of Michigan Departments of Dermatology and Pathology	Study protocol # HUM00042233, HUM00075822, HUM00051875
Chemicals, Peptides, and Recombinant Proteins		
Doxycycline chow (200 mg/kg)	BioServ Inc	Cat # S3888
Nair hair removal lotion	Nair	Cat # B001E6OAM8
Nuclear fast red	Sigma	Cat # N3020-100ML
Tamoxifen	Sigma	Cat # T5648-1G
X-Gal	Roche	Cat # 10651745001
Critical Commercial Assays		
DNeasy Blood & Tissue Kit	Qiagen	Cat # 69504
RNAscope 2.5 HD Reagent Kit-BROWN	ACD (RNAscope)	Cat # 322310
RNAscope 2.5 Pretreat Reagents-H202 and Protease Plus	ACD (RNAscope)	Cat # 322330
RNAscope Target Retrieval	ACD (RNAscope)	Cat # 322000
RNAscope Wash Buffer	ACD (RNAscope)	Cat # 310091
TSA Fluorescein Plus Kit	Akoya Biosciences	Cat # NEL741E001KT
Deposited Data		
WES data	This manuscript	BioProject: PRJNA782990
Experimental Models: Organisms/Strains		
Mouse: Gli1$^{tm3(cre/ERT2)Alj}$ (Gli1-Cre^{ERT2})	The Jackson Laboratory [24]	Cat # 007913
Mouse: Lrig1$^{tm1.1(cre/ERT2)Rjc}$ (Lrig1-Cre^{ERT2})	The Jackson Laboratory [25]	Cat # 018418
Mouse: Ptch1^{tm1Hahn} (Ptch1^{flox})	The Jackson Laboratory [26]	Cat # 012457
Mouse: Gt(ROSA)26Sor$^{tm1(Smo/EYFP)Amc}$/J (SmoM2)	The Jackson Laboratory [27]	Cat # 005130
Mouse: Notch1$^{tm2Rko/GridJ}$ (Notch1^{flox})	The Jackson Laboratory [28]	Cat # 007181
Mouse: Trp53^{tm1Brn} (p53^{flox})	The Jackson Laboratory [29]	Cat # 008462
Mouse: Gt(ROSA)26$^{Sortm1(rtTA,EGFP)Nagy}$	The Jackson Laboratory [30]; Laboratory of Dr. Anj Dlugosz	Cat # 005572
Mouse: TRE-MYCN/Luciferase	Laboratory of Dr. William Weiss [31]	N/A
Oligonucleotides		
In situ probe: mGli1	ACD (RNAscope)	Cat # 311001
In situ probe: mGli2	ACD (RNAscope)	Cat # 405771

In situ probe: mPtch2	ACD (RNAscope)	Cat # 435131
In situ probe: mMycn	ACD (RNAscope)	Cat # 477151
In situ probe: mMycl	ACD (RNAscope)	Cat # 552711
In situ probe: mMyc	ACD (RNAscope)	Cat # 413451
Software and Algorithms		
ImageJ	NIH	https://imagej.nih.gov/ij/
AxioVision, Version 4	Carl Zeiss	https://www.micro-shop.zeiss.com/en/us/
GraphPad Prism 7	GraphPad Prism Software	https://www.graphpad.com/scientific-software/prism/
Burrows-Wheeler Aligner	(32)	http://bio-bwa.sourceforge.net/
Picard	Broad Institute	https://broadinstitute.github.io/picard/
GATK	(33)	https://gatk.broadinstitute.org/hc/en-us
MuTect	(34)	https://software.broadinstitute.org/cancer/cga/mutect
Strelka	(35)	https://github.com/Illumina/strelka/blob/v2.9.x/docs/userGuide/README.md
Control-FREEC	(36)	http://boevalab.inf.ethz.ch/FREEC/
CNVKit	(37)	https://cnvkit.readthedocs.io/en/stable/
ANNOVAR	(38, 39)	https://annovar.openbioinformatics.org/en/latest/
Integrative Genomics Viewer (IGV)	(40)	https://software.broadinstitute.org/software/igv/

2.4 Results

2.4.1 Nascent BCC-like tumors driven by hallmark mutations fail to progress

We and others have previously demonstrated that microscopic BCC-like tumors form efficiently after *Ptch1* deletion in hair follicle and surface mechanosensory touch dome (TD) epithelia [41, 42]. To further assess the growth kinetics of these lesions, we analyzed mice expressing tamoxifen (TAM)-inducible Cre recombinase under the control of the *Gli1* promoter (*Gli1-CreERT2*), coupled with homozygous *Ptch1* floxed alleles (GP mice) [43, 44]. As we previously reported, 5 weeks after TAM administration in GP mice, numerous microscopic lesions arose from Gli1+ stem cells in the hair follicle and TD (**Figure 2-1A-C**). Hair follicle-associated tumors resembled nodular BCC, whereas TD-derived tumors possessed features reminiscent of infundibulocystic BCC and fibroepithelioma of Pinkus.

To examine the long-term fates of these nascent tumors, we collected serial biopsies up to 17 weeks post-TAM. Unexpectedly, we observed that hair follicle-associated lesions spontaneously regressed over time, leaving behind small residual tumor nests (**Figure 2-1A-B**). In no instance did we observe macroscopic tumors in any GP mice (**Figure 2-1A**). By contrast, TD-derived tumors neither progressed nor regressed between 12-17 weeks post-TAM, although we occasionally observed ~1 mm diameter papules that did not enlarge over time (**Figure 2-1C-D**). Macroscopic tumors failed to appear even when we followed GP mice up to 25 weeks post-TAM (**Figure 2-8A**).

To determine whether the lack of tumor progression is generalizable to lesions originating from other stem cell populations, we also targeted Lrig1+ hair follicle stem cells for *Ptch1* deletion (LP mice) [45]. Similar to above, we observed nascent microscopic lesions in LP mice, but no macroscopic tumors (**Figure 2-1E-F**). Finally, we assessed tumor formation following overexpression of a constitutively active form of Smo (SmoM2), targeted to either Gli1+ or Lrig1+ stem cells [46]. Again, abundant microscopic BCC-like tumors emerged, but no macroscopic tumors (**Figure 2-1G**). Altogether, these findings demonstrate that nascent tumors initiated by either loss of Ptch1 or gain of Smo fail to progress in the most widely studied models of BCC (**Figure 2-1H**).

2.4.2 Nascent BCCs become dormant despite constitutively elevated Hh signaling

Sporadic BCCs often arise in aged skin, which undergoes epidermal and dermal changes over time [47]. To better characterize our BCC model, we asked whether aging confers a

permissive environment for GP tumors to progress. We induced *Ptch1* deletion in young or older mice at 4 or 25 weeks of age, respectively, and assessed tumor kinetics relative to animals induced at 8 weeks of age, our standard starting point (**Figure 2-2A**). In all cases, we observed abundant microscopic tumors at 5 weeks post-TAM, followed by spontaneous regression of hair follicle-associated tumors at 12-17 weeks post-TAM (**Figure 2-2B-D**). As before, no macroscopic tumors emerged. These findings indicate that the relative age of the tumor (time after initiation), rather than the absolute age of the animal, likely determines regression kinetics in our system.

Since BCCs regress in response to pharmacological inhibition of Hh signaling [48], we next asked whether spontaneous tumor regression occurs due to the inability to maintain high level Hh signaling. To measure downstream pathway activity, we incorporated a Gli1-responsive *β-galactosidase* (LacZ) allele into GP mice and assessed LacZ activity. Alternatively, we quantitated mRNA *in situ* for the canonical Hh target gene, *Ptch2*. In both cases, we found that Hh pathway activity is maintained even in regressed residual tumors (**Figure 2-2E-F**).

Further characterization of regressing tumors revealed that proliferation is significantly reduced between 12-17 weeks post-TAM (**Figure 2-2E**) , concordant with previous findings in *Ptch1*-deficient skin lesions [49]. This reduction was observed in both hair follicle- and TD-derived tumors in GP mice (**Figure 2-2G-H**), as well as in hair follicle-derived tumors in LP and SmoM2 mice (**Figure 2-2I**, **Figure 2-8B-C**). Notably, regressed GP tumors were not apoptotic and did not express classic markers of senescence, such as p16 and p21 (**Figure 2-9A-B**). Interventions such as treating the skin with a phorbol ester tumor promoter failed to restore proliferation, while depilation caused hair follicles to enter the anagen growth phase without affecting neighboring regressed lesions (**Figure 2-9C-D**). These findings indicate that nascent tumors initiated by deletion of *Ptch1* eventually become suspended in a dormant state where cells are neither highly proliferative, apoptotic nor senescent—features that somewhat resemble those of dormant hair follicle stem cells.

2.4.3 Nascent tumors exhibit hair follicle progenitor-like organization and persist upon Notch1 deletion

Given the parallels between spontaneously regressed GP tumors and slow-cycling hair follicle stem cells, we next investigated whether, conversely, nascent proliferating tumors might

resemble growing hair follicles. Indeed, we previously reported that BCCs can possess two molecularly distinct cellular sub-compartments: peripheral basal layer cells with high Hh pathway activity, and interior suprabasal tumor cells with elevated Notch signaling, as assessed by staining for cleaved Notch1 intracellular domain (NICD) [50] (**Figure 2-3A**). Notably, these features are recapitulated in the normal growing hair follicle bulb, where basal layer matrix progenitor cells exhibit high Hh target gene expression and give rise to NICD+ suprabasal progeny (**Figure 2-3B-C**).

NOTCH1/2 are among the most frequently mutated genes in BCC, and we previously showed that loss of Notch1 enables tumors to persist when Hh signaling is inhibited pharmacologically [50]. To test whether Notch also modulates tumor dormancy, we generated GP mice harboring additional homozygous *Notch1* conditional deletion alleles (GPN1 mice) [51]. In contrast to GP mice, GPN1 animals developed extensive microscopic hair follicle-associated lesions that did not undergo spontaneous regression (**Figure 2-3D-E**). In spite of their increased persistence, however, these tumors still reduced their proliferation over time, which was again not reversible by phorbol ester treatment (**Figure 2-3F**, **Figure 2-10A**). Overall, these findings indicate that losing Notch1 promotes tumor persistence, but does not enable these lesions to escape dormancy. Thus, even after developing substantial microscopic tumor burdens which persisted up to 17 weeks post-TAM, GPN1 mice were largely devoid of macroscopic BCC-like tumors, with rare exceptions (**Figure 2-3G**, **Table 2-2**), which we will discuss in greater detail below.

2.4.4 Loss of p53 is not sufficient to drive BCC tumor progression

TP53 is also commonly mutated in BCC, and loss of *Trp53* promotes tumorigenesis in an irradiated model of BCC; however, the mechanism by which p53 modulates BCC progression remains unclear [52-54]. Indeed, our previous studies demonstrated that deleting *Trp53* neither affects initial tumor formation nor drug-induced regression [50]. To examine whether loss of p53 affects later stages of tumor progression, we first confirmed that p53 is highly expressed in basal layer cells in GP tumors, which again mimics the expression pattern seen in basal matrix progenitors in the normal growing hair follicle [55] (**Figure 2-4A-C**).

We next generated GP mice harboring homozygous *Trp53* conditional deletion alleles (GPP53 mice) [56], and observed that nearly all microscopic GPP53 lesions still underwent spontaneous regression (**Figure 2-4D-E**). As seen in GP and GPN1 mice, GPP53 tumors

similarly exhibited reduced proliferation over time (**Figure 2-4F**), and we confirmed that dormant regressed lesions deleted p53, as expected (**Figure 2-4D**). Along with our previously published data [50], these findings suggest that losing p53 does not affect tumor initiation, persistence, dormancy or drug-response. In contrast to GPN1 mice above, GPP53 animals harbored lower microscopic tumor burdens following spontaneous regression. Nonetheless, most GPP53 mice developed at least one macroscopic tumor between 12-17 weeks post-TAM (**Figure 2-4G**). Below, we explore the pathological and molecular features that distinguish these macroscopic tumors from failed microscopic lesions.

2.4.5 Macroscopic tumors vary histologically

Irradiated *Ptch1*-heterozygous mice have previously been reported to develop multiple types of skin tumors [53, 57]. We therefore assessed the histology of macroscopic tumors from GPP53 and GPN1 mice, and determined that most tumors can be classified into 3 categories (**Figure 2-5A**): Type 1 tumors most resembled human BCC and formed dense basaloid nests with peripheral palisading. Rare Type 2 tumors had myoepithelial features, such as expression of α smooth muscle actin (SMA). Finally, Type 3 tumors were comprised of numerous cell islands with stromal involvement, reminiscent of trichoblastoma. Whereas GPP53 mice mostly developed Type 1 tumors, GPN1 mice formed both Type 1 and Type 3 tumors, with the latter subtype predominating in mice aged beyond 20 weeks post-TAM. In GPP53 mice, Type 3 tumors displayed extensive Notch pathway activation (**Figure 2-5A**). The incidence and distribution of macroscopic tumor subtypes is summarized in **Table 2-2**. For all studies below, we focus exclusively on characterizing Type 1 BCC-like tumors.

2.4.6 Macroscopic tumors acquire downstream Hh pathway hyperactivation

What enables rare macroscopic tumors to "break through," when millions of other *Ptch1*-deleted cells in the skin fail to progress? Since the inability to maintain high level proliferation appears to be a common road block for nascent tumors arising in GP, LP, GPN1, GPP53 and SmoM2 mice, we reasoned that macroscopic tumors likely acquire mutations that confer sustained replicative ability. To identify these somatic changes, we performed whole exome sequencing (WES) on 16 macroscopic GPP53 tumors and 5 GPN1 tumors, along with matched normal control tissue.

Although overall mutational burdens varied widely among tumors, the dominant genomic alterations were somatic DNA copy number changes, with far fewer single nucleotide variations

and insertions/deletions (**Figure 2-11A-B, Supplemental Data S1**). In particular, we detected two recurrent amplifications: 7/16 GPP53 tumors acquired copy number gains in regions of Chromosome 1 encompassing *Gli2*, while 4/16 GPP53 tumors acquired gains in regions of Chromosome 10 encompassing *Gli1* (**Figure 2-5B-D**, **Figure 2-12A-B**). These amplifications were often accompanied by smaller copy number changes on the same chromosome, and notably, no tumor exhibited amplification of both *Gli1* and *Gli2*. Since these genes encode the key transcriptional mediators of Hh signaling, we next validated that GPP53 tumors with amplified Chromosome 1 possessed increased *Gli2* mRNA, whereas tumors with amplified Chromosome 10 had increased *Gli1* mRNA (**Figure 2-5E**). As expected, regressed microscopic lesions presumably lacking these mutations had lower levels of both transcripts and displayed less Hh pathway activation (**Figure 2-5E**). Overall, these findings are consistent with previous studies showing that 8% of human BCCs possess *GLI1*/*GLI2* amplifications [20], and that overexpression of either transcription factor induces BCC formation [58, 59]. Thus, a subset of *Ptch1*-deficient tumors likely overcome dormancy by independently acquiring the ability to hyperactivate downstream Hh signaling in our system.

2.4.7 Macroscopic tumors converge upon Mycn upregulation

Although we observed recurrent *Gli* amplifications, 5/16 macroscopic GPP53 tumors and 5/5 macroscopic GPN1 tumors did not possess either mutation (**Figure 2-12A**). Working from a list of 70 commonly mutated genes in BCC compiled by Villani et al. [60]; from previous studies [20, 21]; as well as from the Catalogue of Somatic Mutations in Cancer (COSMIC) database—we further noted that among the 5 GPP53 tumors without *Gli* amplification, 3 tumors had copy number gains in either *Yap1* or *Kif7*, or copy number loss of *Ptch2* (**Figure 2-12A-B**). These changes may potentially explain how 3/5 GPP53 tumors progressed to macroscopic disease, without amplifying *Gli* [61-64].

For the remaining tumors lacking these mutations, we decided to take a different tack to understand how they overcame dormancy. We reasoned that all Type 1 macroscopic tumors, regardless of mutational status, must share certain downstream outputs which set them apart from failed microscopic lesions. For instance, we confirmed that all GPP53 and GPN1 macroscopic tumors are highly proliferative (**Figure 2-6A**). We also determined that all Type 1 tumors have reduced Notch signaling (**Figure 2-6A**). Finally, we noted that all macroscopic

tumors, regardless of genotype, *Gli* mutation status or Hh pathway activity, possess high levels of Mycn (**Figure 2-6A**).

We next extended these analyses to human BCCs of different subtypes. Indeed, we observed high proliferation and reduced Notch in most tumors, although a subset possessed NICD+ cells in the suprabasal compartment, as we have previously noted [50] (**Figure 2-6B**). In addition, all tumors had increased MYCN, which was either uniformly high throughout the tumor or enriched at the basal periphery, as has also previously been reported (**Figure 2-6B**) [65, 66]. Altogether, we conclude that three characteristics—high proliferation, reduced Notch and high MYCN—are often seen in BCC. These features are also shared by all Type 1 macroscopic tumors in our system, irrespective of mutational status.

2.4.8 MYCN overexpression promotes tumor progression

MYCN amplification occurs in 12% of BCCs, while focal mutations that lead to protein stabilization have been detected in 30% of these tumors [20, 65]. As noted above, nascent GP lesions resemble growing hair follicles and consistent with this theme, we observed enriched Mycn protein and RNA in the basal layer of both early tumors and hair follicle matrix progenitors (**Figure 2-7A**, **Figure 2-13A-C**). In contrast, expression of other Myc family members (Myc, Mycl) was not as highly enriched in these compartments (**Figure 2-13A-C**). In GP tumors, cells with high Mycn are more likely to be proliferative (**Figure 2-7B-C**), suggesting a role in cell cycle regulation [67].

To directly test the role of Mycn in our system, we generated mice expressing *Gli1-CreERT2*, coupled with Cre-inducible reverse Tet transactivator (*rtTA*), and a bi-directional tetracycline-responsive element (*TRE*)-driven *MYCN/luciferase* (GT mice) [31] (**Figure 2-7D**). In this system, GT mice are first injected with TAM to activate *rtTA* expression, which subsequently drives *MYCN/luciferase* overexpression in the presence of doxycycline (DOXY). Following 12-20 weeks of continuous DOXY treatment, GT mice formed dysmorphic anagen hair follicles, but no tumors (**Figure 2-7E**).

Having validated this system, we next incorporated these genetic elements into our *Ptch1*-deficient model (GPT mice). Tumors were initiated by TAM and allowed to grow for 5 weeks, before mice were shifted onto DOXY-chow to activate *MYCN* expression for an additional 12 weeks. We noted that transgene expression was localized primarily to the tumor suprabasal compartment (**Figure 2-7F-G**), which may either reflect biased *TRE* promoter

activity or inward movement of transgene-expressing basal layer tumor cells. Regardless, *MYCN* overexpression induced massive proliferation in nascent tumors (**Figure 2-7F**). Strikingly, we also observed that Notch activation was re-localized away from the tumor suprabasal compartment, to cells residing just inside of the basal layer, possibly reflecting early suprabasal cells that express lower levels of the transgene (**Figure 2-7G**). These results indicate that *MYCN* overexpression is sufficient to promote key features of tumor progression—increased proliferation and reduced Notch—that we observed in human BCC and mouse Type 1 BCC-like tumors.

Despite these findings, most GPT mice did not form macroscopic tumors, likely because *MYCN* overexpression caused increased apoptosis (**Figure 2-7F**). In 3/15 GPT mice, however, we observed small palpable tumors, which contained transgene-expressing basaloid cells (**Figure 2-7H**). We did not allow these lesions to continue growing due to frequent gastrointestinal-related morbidity in GPT mice. Similar to GPN1 and GPP53 macroscopic tumors, these rare GPT tumors likely also acquired additional somatic mutations that enabled them to progress. Collectively, our findings argue that loss of Ptch1 by itself is not sufficient for full BCC progression, and that secondary mutations—resulting in loss of Notch1 or p53, increased Gli, and/or gain of Mycn—contribute functionally to the critical transition from microscopic to macroscopic disease.

2.5 Discussion

Our skin is the most highly mutated organ, and mutations in cancer-associated genes such as *NOTCH1/2*, *TP53* and *RAS* are frequently detected in photoaged epithelia [1-3, 7]. Previously, we and others have observed that mutant cells with aberrant Notch1 or p53 can persist long-term in the epidermis without forming tumors (**Figure 2-13D-E**, **Table 2-3**) [4, 68]. Targeted expression of oncogenic Kras in hair follicle stem cells also causes only temporary tissue disruption that normalizes over time [5, 6]. Along a similar vein and consistent with previous findings [49], we report here that loss of Ptch1 or gain of Smo, both hallmark mutations in BCC, induces nascent tumors that do not progress.

Given the high failure rate for tumor-initiated cells in the skin, it is likely that both cell-intrinsic and -extrinsic factors suppress tumor progression. Indeed, an idiosyncratic feature of the skin is the periodic phases of hair growth and regression, with the anagen growth phase favoring tumor formation and the telogen resting phase associated with tumor regression [6, 57, 69-

[71]. In our GP model, nascent BCC-like tumors share some resemblance to growing hair follicles, including basal layer enrichment for multiple factors—high Hh pathway activation, proliferation, p53 and Mycn—as well as suprabasal activation of Notch signaling (**Figure 2-3C**). Thus, it is conceivable that early tumor growth and spontaneous regression are linked to the hair cycle. However, since regressed tumors in our model remain dormant even during subsequent anagen, other factors likely cause tumor exhaustion over time.

In mice, the absence of macroscopic BCCs has been a major short-coming of both the conditional *Ptch1*-deletion and *SmoM2*-overexpression models, confirming that tumors do not progress regardless of how upstream Hh signaling becomes activated or which Cre driver is utilized [41, 46, 52, 72-74]. Indeed, previous studies have shown that nascent BCC-like tumors induced by non-targeted *Ptch1* deletion similarly regress due to macrophage-induced tumor differentiation [49]. During postnatal brain development, *Ptch1*-heterozygous mice also exhibit transient hyperplasia in the external granular layer, a site of medulloblastoma formation, that subsequently regresses [75]. These data suggest that Hh-activated cells likely encounter steep obstacles to tumor progression across multiple organ systems.

While our findings in mice indicate that Ptch1 loss alone is insufficient for inducing macroscopic tumors, Gorlin patients can develop numerous BCCs, seemingly arguing that loss of heterozygosity of a single tumor suppressor, in most cases *PTCH1*, can lead to palpable tumors. However, although the average mutational burden in Gorlin BCCs is lower than in sporadic BCCs [19, 76], the mutational load in Gorlin tumors is still higher than that of many internal tumors. In addition, *TP53* mutations are present in ~40% of Gorlin BCCs, similar to sporadic tumors [76]. Finally, Gorlin BCCs can manifest a variety of histologic subtypes [77], and Gorlin patients can also develop basaloid follicular hamartoma (BFH), a benign hair follicle tumor [78-81]. While the connection between BFH and BCC remains unclear, some have speculated that these neoplasms are variations of the same disease [78]. Indeed, previous studies have shown that downstream Hh signaling strength can modulate BFH versus BCC tumor phenotype in mice [71, 74]. Altogether, these data suggest that secondary somatic mutations likely play functional roles in modulating tumor phenotype in Gorlin patients, possibly during the transition from BFH-like lesions to BCC.

In contrast to *Ptch1*-conditional mice, *Ptch1*-heterozygous animals form macroscopic BCCs following irradiation, but how these tumors progress remains unknown [52, 82, 83].

Transgenic overexpression of either *GLI1* or *Gli2* from an exogenous promoter also induces macroscopic BCC-like tumors [58, 59]. While these studies demonstrate that high level downstream Hh pathway activity can induce tumorigenesis, *GLI* amplification is not regarded as a primary driver of human BCC. Indeed, human BCCs possess canonical mutations in upstream Hh pathway components, even when *GLI* amplifications are detected [20]. This suggests that constitutive activation of upstream Hh signaling, mediated by primary cilia, may be critical for unlocking the full potential of secondary mutations that activate downstream components of the pathway. In line with this, GPP53 tumors in our study acquired *Gli* amplifications spontaneously, without additional experimental manipulation, again arguing that *Ptch1*-deficient lesions must hyperactivate both upstream and downstream Hh signaling in order to progress.

It is important to note that the prevalence of *Gli* amplification in our GPP53 model is higher than in human BCCs, where analogous amplifications are seen in 8% of tumors and may drive resistance to SMO antagonists [18-20, 84]. Since our mice are not exposed to UV, this likely affects the spectrum of mutations that occurs in our models. Apart from direct *Gli* amplification, there are likely many ways by which BCCs can hyperactivate downstream Hh signaling. For instance, Gli activity can be enhanced by aPKC, TGFβ and AP-1 [85, 86], while the PI3K/Akt and EGF pathways can cooperate with canonical Hh signaling to promote downstream activity [87-89].

Regardless of *Gli* amplification status, all Type 1 macroscopic tumors upregulated Mycn, which plays critical roles in many tumors, including nervous system cancers, prostate cancer and retinoblastoma [90, 91]. We further demonstrated that *MYCN* overexpression induces certain features of tumor progression, including increased proliferation and reduced differentiation. Notably, *Mycn* is a downstream target of Hh signaling [16, 92] (**Figure 2-13F**), yet this gene is still frequently mutated in BCC [20, 65]. This further supports the view that neither loss of Ptch1 nor gain of Smo is sufficient for tumor progression. Rather, mutations that augment MYCN levels may provide a secondary boost for tumors to sustain high level proliferation while limiting differentiation. Collectively, these data indicate that MYCN is likely situated at a critical nexus for driving BCC progression and possibly drug resistance.

In summary, by utilizing BCC models that largely fail to progress, we identify genetic factors that enable rare tumors to succeed. Our findings suggest that BCCs arise through a step-wise process guided by the acquisition of somatic secondary mutations. Activation of upstream Hh signaling, via loss of Ptch1 or gain of Smo, initiates nascent tumors that eventually regress

and become dormant unless additional mutations are acquired. Concomitant loss of Notch1 prevents tumor regression, and loss of p53 likely increases genomic instability; however, neither is sufficient for macroscopic tumors to form. Ultimately, tumor-initiated cells must acquire additional changes that either directly or indirectly cause exuberant downstream Hh pathway activation in order to progress. These findings may explain why some BCCs persist after pharmacological inhibition of upstream Hh signaling, while highlighting the possibility that essential downstream factors such as MYCN may represent viable targets for therapy.

2.6 Limitations of the Study

While our study suggests a role for secondary mutations in driving BCC progression, mouse BCC-like tumors likely do not recapitulate the full panoply of mutations seen in human BCC, since mice are not typically exposed to UV radiation. Thus, other genetic and epigenetic changes may contribute to the progression of human tumors. Mutations within intergenic regions of the chromosome are not detected by WES, and may also affect tumor progression in our system. While all BCC-like tumors in our study exhibited increased Mycn, it remains unclear how this occurs in tumors lacking *Gli* amplification. Aside from Hh signaling, other pathways such as PI3K/Akt have been reported to modulate Mycn expression or stabilization [(93)]. Loss of *Trp53* may also be necessary for over-riding cellular controls that guard against excessive Mycn, leading to cell death. Finally, the mechanisms underlying tumor dormancy and spontaneous regression remain unclear. Given the parallels between nascent BCC formation and hair follicle regeneration, a deeper understanding into how hair follicles normally develop, cycle and regress may inspire additional novel insights into the biology of these tumors.

2.7 Acknowledgements

We are grateful to Dr. S. X. Atwood (UC Irvine) and Dr. J. T. Seykora (University of Pennsylvania) for helpful discussions; Dr. W. A. Weiss (UCSF) for sharing mice; and Linguo Hao (Novogene) for project management. S.Y.W. acknowledges the support of the Leo Foundation (LF18017); the American Cancer Society; the Donald & Patricia Roof Fund for Skin Cancer Research; and the NIH (R21CA209166 and R56AR075638). K.G.T. acknowledges the support of the NIH (F31CA254080). The authors also acknowledge support from the UM Skin Biology and Disease Resource-based Center (P30AR075043) and NCI Cancer Center Support Grant (P30CA046592).

2.8 Figures

Figure 2-1: Microscopic tumors initiated by activation of upstream Hh signaling fail to progress

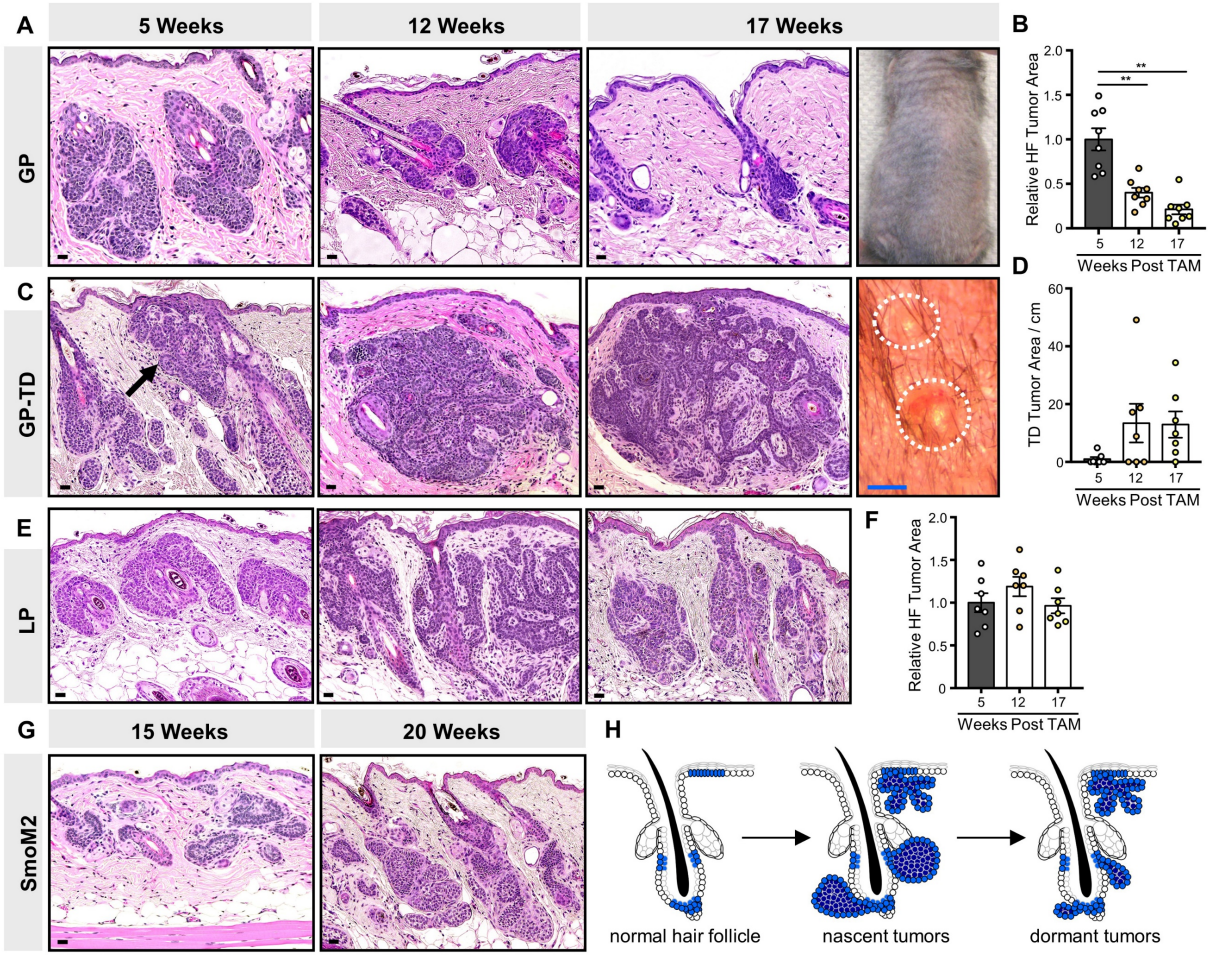

A. Histology of hair follicle (HF)-associated GP tumors, 5-17 weeks post-TAM. Right photo, shaved dorsal skin devoid of palpable tumors, 17 weeks post-TAM.
B. Quantitation of HF-associated tumors.
C. Histology of touch dome (TD)-derived GP tumors (arrow), 5-17 weeks post-TAM. Right photo, view of small TD papules, ~1 mm diameter.
D. Quantitation of TD-derived tumor area, in arbitrary pixel units per cm.
E. Histology of HF-derived LP tumors, 5-17 weeks post-TAM.
F. Quantitation of LP tumors.
G. Histology of microscopic HF-associated SmoM2 tumors arising from Lrig1+ stem cells (left, 15 weeks post-TAM) or Gli1+ stem cells (right, 20 weeks post-TAM)/
H. Schematic of GP tumor kinetics.

Data are represented as mean ± SEM, with significance calculated by one-way ANOVA. **, $p < 0.01$. Scale bar, 50 μm. Blue scale bar, 1 mm.

Figure 2-2: Microscopic tumors exhibit reduced proliferation over time

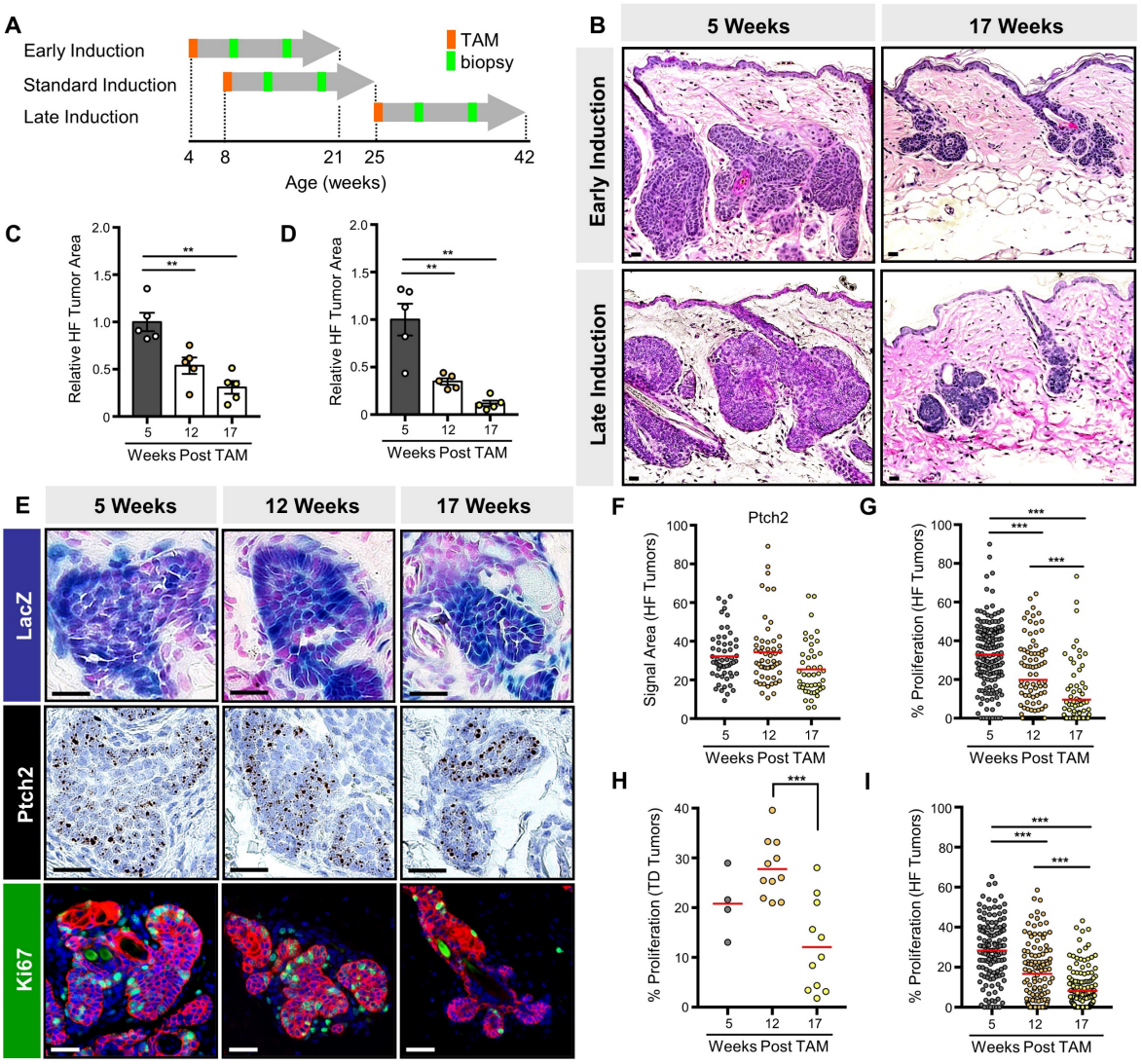

A. Schematic for TAM induction and skin biopsy in GP mice. Mice were also biopsied at the end of the experiment.
B. GP tumors regress by 17 weeks post-TAM, regardless of induction scheme.
C. Quantitation of tumor area in early-induced GP mice.
D. Same as (C), but for late-induced GP mice.
E. GP tumors maintain elevated Hh signaling, as assessed by LacZ (top panels) and *Ptch2* mRNA (middle panels), but reduce their proliferation over time, as assessed by Ki67 (green, lower panels). Red, Keratin 14 (K14).
F. Quantitation for *Ptch2* in HF-associated GP tumors.
G. Quantitation of proliferation in HF-associated GP tumors.
H. Same as (G), but for touch dome-derived GP tumors.
I. Quantitation of proliferation in LP tumors. For E-I, analysis was performed on tumors arising from the standard induction scheme.

Data are represented as mean ± SEM, with significance calculated by one-way ANOVA. Significance for beeswarm plots was calculated using a linear mixed model. **, $p < 0.01$; ***, $p < 0.001$. Scale bar, 50 μm.

Figure 2-3: *Notch1*-deficient microscopic tumors do not undergo spontaneous regression

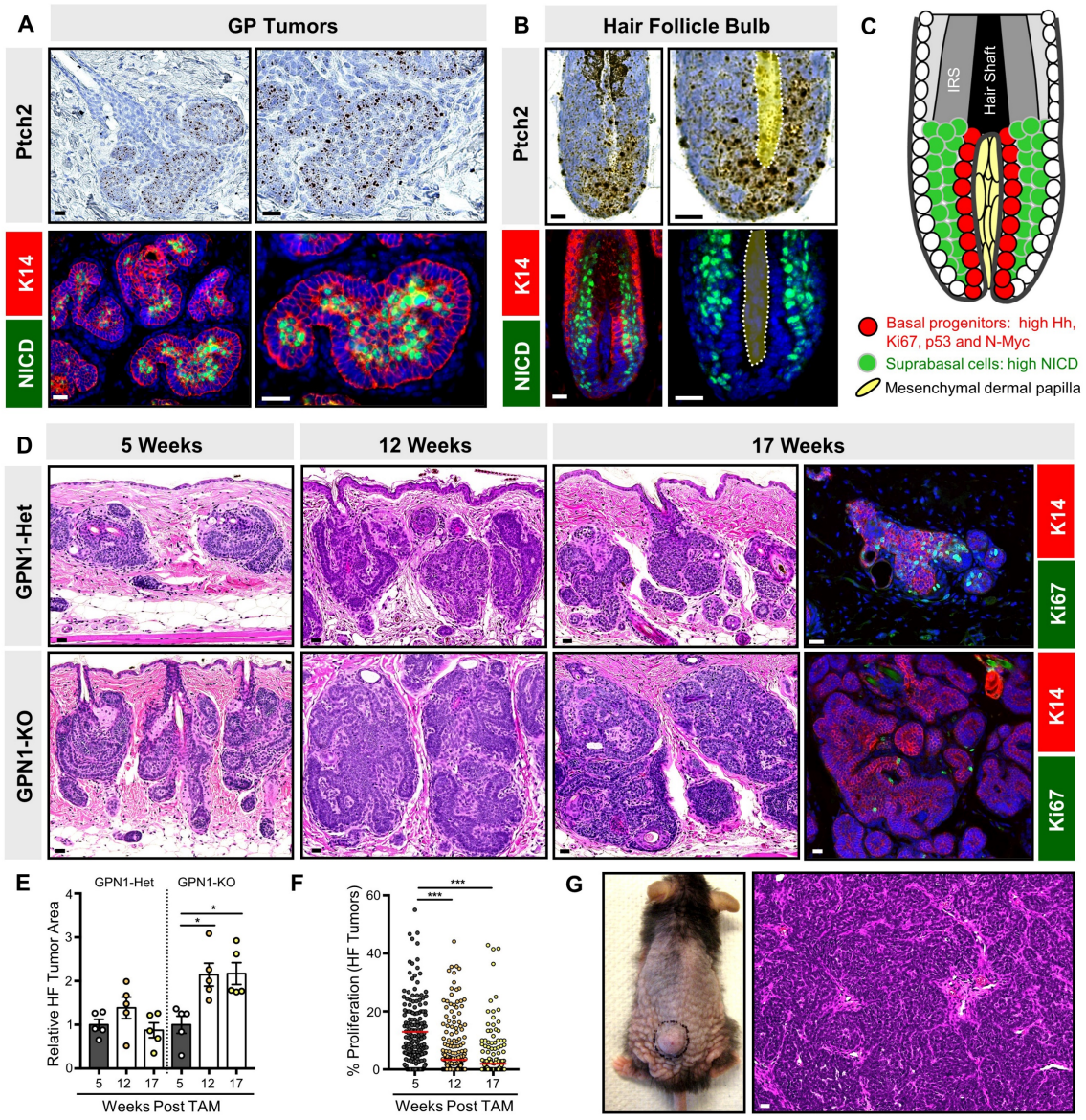

A. GP tumors have elevated Hh target genes, as assessed by *Ptch2* mRNA, in peripheral basal cells (top panels) and high NICD (green) in interior suprabasal cells (lower panels). Red, Keratin 14 (K14).

B. In the growing anagen hair follicle, basal matrix progenitor cells directly abutting the dermal papilla (yellow, dotted) express high *Ptch2* (top panels), whereas their suprabasal progeny express high NICD (green, bottom panels).

C. Schematic for basal progenitors (red) and suprabasal progeny (green) in the hair follicle bulb.

D. Histology of HF-derived GP tumors that are either *Notch1*-heterozygous (GPN1-Het) or -deleted (GPN1-KO), 5-17 weeks post-TAM. Right panels, tumor proliferation, as assessed by Ki67 (green), 17 weeks post-TAM.

E. Quantitaton of GPN1-Het and GPN1-KO tumor area.

F. Quantitation of GPN1-KO tumor proliferation.

G. Photo and histology of GPN1-KO macroscopic tumor.

Data are represented as mean ± SEM, with significance calculated by one-way ANOVA. Significance for beeswarm plots was calculated using a linear mixed model. *, $p < 0.05$; ***, $p < 0.001$. Scale bar, 50 μm.

Figure 2-4: *p53*-deficient microscopic tumors largely do not progress

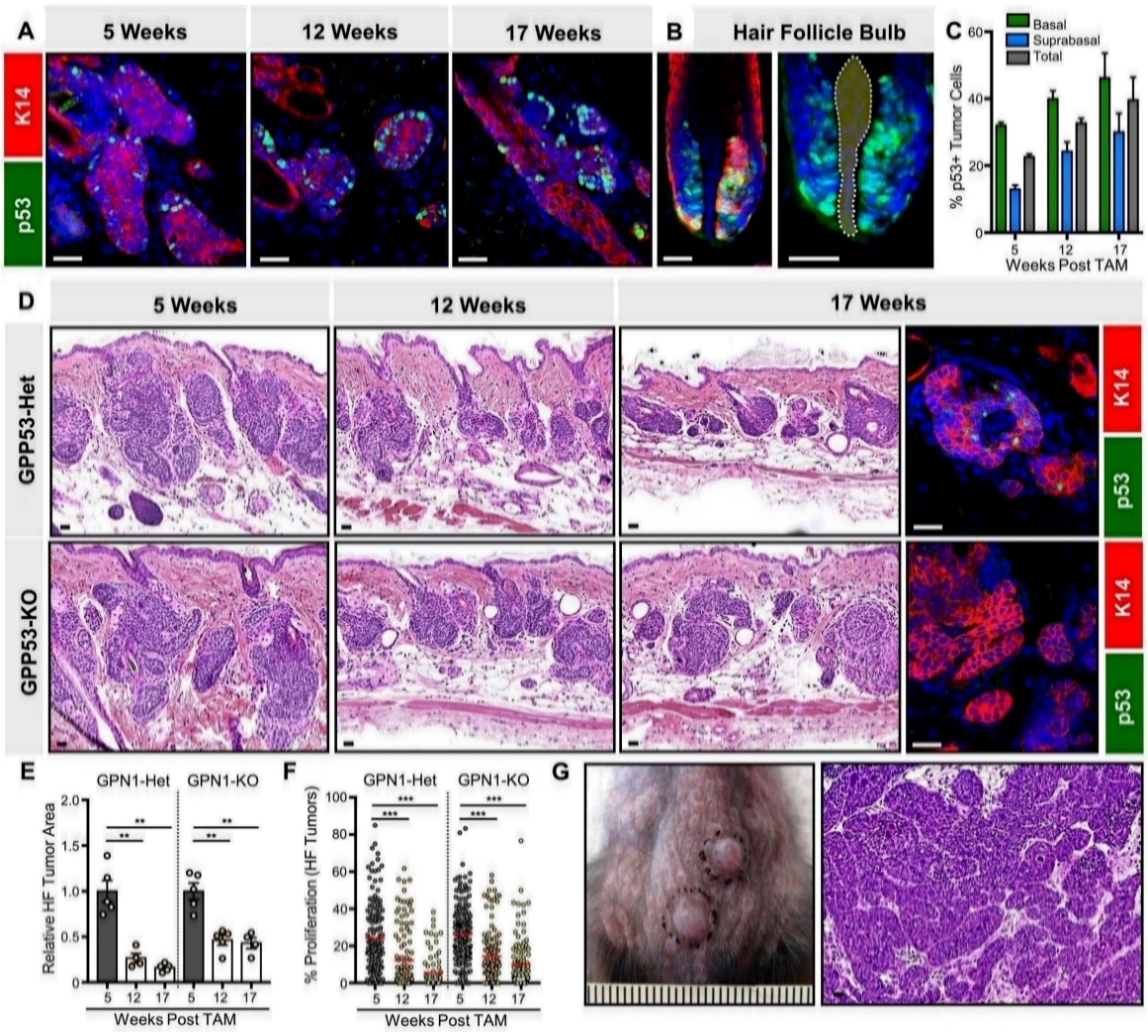

A. Peripheral basal tumor cells express p53 (green) in GP mice, 5-17 weeks post-TAM.
B. Basal matrix progenitors directly abutting the dermal papilla (dotted) also express p53 (green) in the growing hair follicle.
C. Quantitation for p53 in GP basal and suprabasal tumor compartments, 5-17 weeks post-TAM.
D. Histology of HF-derived GP tumors that are either *p53*-heterozygous (GPP53-Het) or -deleted (GPP53-KO), 5-17 weeks post-TAM. Right panels, validation of p53 loss (green) in GPP53-KO tumors, 17 weeks post-TAM.
E. Quantitation of GPP53-Het and GPP53-KO tumor area.
F. Quantitation of GPP53-Het and GPP53-KO tumor proliferation.
G. Photo and histology of GPP53-KO macroscopic tumors.

Data are represented as mean ± SEM, with significance calculated by one-way ANOVA. Significance for beeswarm plots was calculated using a linear mixed model. **, $p < 0.01$; ***, $p < 0.001$. Scale bar, 50 μm. Ruler marks, 1 mm.

Figure 2-5: Characterization of GPP53 and GPN1 macroscopic tumors

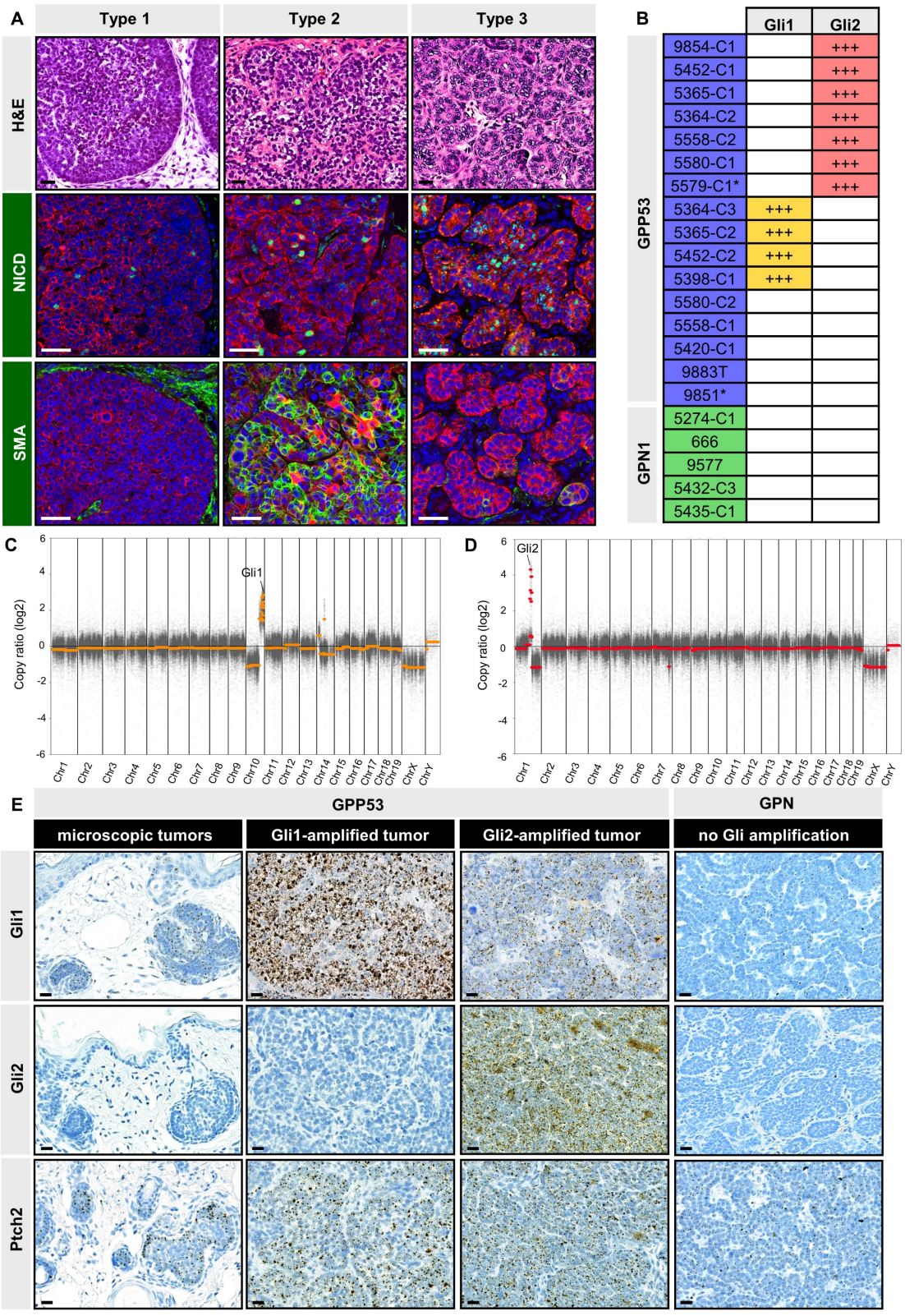

A. Histologic classification of macroscopic tumors (top panel), and immunohistochemistry for NICD (green, middle panels) and α smooth muscle actin (SMA) (green, lower panels). Red, K14 staining. All examples shown are from GPP53 mice.
B. Table showing tumors with somatic *Gli1* or *Gli2* copy number gains (+++, amplified). Asterisk, GPP53-Het tumor.
C. Representative DNA copy number plot of a GPP53 tumor that amplified a region of Chromosome 10 containing *Gli1*.
D. Same as (C), but of a different GPP53 tumor that amplified a region of Chromosome 1 containing *Gli2*.
E. mRNA *in situ* staining for *Gli1* (top panels), *Gli2* (middle panels) and *Ptch2* (lower panels) in GPP53 tumors (microscopic, *Gli1*- or *Gli2*-amplified) and in macroscopic GPN1 tumors. Scale bar, 50 μm.

Figure 2-6: Macroscopic GPP53 and GPN1 tumors share common features with human BCCs

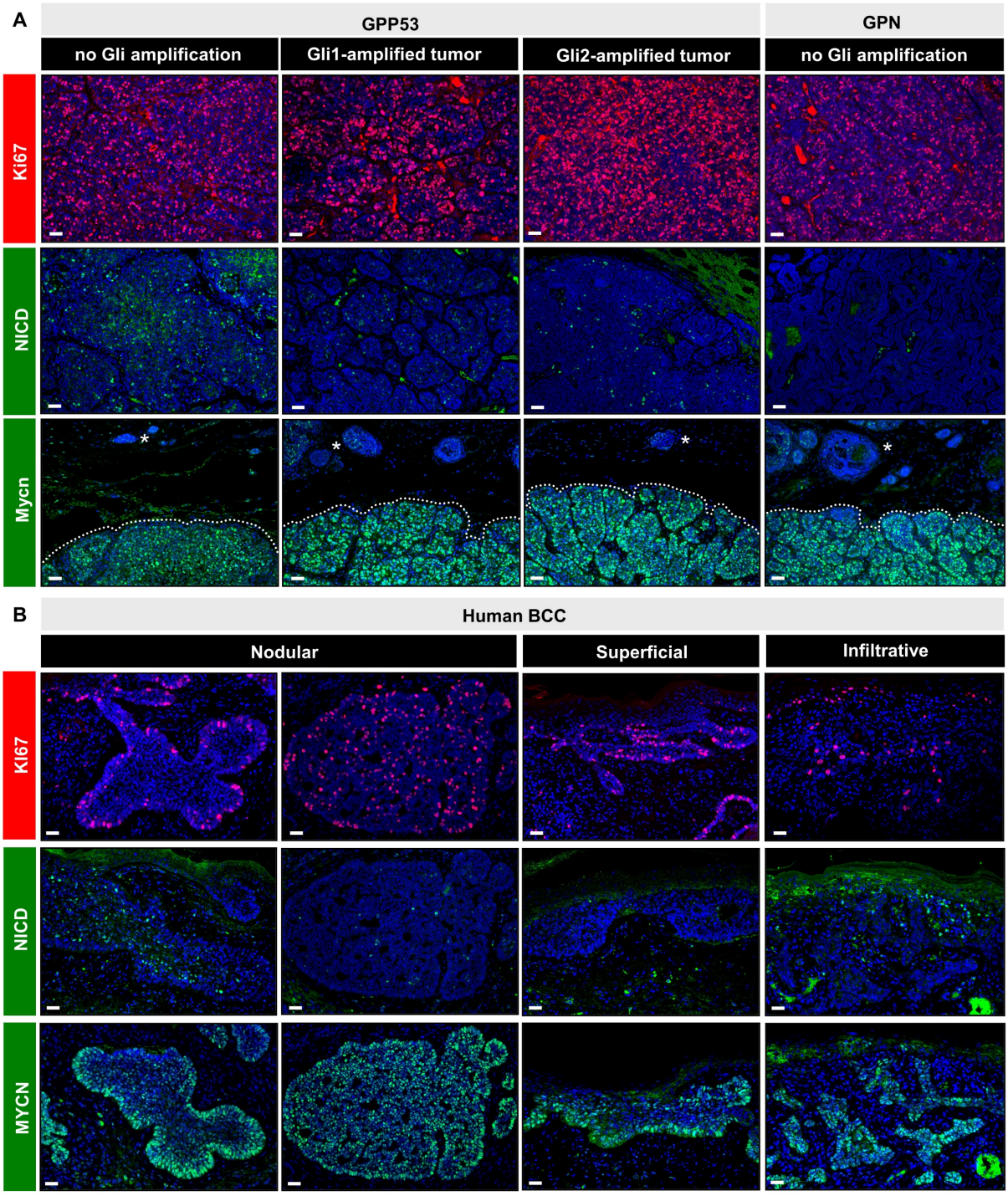

A. Immunohistochemistry for Ki67 (red, top panels), NICD (green, middle panels) and Mycn (green, lower panels) in GPP53 tumors, sub-divided by *Gli* amplification status (non-amplified, *Gli1*-amplified or *Gli2*-amplified), and in macroscopic GPN1 tumors lacking *Gli* amplification. Regardless of genotype, all macroscopic tumors express higher levels of Mycn relative to adjacent microscopic lesions (asterisks).

B. Same markers as in (A), probing human BCCs sub-divided by histological subtype. Two representative examples of nodular BCCs with variable marker expression are shown. Scale bar, 50 μm.

Figure 2-7: *MYCN* overexpression promotes tumor progression

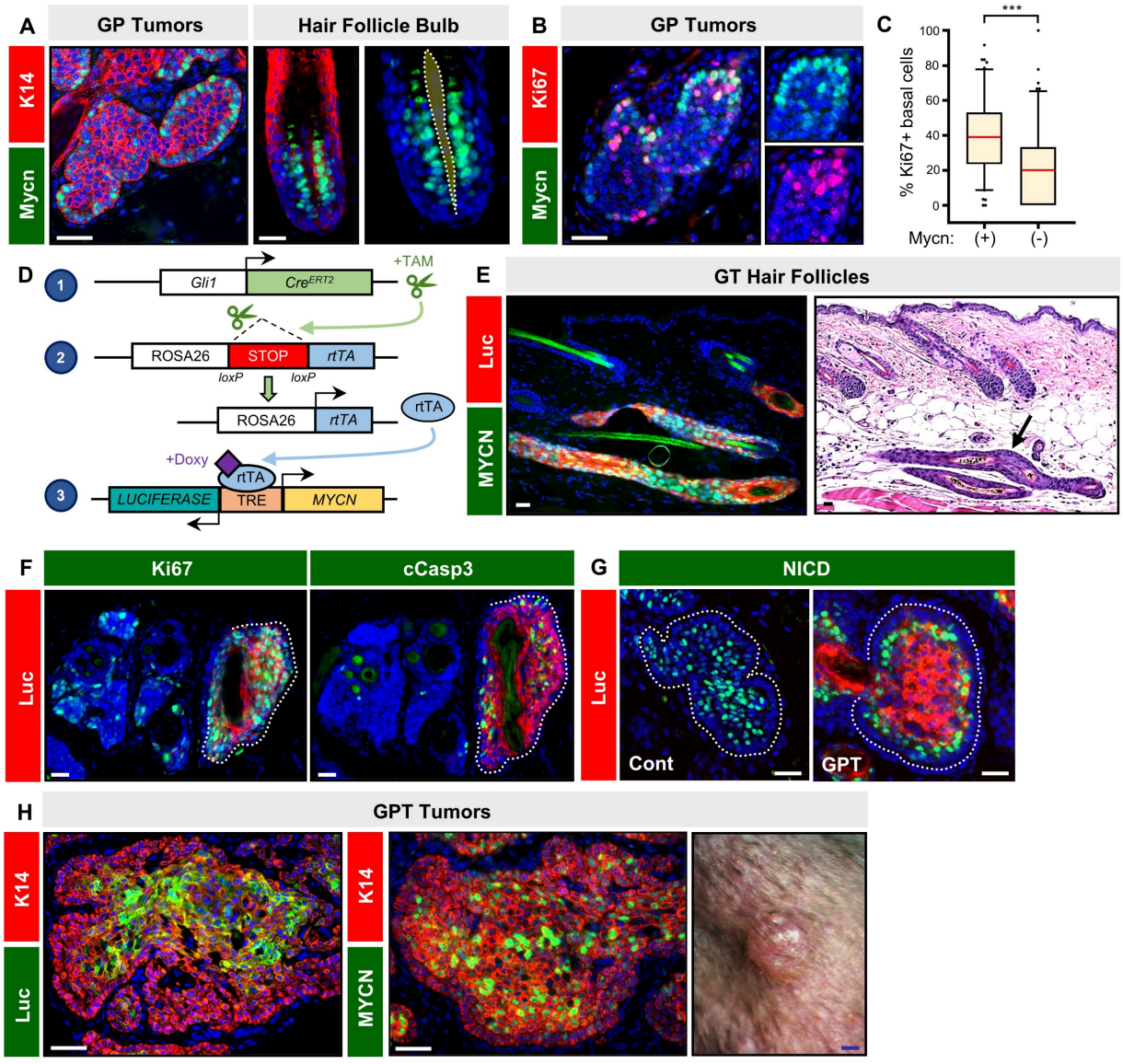

A. Peripheral basal tumor cells and basal matrix progenitors in anagen hair follicles express Mycn (green). Dotted region, mesenchymal dermal papilla.
B. Co-localization of Mycn (green) and Ki67 (red) in microscopic GP tumor, 5 weeks post-TAM.
C. Quantitation showing that Mycn+ basal tumor cells are more likely to be proliferative.
D. Schematic for *MYCN*/*Luciferase* overexpression system.
E. Histology of dysmorphic anagen hair follicles (arrow) expressing MYCN (green) and Luciferase (red) in GT mice.
F. Microscopic GPT tumors expressing *MYCN*/*Luciferase* (red, dotted) display increased Ki67 (green, left panel) and cleaved Caspase 3 (green, right panel).
G. Microscopic GP tumors possess extensive suprabasal NICD expression (left panel, green), whereas GPT tumors expressing *MYCN*/*Luciferase* (right panel, red) re-localize NICD to suprabasal tumor cells just inside of the basal layer.
H. Immunohistochemistry showing expression of Luciferase (green, left photo) and exogenous MYCN/endogenous Mycn (green, middle photo) in macroscopic GPT tumor (right photo).

p-values were calculated by a Wilcoxon rank sum test with continuity correction. ***, $p < 0.001$. Scale bar, 50 μm. Blue scale bar, 1 mm.

Figure 2-8: Tumors arising in GP and SmoM2 mice fail to progress.

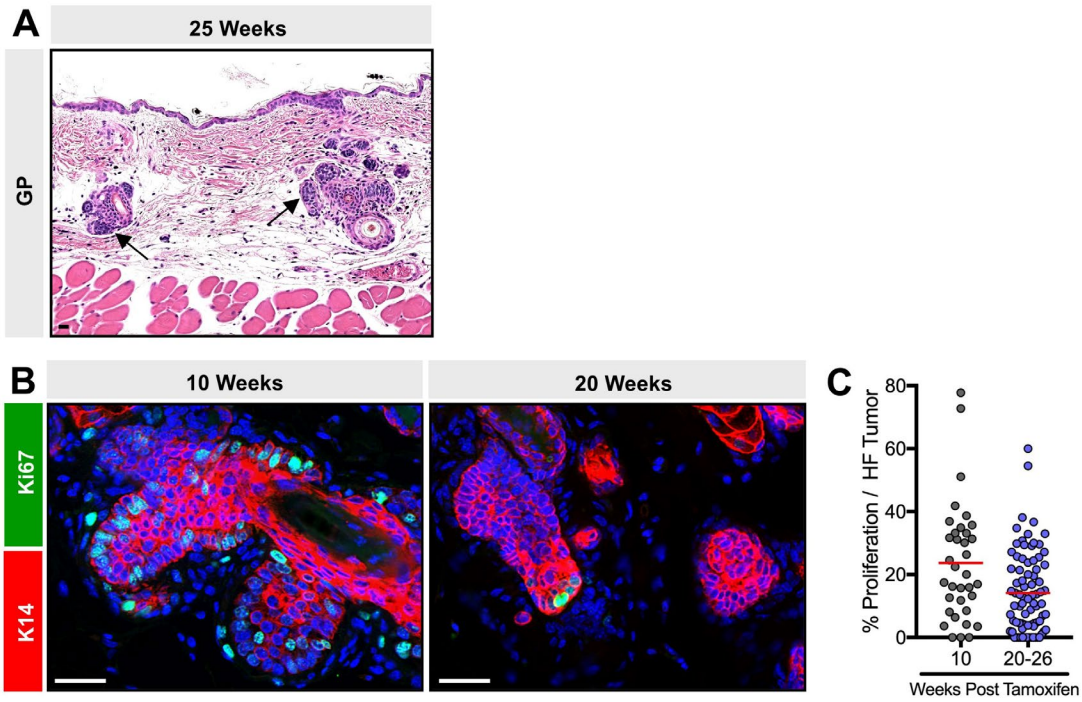

A. Histology of microscopic hair follicle (HF)-associated GP tumors (arrows), 25 weeks post-TAM.
B. HF-associated SmoM2 tumors exhibit reduced proliferation over time, as assessed by Ki67 (green).
C. Quantitation of proliferation in HF-associated SmoM2 tumors.

Significance for beeswarm plot was calculated using a linear mixed model ($p = 0.02$). Scale bar, 50 µm.

Figure 2-9: Dormant GP tumors do not progress in response to phorbol ester treatment or depilation.

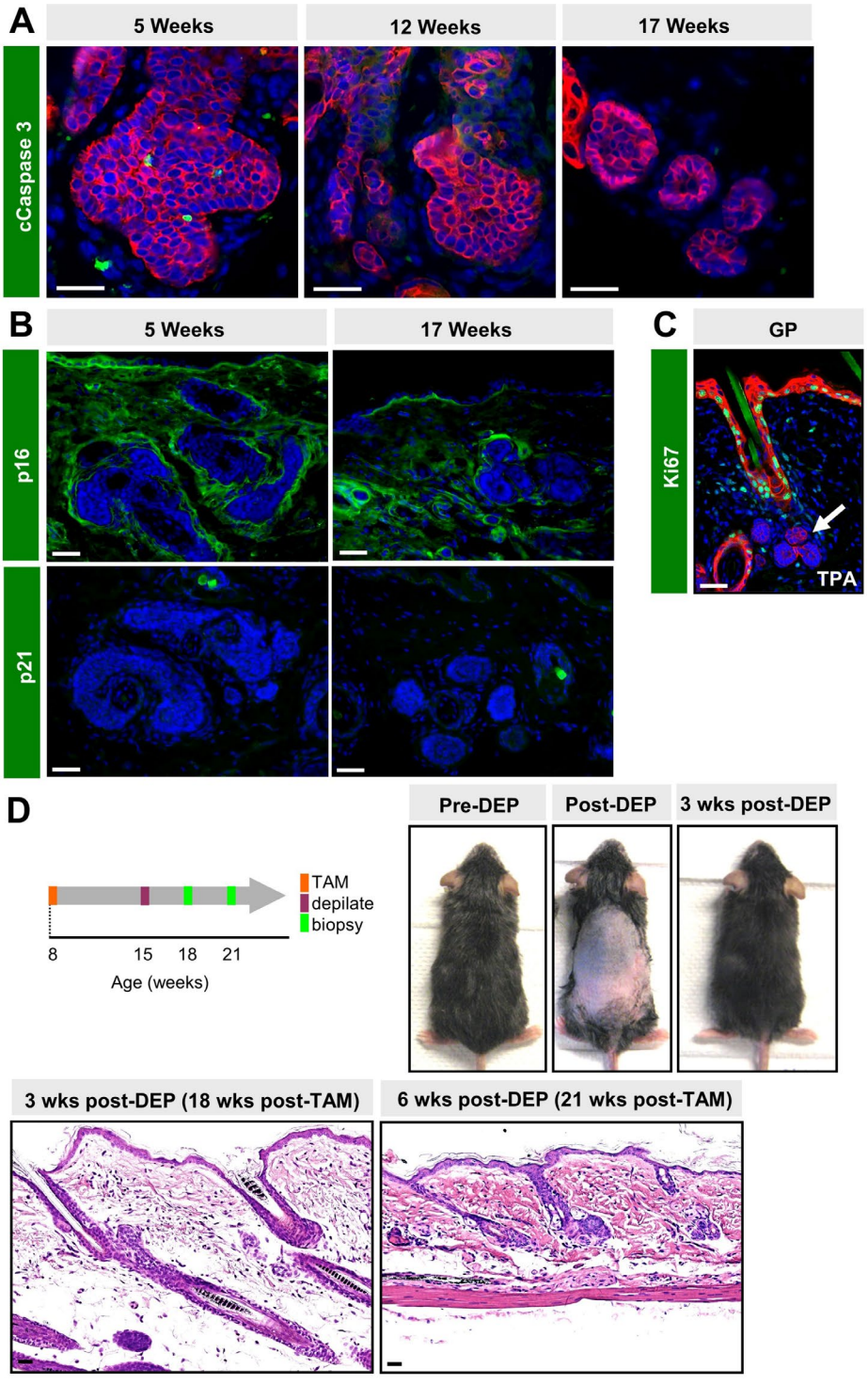

A. Staining for cleaved Caspase 3 (green) in GP tumors, 5-17 weeks post-TAM. Red, K14.

B. Lack of staining for senescence markers p16 (green, top) and p21 (green, bottom) in GP tumors, 5 and 17 weeks post-TAM.
C. TPA treatment does not induce proliferation, as assessed by Ki67 (green) in GP tumors (arrow).
D. Schematic for depilation and skin biopsy in GP mice. Mice were also biopsied at the end of the experiment. Right, photos showing dorsal skin from GP mice, pre- and post-depilation (DEP). Bottom photos, histology of GP mice, 3-6 weeks post-depilation. Scale bar, 50 μm.

Figure 2-10: Phorbol ester treatment does not restore proliferation in GPN1 tumors.

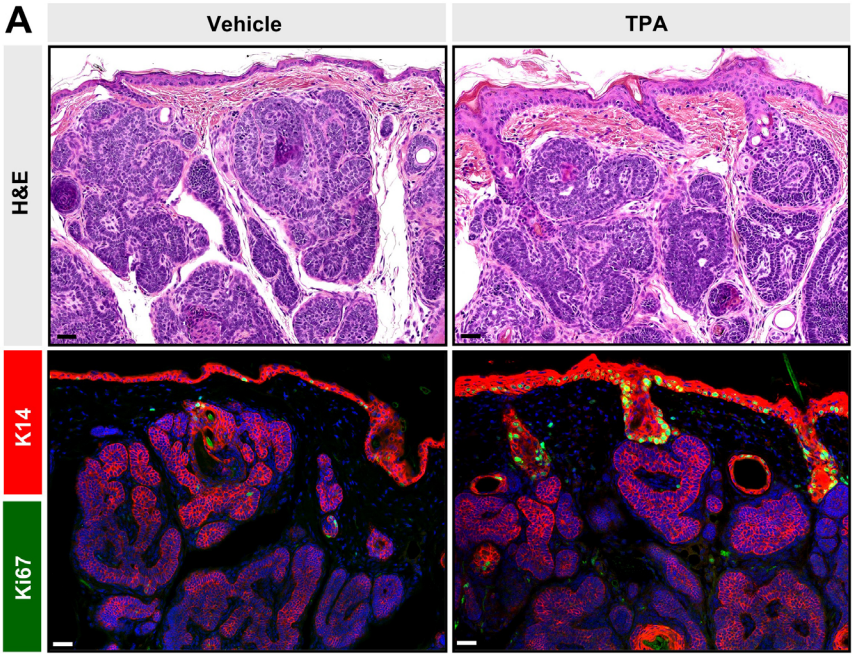

A. Top, histology of vehicle- and TPA-treated GPN1-KO tumors. Bottom, proliferation, as assessed by Ki67 (green), is not restored in GPN1 tumors treated with TPA, even though elevated proliferation is seen in the interfollicular epidermis and upper hair follicle. Scale bar, 50 μm.

Figure 2-11: Summary of genomic alterations in GPP53 and GPN1 macroscopic tumors.

A

		Tumor Code	CNV	SNV	InDel
GPP53	9854-C1	C1_9854	116	10	0
	5452-C1	A2_1	294	5	1
	5365-C1	A5_1	182	10	0
	5364-C2	A4_2	304	4	0
	5558-C2	A58_2	512	3	0
	5580-C1	A80_C1	191	9	2
	5579-C1*	A79_1	151	8	2
	5364-C3	A4_3	503	6	1
	5365-C2	A5_2	335	6	0
	5452-C2	A2_2	510	7	0
	5398-C1	A8_1	554	5	3
	5580-C2	A80_C2	77	5	3
	5558-C1	A58_1	870	3	0
	5420-C1	A20_1	239	3	0
	9883T	A83_1	72	5	0
	9851*	C1_9851	37	3	0
GPN1	5274-C1	A74_1	135	10	0
	666	C1_666	36	6	3
	9577	C1_9577	76	7	0
	5432-C3	A32_3	55	4	0
	5435-C1	A35_1	39	7	1

B

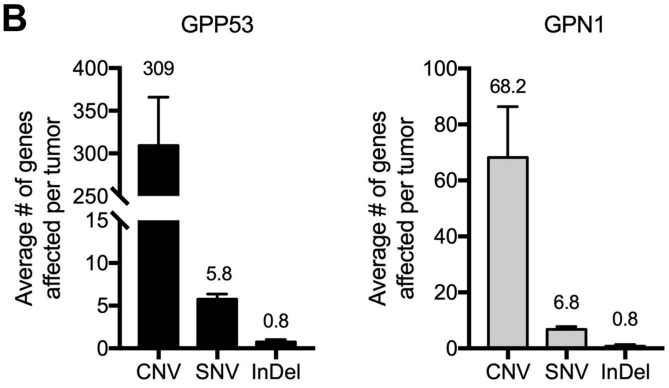

A. Table indicating the number of genes affected by different classes of somatic DNA mutations for each tumor analyzed by WES: copy number variation (CNV), single nucleotide variation (SNV) and insertion/deletion (InDel). Asterisk, GPP53-Het tumor.

B. Average number of genes affected by CNVs, SNVs and InDels in GPP53 and GPN1 macroscopic tumors.

Figure 2-12:Summary of somatic CNVs in macroscopic tumors

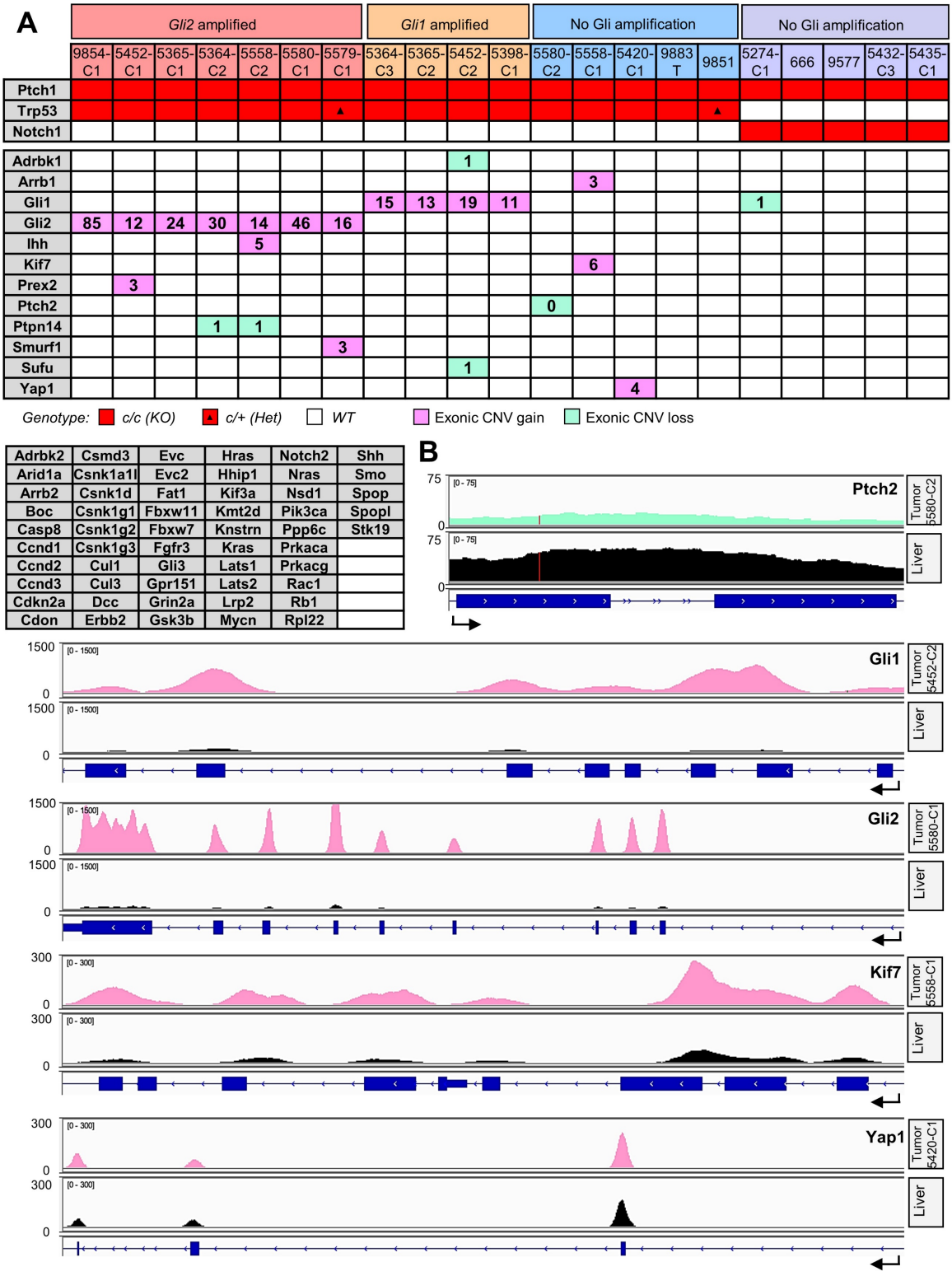

A. List of 70 commonly mutated genes in BCC (gray), and table showing CNVs affecting these genes across 16 GPP53 and 5 GPN1 macroscopic tumors. Bottom table is the remaining list of genes that were not found to be mutated in any of the 21 tumors.

B. Visualization of WES traces for *Ptch2* loss (tumor 5580-C2), *Gli1* amplification (tumor 5452-C2), *Gli2* amplification (tumor 5580-C1), *Kif7* amplification (tumor 5558-C1) and *Yap1* amplification (tumor 5420-C1). Each tumor (pink or teal trace) is compared against its matched normal (liver, black trace).

Figure 2-13: Expression of Myc family proteins in GP tumors and lack of tumor formation in *Notch1*- or *p53*-deficient skin.

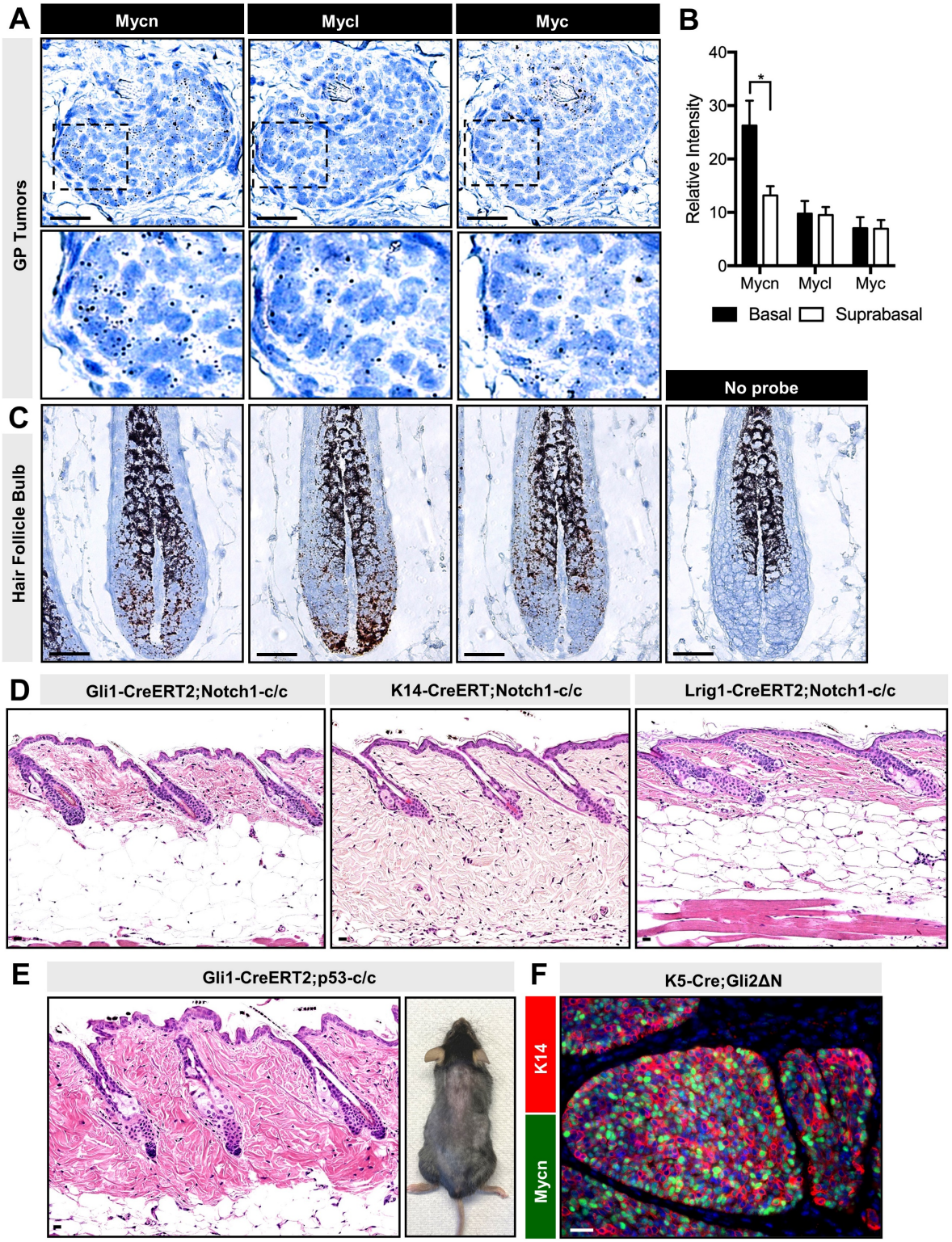

A. *In situ* staining for *Mycn*, *Mycl* and *Myc* in GP tumors. Bottom panels are magnified views of the boxed areas.
B. Quantitation of mRNA in tumor basal and suprabasal compartments.
C. *In situ* staining for *Mycn*, *Mycl* and *Myc* in normal anagen hair follicle bulb. Right image, staining with probe omitted, showing only background staining for hair shaft and melanocytes.
D. Histology of *Notch1*-deleted skin using 3 different inducible Cre drivers, as indicated, 15-20 weeks post-TAM.
E. Histology of skin where *p53* was deleted from Gli1+ hair follicle stem cells, 25 weeks post-TAM. Right, photo of mouse with shaved dorsal skin devoid of palpable tumors.
F. Mycn (green) is highly expressed in macroscopic BCC-like tumors following overexpression of a constitutively active form of Gli2 (Gli2ΔN).

Data are represented as mean ± SEM, with statistics calculated by an unpaired *t*-test. *, $p < 0.05$. Scale bar, 50 μm.

Table 2-2: Supplemental Table S1. *Ptch1*-deficient mice

Genotype	Total # of mice	# of mice with macro tumors within 17 weeks post-TAM	Total # of mice with macro tumors (any age)	Total # of macro tumors collected*	# of Type 1 macro tumors	# of Type 2 macro tumors	# of Type 3 macro tumors	# of macro tumors with other subtype
GP (Gli1-CreERT2 + Ptch1-c/c)	18	0	0	0	-	-	-	-
GP + Notch1-c/c (GPN1)	25	6	12	24	9	1	14	0
GP + Notch1-c/+ (GPN1-Het)	9	0	0	0	-	-	-	-
GP + Trp53-c/c (GPP53)	14	9	14	30	22	7	4	2
GP + Trp53-c/+ (GPP53-Het)	11	1	3	3	2	0	1	0
GP + rtTA + TRE-MYCN (GPT)	15	3	3	3	3	0	1	0

***** Tumors that contained ~50/50 mixed histological subtypes were scored as positive for both subtypes.

Table 2-3: Supplemental Table S2. Other mice

Genotype	Total # of mice	Weeks post-TAM assessed for tumors	Total # of mice with tumors
Gli1-CreERT2 + Notch1-c/c	9	21-28	0
K14-CreERT + Notch1-c/c	7	20	0
Lrig1-CreERT2 + Notch1-c/c	5	15	0
Gli1-CreERT2 + Trp53-c/c	11	17-25	0
Gli1-CreERT2 + rtTA + TRE-MYCN	4	12-20	0

2.9 Reference

1. Martincorena, I., et al., *Tumor evolution. High burden and pervasive positive selection of somatic mutations in normal human skin.* Science, 2015. **348**: p. 880-886.

2. Fowler, J.C., et al., *Selection of oncogenic mutant clones in normal human skin varies with body site.* Cancer Discov, 2021. **11**: p. 340-361.

3. Lynch, M.D., et al., *Spatial constraints govern competition of mutant clones in human epidermis.* Nat Commun, 2017. **8**: p. 1119.

4. Murai, K., et al., *Epidermal tissue adapts to restrain progenitors carrying clonal p53 mutations.* Cell Stem Cell, 2018. **23**: p. 687-699.

5. Brown, S., et al., *Correction of aberrant growth preserves tissue homeostasis.* Nature, 2017. **548**: p. 334-337.

6. Pineda, C.M., et al., *Hair follicle regeneration suppresses Ras-driven oncogenic growth.* J Cell Biol, 2019. **218**: p. 3212-3222.

7. Ren, Z.P., et al., *Benign clonal keratinocyte patches with p53 mutations show no genetic link to synchronous squamous cell precancer or cancer in human skin.* Am J Pathol, 1997. **150**: p. 1791-1803.

8. Crowson, A.N., *Basal cell carcinoma: biology, morphology and clinical implications.* Modern Pathology, 2006. **19**: p. S127-S147.

9. Epstein, E.H., *Basal cell carcinomas: attack of the hedgehog.* Nat Rev Cancer, 2008. **8**: p. 743-754.

10. Johnson, R.L., et al., *Human homolog of patched, a candidate gene for the basal cell nevus syndrome.* Science, 1996. **272**: p. 1668-1671.

11. Hahn, H., et al., *Mutations of the human homolog of Drosophila patched in the nevoid basal cell carcinoma syndrome.* Cell, 1996. **85**: p. 841-851.

12. Bonifas, J.M., et al., *Parental origin of chromosome 9q22.3-q31 lost in basal cell carcinomas from basal cell nevus syndrome patients.* Hum Mol Genet, 1994. **3**: p. 447-448.

13. Kasper, M., et al., *Basal cell carcinoma - molecular biology and potential new therapies.* J Clin Invest, 2012. **122**: p. 455-463.

14. Bonifas, J.M., et al., *Activation of expression of hedgehog target genes in basal cell carcinomas.* J Invest Dermatol, 2001. **116**: p. 739-742.

15. Tojo, M., et al., *Expression of sonic hedgehog signal transducers, patched and smoothened, in human basal cell carcinoma.* Pathology International, 1999. **49**: p. 687-694.

16. Mill, P., et al., *Shh controls epithelial proliferation via independent pathways that converge on N-myc.* Dev Cell, 2005. **9**: p. 293-303.

17. Regl, G., et al., *Human GLI2 and GLI1 are part of a positive feedback mechanism in Basal Cell Carcinoma.* Oncogene, 2002. **21**: p. 5529-5539.

18. Atwood, S.X., et al., *Smoothened variants explain the majority of drug resistance in basal cell carcinoma.* Cancer Cell, 2015. **27**: p. 342-353.

19. Sharpe, H.J., et al., *Genomic analysis of smoothened inhibitor resistance in basal cell carcinoma.* Cancer Cell, 2015. **27**: p. 327-341.

20. Bonilla, X., et al., *Genomic analysis identifies new drivers and progression pathways in skin basal cell carcinoma.* Nat Genet, 2016. **48**: p. 398-406.

21. Jayaraman, S.S., et al., *Mutational landscape of basal cell carcinomas by whole-exome sequencing.* J Invest Dermatol, 2014. **134**: p. 213-220.

22. Kilgour, J.M., J.L. Jia, and K.Y. Sarin, *Review of the molecular genetics of basal cell carcinoma; inherited susceptibility, somatic mutations, and targeted therapeutics.* Cancers, 2021. **13**: p. 3870.

23. Nardo, L.D., et al., *Molecular alterations in basal cell carcinoma subtypes.* Sci Rep, 2021. **11**: p. 13206.

24. Ahn, S. and A.L. Joyner, *Dynamic changes in the response of cells to positive hedgehog signaling during mouse limb patterning.* Cell, 2004. **118**(4): p. 505-16.

25. Powell, Anne E., et al., *The Pan-ErbB Negative Regulator Lrig1 Is an Intestinal Stem Cell Marker that Functions as a Tumor Suppressor.* Cell, 2012. **149**(1): p. 146-158.

26. Uhmann, A., et al., *The Hedgehog receptor Patched controls lymphoid lineage commitment.* Blood, 2007. **110**(6): p. 1814-1823.

27. Mao, J., et al., *A novel somatic mouse model to survey tumorigenic potential applied to the Hedgehog pathway.* Cancer Res, 2006. **66**(20): p. 10171-8.

28. Yang, X., et al., *Notch activation induces apoptosis in neural progenitor cells through a p53-dependent pathway.* Developmental Biology, 2004. **269**(1): p. 81-94.

29. Marino, S., et al., *Induction of medulloblastomas in p53-null mutant mice by somatic inactivation of Rb in the external granular layer cells of the cerebellum.* Genes Dev, 2000. **14**(8): p. 994-1004.

30. Belteki, G., et al., *Conditional and inducible transgene expression in mice through the combinatorial use of Cre-mediated recombination and tetracycline induction.* Nucleic Acids Research, 2005. **33**(5): p. e51-e51.

31. Swartling, F.J., et al., *Pleiotropic role for MYCN in medulloblastoma.* Genes Dev, 2010. **24**: p. 1059-1072.

32. Li, H. and R. Durbin, *Fast and accurate short read alignment with Burrows-Wheeler transform.* Bioinformatics, 2009. **25**(14): p. 1754-60.

33. DePristo, M.A., et al., *A framework for variation discovery and genotyping using next-generation DNA sequencing data.* Nat Genet, 2011. **43**(5): p. 491-8.

34. Cibulskis, K., et al., *Sensitive detection of somatic point mutations in impure and heterogeneous cancer samples.* Nature Biotechnology, 2013. **31**(3): p. 213-219.

35. Saunders, C.T., et al., *Strelka: accurate somatic small-variant calling from sequenced tumor-normal sample pairs.* Bioinformatics, 2012. **28**(14): p. 1811-7.

36. Boeva, V., et al., *Control-FREEC: a tool for assessing copy number and allelic content using next-generation sequencing data.* Bioinformatics (Oxford, England), 2012. **28**(3): p. 423-425.

37. Talevich, E., et al., *CNVkit: Genome-Wide Copy Number Detection and Visualization from Targeted DNA Sequencing.* PLoS Comput Biol, 2016. **12**(4): p. e1004873.

38. Yang, H. and K. Wang, *Genomic variant annotation and prioritization with ANNOVAR and wANNOVAR.* Nat Protoc, 2015. **10**(10): p. 1556-66.

39. Wang, K., M. Li, and H. Hakonarson, *ANNOVAR: functional annotation of genetic variants from high-throughput sequencing data.* Nucleic Acids Research, 2010. **38**(16): p. e164-e164.

40. Robinson, J.T., et al., *Integrative genomics viewer.* Nat Biotechnol, 2011. **29**: p. 24-26.

41. Peterson, S.C., et al., *Basal cell carcinoma preferentially arises from stem cells within hair follicle and mechanosensory niches.* Cell Stem Cell, 2015. **16**: p. 400-412.

42. Sun, X., et al., *Coordinated hedgehog signaling induces new hair follicles in adult skin.* eLife, 2020. **9**: p. doi: 10.7554/eLife.46756.

43. Ahn, S. and A.L. Joyner, *Dynamic changes in the response of cells to positive hedgehog signaling during mouse limb patterning.* Cell, 2004. **118**: p. 505-516.

44. Uhmann, A., et al., *The Hedgehog receptor Patched controls lymphoid lineage commitment.* Blood, 2007. **110**: p. 1814-1823.

45. Powell, A.E., et al., *The pan-ErbB negative regulator Lrig1 is an intestinal stem cell marker that functions as a tumor suppressor.* Cell, 2012. **149**: p. 146-158.

46. Mao, J., et al., *A novel somatic mouse model to survey tumorigenic potential applied to the Hedgehog pathway.* Cancer Res, 2006. **66**: p. 10171-10178.

47. Rittié, L. and G.J. Fisher, *Natural and sun-induced aging of human skin.* Cold Spring Harb Perspect Med, 2015. **5**: p. a015370.

48. Hoff, D.D.V., et al., *Inhibition of the hedgehog pathway in advanced basal-cell carcinoma.* N Engl J Med, 2009. **361**: p. 1164-1172.

49. Nitzki, F., et al., *Tumor Stroma-Derived Wnt5a Induces Differentiation of Basal Cell Carcinoma of Ptch-Mutant Mice via CaMKII.* Cancer Res, 2010. **70**: p. 2739-2748.

50. Eberl, M., et al., *Tumor architecture and Notch signaling modulate drug response in basal cell carcinoma.* Cancer Cell, 2018. **33**: p. 229-243.

51. Yang, X., et al., *Notch activation induces apoptosis in neural progenitor cells through a p53-dependent pathway.* Dev Biol, 2004. **269**: p. 81-94.

52. Wang, G.Y., et al., *Differing tumor-suppressor functions of Arf and p53 in murine basal cell carcinoma initiation and progression.* Oncogene, 2017. **36**: p. 3772-3780.

53. Wang, G.Y., et al., *Basal cell carcinomas arise from hair follicle stem cells in Ptch1+/- mice.* Cancer Cell, 2011. **19**: p. 1-11.

54. Ponten, F., et al., *Molecular pathology in basal cell cancer with p53 as a genetic marker.* Oncogene, 1997. **15**: p. 1059-1067.

55. Xue, Y., B.S. Luis, and D.P. Lane, *Intratumour heterogeneity of p53 expression; causes and consequences.* J Pathol, 2019. **249**: p. 274-285.

56. Marino, S., et al., *Induction of medulloblastomas in p53-null mutant mice by somatic inactivation of Rb in the external granular layer cells of the cerebellum.* Genes Dev, 2000. **14**: p. 994-1004.

57. Mancuso, M., et al., *Hair cycle-dependent basal cell carcinoma tumorigenesis in Ptc1-neo67/+ mice exposed to radiation.* Cancer Res, 2006. **66**: p. 6606-6614.

58. Grachtchouk, M., et al., *Basal cell carcinomas in mice overexpressing Gli2 in skin.* Nat Genet, 2000. **24**: p. 216-217.

59. Nilsson, M., et al., *Induction of basal cell carcinomas and trichoepitheliomas in mice overexpressing Gli-1.* Proc Natl Acad Sci USA, 2000. **97**: p. 3438-3443.

60. Villani, R., et al., *Subtype-specific analyses reveal infiltrative basal cell carcinomas are highly interactive with their environment.* J Invest Dermatol, 2021. **141**: p. 2380-2390.

61. Adolphe, C., et al., *Patched1 and Patched2 redundancy plays a key role in regulating epidermal differentiation.* J Invest Dermatol, 2014. **134**: p. 1981-1990.

62. Maglic, D., et al., *YAP-TEAD signaling promotes basal cell carcinoma development via a c-JUN/AP1 axis.* EMBO J, 2018. **37**: p. e98642.

63. Li, Z.J., et al., *Kif7 regulates Gli2 through Sufu-dependent and -independent functions during skin development and tumorigenesis* Development, 2012. **139**: p. 4152-4161.

64. Debaugnies, M., et al., *YAP and TAZ are essential for basal and squamous cell carcinoma initiation.* EMBO Rep, 2018. **19**: p. e45809.

65. Freier, K., et al., *Recurrent NMYC copy number gain and high protein expression in basal cell carcinoma.* Oncol Rep, 2006. **15**: p. 1141-1145.

66. Brandl, L., et al., *Expression of n-MYC, NAMPT and SIRT1 in basal cell carcinomas and their cells of origin.* Acta Derm Venereol, 2019. **99**: p. 63-71.

67. Ellis, S.J., et al., *Distinct modes of cell competition shape mammalian tissue morphogenesis.* Nature, 2019. **569**: p. 497-502.

68. Veniaminova, N.A., et al., *Niche-specific factors dynamically regulate sebaceous gland stem cells in the skin.* Dev Cell, 2019. **51**: p. 326-340.

69. White, A.C., et al., *Stem cell quiescence acts as a tumour suppressor in squamous tumours.* Nat Cell Biol, 2014. **16**: p. 99-107.

70. Oro, A.E. and K. Higgins, *Hair cycle regulation of Hedgehog signal reception.* Dev Biol, 2003. **255**: p. 238-248.

71. Grachtchouk, M., et al., *Basal cell carcinomas in mice arise from hair follicle stem cells and multiple epithelial progenitor populations.* J Clin Invest, 2011. **121**: p. 1768-1781.

72. Youssef, K.K., et al., *Identification of the cell lineage at the origin of basal cell carcinoma.* Nat Cell Biol, 2010. **12**: p. 299-305.

73. Kasper, M., et al., *Wounding enhances epidermal tumorigenesis by recruiting hair follicle keratinocytes.* Proc Natl Acad Sci USA, 2011. **108**: p. 4099-4104.

74. Grachtchouk, V., et al., *The magnitude of hedgehog signaling activity defines skin tumor phenotype.* EMBO J, 2003. **22**: p. 2741-2751.

75. Thomas, W.D., et al., *Patched1 deletion increases N-Myc protein stability as a mechanism of medulloblastoma initiation and progression.* Oncogene, 2009. **28**: p. 1605-1615.

76. Chiang, A., et al., *Genomic stability in syndromic basal cell carcinoma.* J Invest Dermatol, 2018. **138**: p. 1044-1051.

77. Rehefeldt-Erne, S., et al., *Nevoid basal cell carcinoma syndrome: report from the Zurich nevoid basal cell carcinoma syndrome cohort.* Dermatology, 2016. **232**: p. 285-292.

78. Ponti, G., et al., *PTCH1 germline mutations and the basaloid follicular hamartoma values in the tumor spectrum of basal cell carcinoma syndrome (NBCCS).* Anticancer Res, 2018. **38**: p. 471-476.

79. Besagni, F., et al., *Basaloid follicular hamartomas in pediatric Basal Cell Nevus Syndrome: A diagnostic challenge.* J Dermatol, 2021. **48**: p. 1101-1105.

80. Requena, L. and O. Sangueza, *Basaloid follicular hamartoma*, in *Cutaneous adnexal neoplasms*, L. Requena and O. Sangueza, Editors. 2017, Springer. p. 457– 68.

81. Chikeka, I., et al., *Basaloid follicular hamartoma: an additional criterion of nevoid basal cell carcinoma syndrome.* Am J Dermatopathol, 2021: p. doi: 10.1097/DAD.0000000000001987.

82. Chaudhary, S.C., et al., *Shh and p50/Bcl3 signaling crosstalk drives pathogenesis of BCCs in Gorlin syndrome.* Oncotarget, 2015. **6**: p. 36789-36814.

83. Aszterbaum, M., et al., *Ultraviolet and ionizing radiation enhance the growth of BCCs and trichoblastomas in patched heterozygous knockout mice.* Nat Med, 1999. **5**: p. 1285-1291.

84. Buonamici, S., et al., *Interfering with resistance to smoothened antagonists by inhibition of the PI3K pathway in medulloblastoma.* Sci Transl Med, 2010. **2**: p. 51ra70.

85. Atwood, S.X., et al., *GLI activation by atypical protein kinase Cl/gamma regulates the growth of basal cell carcinomas.* Nature, 2013. **494**: p. 484-488.

86. Yao, C.D., et al., *AP-1 and TGFß cooperativity drives non-canonical Hedgehog signaling in resistant basal cell carcinoma.* Nat Commun, 2020. **11**: p. 5079.

87. Eberl, M., et al., *Hedgehog-EGFR cooperation response genes determine the oncogenic phenotype of basal cell carcinoma and tumor-initiating pancreatic cancer cells.* EMBO Mol Med, 2012: p. 218-233.

88. Kim, A.L., et al., *AKT1 activation is obligatory for spontaneous BCC tumor growth in a murine model that mimics some features of basal cell nevus syndrome.* Cancer Prev Res (Phila), 2016. **9**: p. 794-802.

89. Chow, R.Y., et al., *MTOR promotes basal cell carcinoma growth through atypical PKC.* Exp Dermatol, 2021. **30**: p. 358-366.

90. Rickman, D.S., J.H. Schulte, and M. Eilers, *The expanding world of N-MYC-driven tumors.* Cancer Discov, 2018. **8**: p. 150-163.

91. Wu, N., et al., *A mouse model of MYCN-driven retinoblastoma reveals MYCN-independent tumor reemergence.* J Clin Invest, 2017. **127**: p. 888-898.

92. Hatton, B.A., et al., *N-myc Is an Essential Downstream Effector of Shh Signaling during both Normal and Neoplastic Cerebellar Growth.* Cancer Res, 2006. **66**: p. 8655-8661.

93. Liu, Z., et al., *Targeting MYCN in Pediatric and Adult Cancers.* Front Oncol, 2021. **10**: p. 623679.

Chapter 3: Generation of Various Combinatorial Mouse Models of BCC

3.1 Summary

NOTCH1/2, *TRP53*, and *MYCN* are frequently mutated genes seen in human BCCs. However, it is unclear if combinatorial manipulation of these genetic factors modulates tumor progression in our system. To address this question, I assessed tumor growth kinetics by generating *Gli1;Ptch1;Notch1;Trp53*-deficient tumors (GPNP) and *Gli1;Ptch1;Notch1*-deficient tumors with *MYCN* overexpression (GPNT). Preliminary results suggest GPNP and GPNT tumors resist regression and can develop into successful macroscopic tumors. I also generated *Gli1;Ptch1;Mycn*-deficient tumors (GP-Mycn) and observed deleting *Mycn* affects initial tumor size. Altogether, these data suggest genetic manipulations in *Notch1*, *Trp53*, or *Mycn* in various tumor genetic backgrounds modulates BCC tumorigenesis.

3.2 Introduction

Exome sequencing studies have revealed that *NOTCH1/2*, *TRP53*, and *MYCN* are frequently mutated genes in BCCs [1-3]. As described in chapter 2, we observed macroscopic BCC-like tumors when *Notch1* or *Trp53* are deleted in *Gli1;Ptch1*-deficient (GP) tumors (**GPN1** and **GPP53 mice**). Furthermore, we observed that overexpression of *MYCN* promotes the progression of tumors induced by loss of *Ptch1* (**GPT tumors**). While individual genetic manipulations in *Notch1, Trp53,* or *MYCN* promotes progression in GP tumors, it is unclear how combinatorial genetic manipulations of these factors modulates tumor progression.

Our data from chapter 2 therefore raises three additional ongoing questions addressed in chapter 3. We first investigated if concomitant deletion of *Notch1* and *Trp53* promotes the progression of tumors induced by the loss of *Ptch1*. We decided to perform these experiments because GPP53 macroscopic tumors possess reduced Notch signaling (**Figure 2-6A**). Second, we addressed if overexpressing *MYCN* in GPN1 tumors increases macroscopic tumor multiplicity. We generated this mouse model because we observed GPN1 macroscopic tumors possess upregulated Mycn (**Figure 2-6A**). Finally, while we found that overexpressing *MYCN* provides a tumor cell advantage in our system (**Figure 2-7**), does deleting *Mycn* in GP tumors

provide a disadvantage? We therefore generated GP tumors that delete *Mycn* to address this question.

Here, we demonstrate that simultaneously losing *Notch1* and *Trp53* causes early nascent microscopic tumors to persist and progress into successful macroscopic tumors. In most cases, GPNP macroscopic tumors can be group into three distinct subtypes. GPNT mice develop rare palpable tail lesion tumors and express K8, a neuroendocrine marker. Finally, deleting *Mycn* in GP tumors affects initial tumor size.

3.3 Methods

3.3.1 Mice

The following strains were used in this study: *Gli1*$^{tm3(cre/ERT2)Alj}$ (*Gli1-Cre*^{ERT2}) [4]; *Ptch1*^{tm1Hahn} (*Ptch1*^{flox}) [5]; *Notch1*$^{tm2Rko/GridJ}$ (*Notch1*^{flox}) [6]; *Trp53*^{tm1Brn} (*p53*^{flox}) [7]; Rosa26$^{Lox\text{-}STOP\text{-}LOX\text{-}rtTA/+}$ (*R26-LSL-rtTA*) [8]; *TRE-MYCN/Luciferase* [9, 10]; and *Mycn*^{tm1Psk} (*Mycn*^{flox}) [11]. GPNP, GP-Mycn, and GPNT mice were induced with 5 mg tamoxifen per 40 g body weight at 8 weeks of age. Five to seventeen weeks later, dorsal skin biopsies were collected. GPNT mice were subsequently transferred to 200mg / kg doxycycline chow 5 weeks post-tamoxifen injection to overexpress *MYCN* and *Luciferase*. All studies were performed on mice of both genders on wild-type C57BL/6 mice or mixed genetic background, using littermate animals for comparisons when possible. All mice were maintained in pathogen free housing and in accordance with regulations established by the University of Michigan Unit for Laboratory Animal Medicine.

3.3.2 Immunohistochemistry

Skin biopsies were fixed in 3.7% formalin overnight for paraffin embedding. For information regarding antibodies and dilutions, please refer to **Table 3-1**. For Mycn staining, paraffin-embedded sections were amplified by TSA Fluorescein Plus kit. Paraffin sections were antigen-retrieved by simmering slides in 1 mM EDTA, pH 8.0, for 10 minutes, and probed for Mycn. In some cases, fluorescent images were processed using the auto-blend feature of Adobe Photoshop to sharpen images across multiple focal planes.

3.3.3 Tamoxifen

Tamoxifen was dissolved in corn oil by vortexing for a minimum of 1 hour at room temperature. A volume of 200 µL tamoxifen solution was injected intraperitoneally per 20 grams mouse body weight.

3.3.4 Antibodies

Table 3-1: Antibodies used in Chapter 3

Antibody	Species	Catalogue #	Source	Dilution	Notes
Luciferase	Goat	NB100-1677SS	Novus	1:1000	
Keratin 14	Chicken	906004	Biolegend	1:1000	
Keratin 8	Rat	AB-531826	Developmental Studies Hybridoma Bank	1:500	
Ki67	Mouse	550609	BD Biosciences	1:100	
Mycn	Rabbit	D4B2Y	Cell Signaling	1:500	TSA amplification (10')

3.3.5 Quantification

For tumor area measurement, H&E images using identical magnification (20x) were taken spanning the entire biopsy (~1 cm) and quantitated using ImageJ software. The average tumor area per field (total sum of all tumors) was then calculated for each animal/biopsy. For each mouse, 3 random fields were assessed, and a single average tumor area sum was calculated for each field, followed by an overall average. These values were expressed relative to the tumors at 5-weeks heterozygous tumors, which was set to '1'. Mycn+ tumor periphery (basal) compartment and was quantitated from 3 representative fields per sample and expressed as the percentage of Mycn+ tumor basal cells / K14+ total tumor cells.

3.4 Results

3.4.1 Simultaneously deleting Notch1 and p53 promotes tumor progression

We previously generated two separate systems where we incorporated homozygous conditional *Notch1* (*N1*) and *Trp53* (*p53*) loss-of-function alleles into our GP tumor model (GPN1 and GPP53 mice). As described in chapter 2, we observed the majority of GPN1 microscopic tumors persist and fail to progress, whereas GPP53 microscopic tumors spontaneously regress. However, we observed GPN1 mice develop rare macroscopic BCC-like tumors and all GPP53 develop ≥ 1 macroscopic BCC-like tumor.

Because GPN1 mice occasionally developed macroscopic tumors and GPP53 macroscopic tumors possessed reduced Notch signaling, we therefore asked if deletion of *Notch1* and *Trp53* increases macroscopic tumor multiplicity. To examine if concomitant deletion of *Notch1* and *Trp53* promotes macroscopic tumor efficiency, we incorporated homozygous conditional *Notch1* and *p53* loss-of-function alleles into our GP tumor model (*Gli1;Ptch1;N1;p53* mice, **GPNP mice**). To assess the growth kinetics of these lesions, we injected GPNP mice and *Gli1;Ptch1;N1*-heterozygous*;p53* mice (**GPNP-N1-Het**) at 8 weeks of age, and harvested skin biopsied 5-17 post-tamoxifen injection (**Figure 3-1A**). We observed

robust formation of nascent microscopic tumors in both GPNP and GPNP-N1-Het mice 5 weeks after tamoxifen induction. At 12-17 weeks post-tamoxifen, we observed GPNP and GPNP-N1-Het microscopic tumors persist. These data are consistent with our previous observations that losing Notch1 promotes tumor persistence.

By 17 weeks post-tamoxifen induction, we observed both GPNP and GPNP-N1-Het mice develop ≥ 1 macroscopic BCC-like tumor (**Figure 3-1B and C**). We assessed the histology of macroscopic tumors from GPNP and GPNP-N1-Het mice and determined that tumors exhibited heterogeneous tumor morphology. Most GPNP and GPNP-N1-Het macroscopic tumors can be classified into 3 subtypes, consistent with our observations seen in GPN1 and GPP53 macroscopic tumors (see chapter 2). In nearly all cases, GPNP and GPNP-N1-Het mice predominantly formed type 1 and type 3 tumors. In more rare cases, GPNP mice also developed heterogeneous type 1 and type 2 hybrid tumors. The distribution of macroscopic tumor subtypes is summarized in **Table 3-2**. Altogether, these data confirm simultaneous deletion of *Notch1* and *Trp53* drives nascent microscopic tumors to progress and succeed into macroscopic BCC-like tumors. However, the efficiency of macroscopic tumor multiplicity between GPNP and GPP53 mice are largely similar. Since our GPP53 mice efficiently develop ≥ 1 macroscopic tumor, incorporating concomitant *Notch1* deletion in this system may not be necessary.

3.4.2 Overexpressing MYCN in GPN1 tumors promotes tumor progression

Because we also observed all GPN1 tumors exhibit increased Mycn, we next asked if overexpressing *MYCN* in GPN1 tumors increases macroscopic tumor multiplicity. We therefore incorporated a Cre-inducible reverse Tet transactivator (*R26-LSL-rtTA*), and a tetracycline-responsive element (TRE)-driven *MYCN/Luciferase* into GPN1 mice (**GPNT mice**). While we have previously confirmed *MYCN* overexpression in our system (see chapter 2), this new GPNT mouse model allows us to determine if *MYCN* overexpression in GPN1 tumors increases macroscopic tumor formation.

We therefore injected GPNT mice with tamoxifen at 8 weeks to activate *rtTA* expression and subsequently allowed microscopic tumors to develop for 5 weeks post-tamoxifen injection. After 5 weeks post-tamoxifen, GPNT mice were then transferred to doxycycline chow to turn on *MYCN*/*Luciferase* overexpression. Skin biopsies were harvested 12-17 weeks post-tamoxifen induction (**Figure 3-2A**). The majority of GPNT tumors persisted in the skin 12-17 weeks post-tamoxifen induction, as expected (**Figure 3-2B**). In rare cases, we observed palpable GPNT

tumors develop on the tail (**Figure 3-2C**). We next confirmed GPNT tail tumors express Luciferase and unexpectedly colocalizes with the neuroendocrine marker Keratin 8 (K8) (**Figure 3-2C**). This preliminary result may suggest GPNT tumors undergo a neuroendocrine cell fate switch; however, additional studies are needed to support this conclusion. Finally, it is important to note that MYCN/luciferase recombination is mosaic in this system and likely explains why we observe rare palpable macroscopic GPNT tail tumors.

3.4.3 Deleting Mycn affects initial tumor size

While we have observed and validated that overexpressing *MYCN* promotes tumor progression, we next asked if deleting *Mycn* provides a tumor cell disadvantage. We therefore generated mice expressing tamoxifen-inducible *Gli1* promoter-driven Cre^{ERT2} to target deletion of *Ptch1* and *Mycn* to hair follicle stem cells (GP-Mycn mice). To assess the growth kinetics of these lesions, we analyzed GP-Mycn mice and *Gli1;Ptch1;Mycn*-heterozygous mice (GP-Mycn-Het) that were induced with tamoxifen at 8 weeks of age, and biopsied 5-17 weeks later. We observed robust nascent microscopic tumor formation in both GP-Mycn and GP-Mycn-Het mice 5 weeks after tamoxifen induction. By 17-weeks post-tamoxifen induction, however, tumors spontaneously regress (**Figure 3-3A**). Interestingly at 5 weeks post-tamoxifen induction, we observed a ~2-fold tumor size reduction when compared to GP-Mycn-Het tumors (**Figure 3-3A-B**). We also observed incomplete deletion of Mycn and GP-Mycn tumors appear to be proliferative at this 5-week timepoint (**Figure 3-3C-E**). Altogether, these data suggest that deletion of Mycn is not required for BCC formation but affects initial tumor size. It is possible other Myc family members (Myc and Mycl) may compensate for the loss of Mycn and I propose additional experiments below.

3.5 Discussion

The findings in this chapter reveal how combinatorial genetic manipulations in *Notch1, Trp53,* and *MYCN* modulate BCC progression. When we first observed GPN1 mice develop rare macroscopic BCC-like tumors, we reasoned that losing *Trp53* in our system may increase macroscopic tumor multiplicity. Indeed, when *Notch1* and *Trp53* are concomitantly deleted in our system, we observed efficient macroscopic BCC-like tumor formation. Not surprisingly, GPNP and GPNP-N1-Het mice develop heterogenous tumors that can be classified into 3 subtypes. This observation is consistent in GPN1 and GPP53 tumors as discussed in chapter 2. Our findings therefore raise an important ongoing question. What acquired somatic mutations

allowed GPNP and GPNP-N1-Het macroscopic tumors to succeed? Additional whole exome sequencing or RNA-seq experiments are needed to help resolve this question.

Next, we provide evidence that overexpressing *MYCN* in GPN1 tumors drives rare palpable macroscopic tumors on the tail. Unexpectedly, we observed GPNT tumors express K8, an established neuroendocrine marker. Indeed, many reports have identified Mycn as a driver in neuroendocrine prostate cancer [12-15]. Furthermore, Notch pathway is reported to suppress the neuroendocrine phenotype [16]. Our preliminary finding of this phenotype raises the question of whether GPNT tumors undergo a neuroendocrine cell fate switch.

While our findings demonstrate that overexpressing *MYCN* in GP or GPN1 tumors promotes BCC progression, we also provide preliminary evidence that losing *Mycn* affects initial tumor size. It is possible other Myc family members may compensate for the loss of Mycn. Indeed, we have previously observed *Myc* and *Mycl* transcripts expressed in hair follicles and BCC (**Figure 2-13**). It is important to note that *Mycn* is predominantly expressed in the basal tumor layer in GP tumors and is also restricted to basal hair follicle matrix cells (**Figure 2-13**). We also observed no apparent hair follicle phenotype in *Keratin5-Cre;Mycn*$^{fl/fl}$ mice (**Figure 3-4**). These data likely suggest Mycn is not required for hair follicle development.

Nonetheless, it is unclear if ablating all three Myc family members may cause a more severe phenotype. To address this question, previous studies have utilized a dominant negative *Omomyc* allele to suppress all Myc activity [17, 18]. In this system, Omomyc heterodimerizes with wild type Myc-Max complex to suppress Myc activity. Indeed, *Omomyc* expression has been demonstrated to reduce skin papillomatosis and *Kras*-driven lung cancer in mice [19-21]. It is therefore tempting to speculate if ablating *Mycn* or coupling the dominant negative function of *Omomyc* in macroscopic tumors reduces tumor size. To address this question, coupling loss-of-function *Mycn* or *Omomyc* alleles into our established GPP53 mice may provide an answer. We are currently in the process of breeding in *Mycn* floxed alleles into GPP53 mice (discussed more in chapter 6). Finally, previous reports have demonstrated p53 as a direct target and co-regulator of MYCN in neuroblastoma [22, 23]. These data may partially explain why neuroblastomas are initially chemo sensitive; however, it is likely that *MYCN*-amplified tumors eventually develop mechanisms to avoid MYCN/p53-driven apoptosis [24]. Because we observed GPT tumors possess increased proliferation and apoptosis (**Figure 2-7**), future studies are needed to

determine if losing *Trp53* in GPT tumors promotes macroscopic tumor multiplicity. We are in the process of incorporating *Trp53* floxed alleles into GPT mice (discussed more in chapter 6).

Altogether, we have clarified how *Notch1, Trp53,* and *MYCN* modulates BCC tumorigenic potential. We show GPNP and GPNT mice have the capacity to develop macroscopic tumors. Follow up characterization and sequencing experiments are needed to be done to better understand these tumors. Ultimately, understanding the complicated mutational combinations and mechanisms that drive tumor progression could open future novel therapeutic targets.

3.6 Acknowledgements

We are grateful to Dr. Andrzej Dlugosz's lab at the University of Michigan for lab discussions and sharing reagents. S.Y.W. acknowledges the support of the Leo Foundation (LF18017); the American Cancer Society; the Donald & Patricia Roof Fund for Skin Cancer Research; and the NIH (R21CA209166 and R56AR075638). S.Y.W. also acknowledges the support from the UM Skin Biology and Disease Resource-based Center (P30AR075043) and NCI Cancer Center Support Grant (P30CA046592). K.G.T. was supported by the National Institute of Health Ruth L. Kirschstein Predoctoral Individual National Research Service Award (NRSA F31 CA254080).

3.7 Figures

Figure 3-1: GPNP mice develop macroscopic tumors

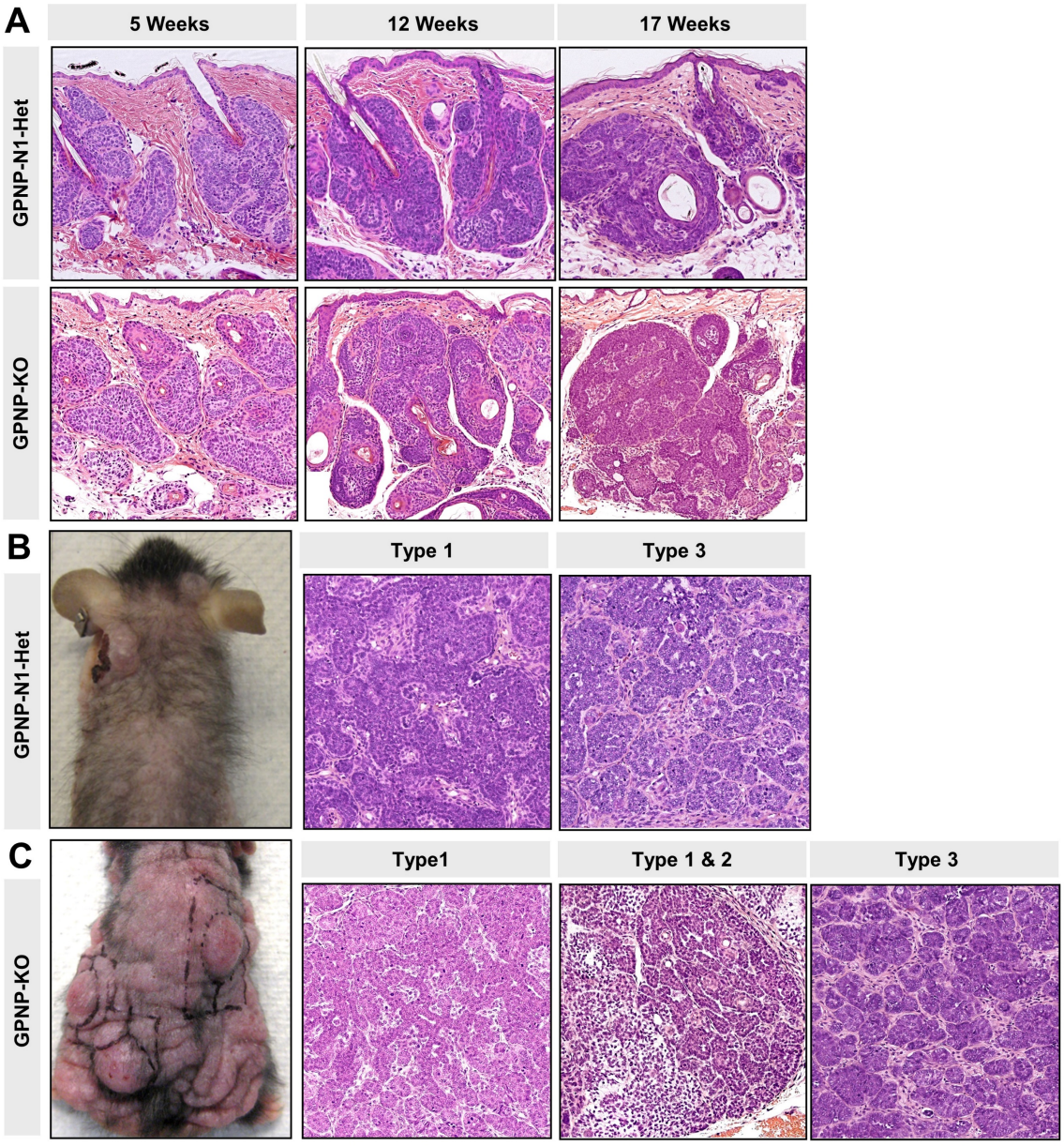

A. Histology of GPNP-N1-Het and GPNP tumors 5, 12, and 17-weeks post-tamoxifen induction.
B. Image and histology of GPNP-N1-Het mice with visible macroscopic tumors.
C. Image and histology of GPNP mice with mice visible macroscopic tumors.

Figure 3-2: GPNT mice develop palpable tail tumors

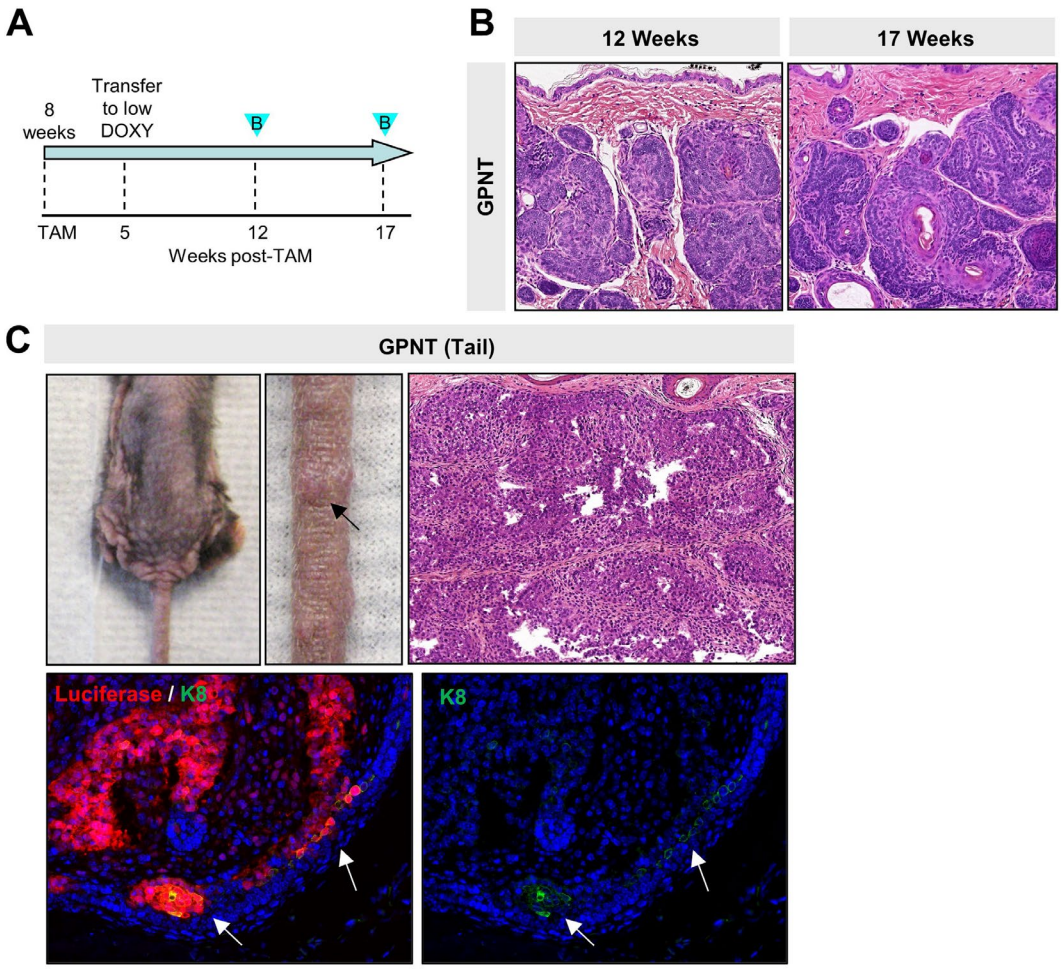

A. Experimental timeline for GPNT mice. GPNT mice are injected with tamoxifen at 8 weeks of age and subsequently transferred to low doxycycline chow 5 weeks post-tamoxifen induction. Skin biopsies are then collected 12-17 weeks post-tamoxifen induction.
B. Histology of GPNT tumors 12- and 17-weeks post-tamoxifen induction.
C. Image and histology of GPNT tail tumor. K8 (green) colocalizes with Luciferase (red) in GPNT tail tumor.

Figure 3-3: Deleting *Mycn* does not affect tumor initiation or proliferation, but affects initial tumor size

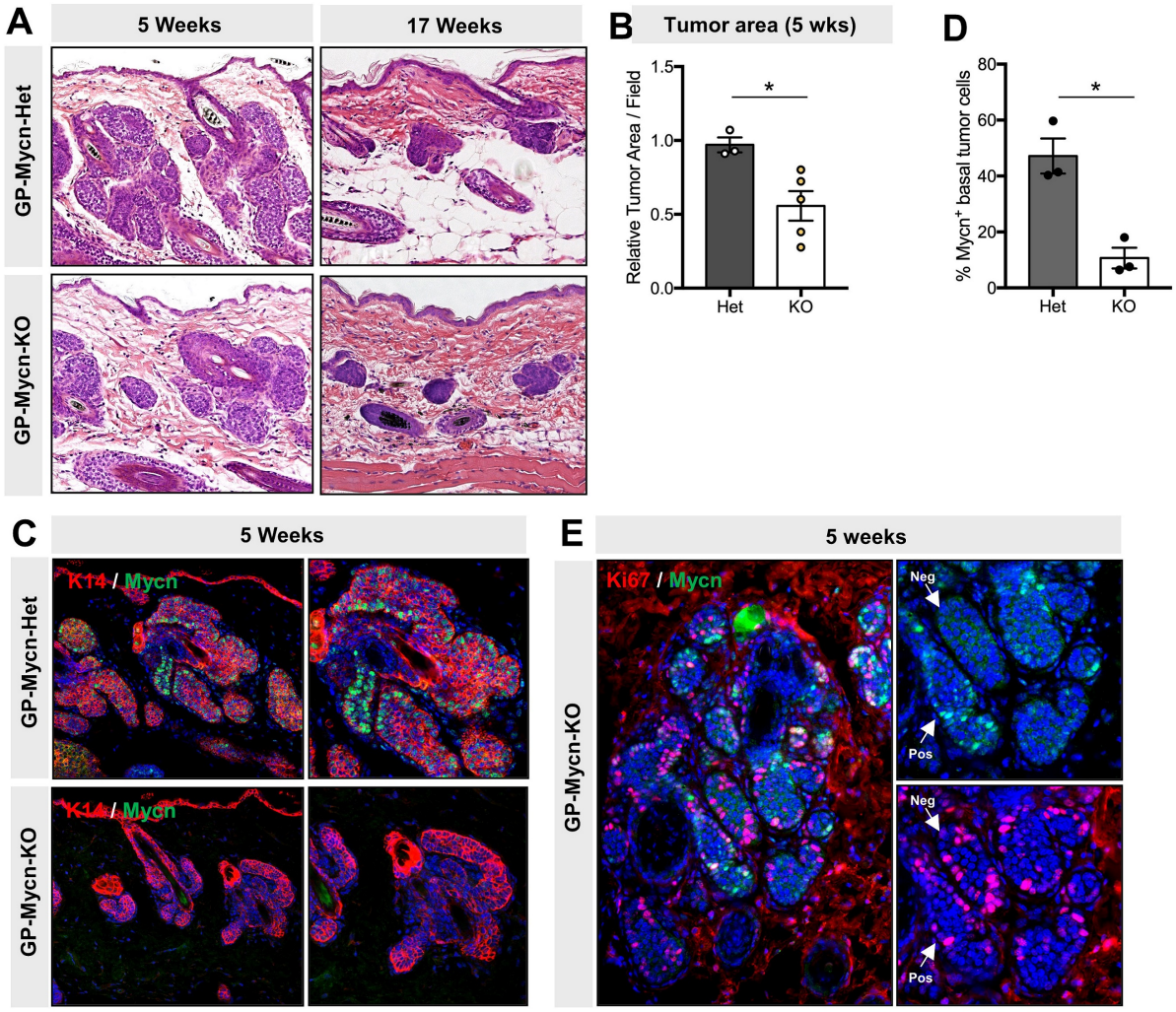

A. Histology of GP-Mycn-Het and GP-Mycn-KO tumors 5- and 17-weeks post-tamoxifen induction.
B. 5-week GP-Mycn-KO tumors exhibit at 2-fold reduction in tumor area.
C. IHC for Mycn (green) in GP-Mycn-Het and KO tumors. Red, co-staining for K14.
D. Quantification of Mycn basal tumor cells. Data are represented as mean ± SEM, with statistics calculated by an unpaired t-test. *, $p < 0.05$.
E. IHC for Mycn (green) and Ki67 (red) in 5-week GP-Mycn KO tumors. Loss of Mycn does not affect proliferation (zoomed inset).

Figure 3-4: Deleting *Mycn* does not affect hair follicle development

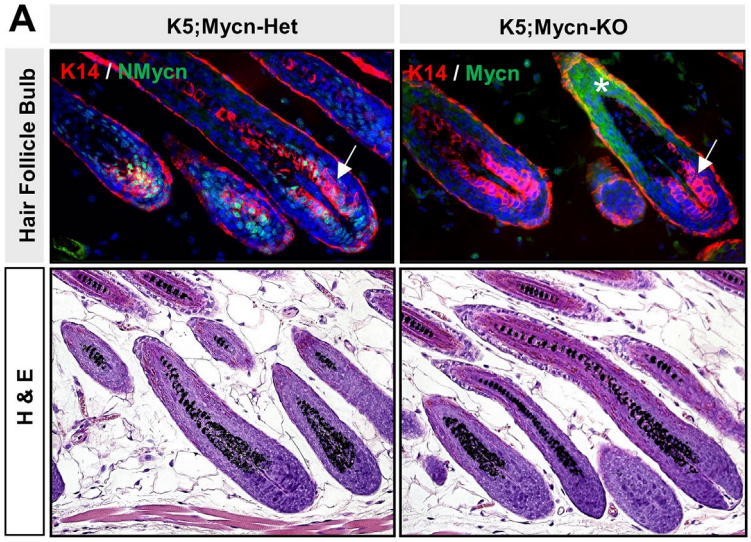

A. IHC for Mycn (green) in anagen hair follicles. Red, co-staining for K14. Bottom photos, histology of K5;Mycn-Het (control) and K5;Mycn-KO hair follicles. The asterisk (*) shown in the K5;Mycn-KO hair follicle indicates non-specific staining in the outer root sheath.

Table 3-2: GPNP and GPNP-N1-Het macroscopic tumor subtypes

Tumor #	Type	Age of tumor (weeks post-TAM)	Notch1	P53	Gender
5220-C1	1	17 weeks	KO	KO	Female
5220-C2	2 (70%) ; 1 (30%)				
5220-C3	1				
5223-C1	1	19 weeks	KO	KO	Male
5223-C2	1				
5223-C3	1				
5223-C4	1 (50%) ; 3 (50%)				
5218-C1	3	21 weeks	KO	KO	Female
5218-C2	3				
5218-C3	3				
5216-C1	3	22 weeks	KO	KO	Female
5216-C2	3				
5216-C3	3				
5227-C1	1	22 weeks	KO	KO	Male
5227-C2	3				
5227-C3	1				
5256-C1	1 (70%) ; 3 (30%)	19 weeks	KO	KO	Female
5256-C2	3				
5222-C1	1	20 weeks	Het	KO	Male
5246-C1	1 (90%) ; 3 (10%)	17 weeks	Het	KO	Male
5246-C2	3				
5246-C3	1 (90%) ; 3 (10%)				
5225-C1	1	20 weeks	Het	KO	Male
5225-C2	3				
5249-C1	1	20 weeks	Het	KO	Female
5249-C2	1 (50%) ; 3 (50%)				
5249-C3	1 (50%) ; 3 (50%)				

3.8 References

1. Bonilla, X., et al., *Genomic analysis identifies new drivers and progression pathways in skin basal cell carcinoma.* Nat Genet, 2016. **48**(4): p. 398-406.

2. Jayaraman, S.S., et al., *Mutational landscape of basal cell carcinomas by whole-exome sequencing.* J Invest Dermatol, 2014. **134**(1): p. 213-220.

3. Atwood, S.X., et al., *Smoothened variants explain the majority of drug resistance in basal cell carcinoma.* Cancer Cell, 2015. **27**(3): p. 342-53.

4. Ahn, S. and A.L. Joyner, *Dynamic changes in the response of cells to positive hedgehog signaling during mouse limb patterning.* Cell, 2004. **118**(4): p. 505-16.

5. Uhmann, A., et al., *The Hedgehog receptor Patched controls lymphoid lineage commitment.* Blood, 2007. **110**(6): p. 1814-1823.

6. Yang, X., et al., *Notch activation induces apoptosis in neural progenitor cells through a p53-dependent pathway.* Developmental Biology, 2004. **269**(1): p. 81-94.

7. Marino, S., et al., *Induction of medulloblastomas in p53-null mutant mice by somatic inactivation of Rb in the external granular layer cells of the cerebellum.* Genes Dev, 2000. **14**(8): p. 994-1004.

8. Belteki, G., et al., *Conditional and inducible transgene expression in mice through the combinatorial use of Cre-mediated recombination and tetracycline induction.* Nucleic Acids Research, 2005. **33**(5): p. e51-e51.

9. Swartling, F.J., et al., *Pleiotropic role for MYCN in medulloblastoma.* Genes Dev, 2010. **24**(10): p. 1059-72.

10. Wu, N., et al., *A mouse model of MYCN-driven retinoblastoma reveals MYCN-independent tumor reemergence.* J Clin Invest, 2017. **127**(3): p. 888-898.

11. Knoepfler, P.S., P.F. Cheng, and R.N. Eisenman, *N-myc is essential during neurogenesis for the rapid expansion of progenitor cell populations and the inhibition of neuronal differentiation.* Genes Dev, 2002. **16**(20): p. 2699-712.

12. Lee, J.K., et al., *N-Myc Drives Neuroendocrine Prostate Cancer Initiated from Human Prostate Epithelial Cells.* Cancer Cell, 2016. **29**(4): p. 536-547.

13. Dardenne, E., et al., *N-Myc Induces an EZH2-Mediated Transcriptional Program Driving Neuroendocrine Prostate Cancer.* Cancer Cell, 2016. **30**(4): p. 563-577.

14. Berger, A., et al., *N-Myc-mediated epigenetic reprogramming drives lineage plasticity in advanced prostate cancer.* J Clin Invest, 2019. **129**(9): p. 3924-3940.

15. Unno, K., et al., *Activated ALK Cooperates with N-Myc via Wnt/β-Catenin Signaling to Induce Neuroendocrine Prostate Cancer.* Cancer Res, 2021. **81**(8): p. 2157-2170.

16. Crabtree, J.S., C.S. Singleton, and L. Miele, *Notch Signaling in Neuroendocrine Tumors.* Frontiers in oncology, 2016. **6**: p. 94-94.

17. Soucek, L., et al., *Design and properties of a Myc derivative that efficiently homodimerizes.* Oncogene, 1998. **17**: p. 2463.

18. Soucek, L., et al., *Omomyc, a potential Myc dominant negative, enhances Myc-induced apoptosis.* Cancer Res, 2002. **62**(12): p. 3507-10.

19. Soucek, L., S. Nasi, and G.I. Evan, *Omomyc expression in skin prevents Myc-induced papillomatosis.* Cell Death Differ, 2004. **11**(9): p. 1038-45.

20. Soucek, L., et al., *Modelling Myc inhibition as a cancer therapy.* Nature, 2008. **455**(7213): p. 679-83.

21. Soucek, L., et al., *Inhibition of Myc family proteins eradicates KRas-driven lung cancer in mice.* Genes Dev, 2013. **27**(5): p. 504-13.

22. Chen, L., et al., *p53 is a direct transcriptional target of MYCN in neuroblastoma.* Cancer Res, 2010. **70**(4): p. 1377-88.

23. Agarwal, S., et al., *MYCN acts as a direct co-regulator of p53 in MYCN amplified neuroblastoma.* Oncotarget, 2018. **9**(29): p. 20323-20338.

24. Hogarty, M.D., *The requirement for evasion of programmed cell death in neuroblastomas with MYCN amplification.* Cancer Lett, 2003. **197**(1-2): p. 173-9.

Chapter 4: Targeting CD200 in a Mouse Model of BCC

4.1 Summary

CD200 is thought to be a potential immunosuppressive molecule in the hair follicle. How CD200 modulates BCC initiation is a gap in knowledge. In this chapter, we address if inhibiting CD200 suppresses tumor initiation. Upon anti-CD200 injections, we observe nascent tumor formation and find no change in tumor size when compared to control IgG injected tumors. Furthermore, nascent anti-CD200^{+} treated tumors possess no changes in Tregs, T cells, macrophages, and leukocytes. Finally, while we observe robust CD200 neutralizing antibodies in early nascent 5-week tumors, we are unable to observe neutralizing antibodies persist in late stage tumors. Altogether, these preliminary data suggest inhibition of CD200 during tumor initiation does not suppress tumor size or promote immune cell numbers in tumor-containing skin.

4.2 Introduction

While inhibitors of the Hedgehog pathway are often proven to be effective, advanced BCCs can persist, develop resistance, or undergo tumor evolution (BCC to SCC) during treatment [1-8]. These data all support the need to identify alternative therapeutic approaches in BCC. In many skin cancers such as melanoma, Merkel cell carcinoma and squamous cell carcinoma, immunotherapy is becoming a viable treatment option [9-12]. An expanding emphasis has been proposed on targeting immunosuppressive molecules that inhibit anti-tumor T cell mediated cytotoxic responses. Inhibiting T-lymphocyte-associated protein 4 (CTLA-4) and programmed cell death protein 1 (PD-1) are two therapeutic immunosuppressive strategies currently being assessed in the clinic [13-15]. Indeed, previous studies have reported human BCCs express PD-Ligand-1 (PD-L1) and clinical trials for the treatment of pembrolizumab (anti-PD-1 antibody) have yielded promising response in advanced BCCs [16-18]. Chang et al. observed BCC patients treated with pembrolizumab have an overall response rate of 44%. Furthermore, the overall response rate for patients treated with pembrolizumab and vismodegib was 29% [18].

Collectively, these data demonstrate pembrolizumab is active against BCC and supports the rationale to use immunotherapy as a potential treatment option for BCCs.

As mentioned briefly in **section 1.5**, CD200 is primarily thought to function by suppressing cells of the myeloid lineage and is expressed across many cancer types [19-25]. It has been demonstrated that $CD200^{-/-}$ mice displayed chronic central nervous system inflammation due to increased macrophages [26]. However, this study did not assess for immune phenotypes in the skin. Our interest in CD200 originated from previous observations where CD200 is expressed in microscopic BCC-like tumors in mice, and Hh signaling increases *CD200* expression in *Ptch1*-deficient keratinocytes [27]. In the skin, CD200 is preferentially expressed in the outer root sheath of the hair follicle and interacts with variety of immune cells that express the receptor for CD200 (CD200R) in the surrounding dermis [28-30]. This ligand and receptor communication is thought to reduce inflammation, prevent hair follicle-specific autoimmunity and may protect epidermal stem cells from autoimmune destruction [31]. Because CD200 modulates an inhibitory role with immune cells, the role of suppressing CD200 in BCC remains unclear. We specifically address if inhibition of CD200 suppresses tumor area during BCC initiation.

Here, our preliminary results suggest inhibition of CD200 does not suppress tumor size during initiation. We also observe no apparent changes in Treg, T cells, macrophages, and leukocytes in tumor-containing skin. Finally, we observe tumors subsequently lose anti-CD200 antibodies in late stage tumor-containing skin. Altogether, our results suggest suppression of CD200 does not suppress tumor area or promote immune cell number during initiation. For future studies, we are further motivated to understand if inhibiting CD200 suppresses pre-existing tumors and hair regeneration.

4.3 Methods

4.3.1 Mice

The following strains were used in this study: *Gli1*$^{tm3(cre/ERT2)Alj}$ (*Gli1-Cre*^{ERT2}) [32]; *Ptch1*^{tm1Hahn} (*Ptch1*^{flox}) [33]. GP mice were induced with 5 mg tamoxifen per 40 g body weight at 8 weeks of age. Five to seventeen weeks later, dorsal skin biopsies were collected. All studies were performed on mice of both genders on wild-type C57BL/6 mice or mixed genetic background, using littermate animals for comparisons when possible. All mice were maintained

in pathogen free housing and in accordance with regulations established by the University of Michigan Unit for Laboratory Animal Medicine.

4.3.2 CD200 treatment

At 3 weeks post-tamoxifen, GP mice were injected with 200 μg (6 total injections every 2-3 days) of a neutralizing rat monoclonal antibody against CD200 (Cat#: BE0299; Bio X Cell) or isotype control (Cat#: BE0089; Bio X Cell).

4.3.3 Immunohistochemistry

Skin biopsies were fixed in 3.7% formalin overnight for paraffin embedding. For frozen sections, samples were fixed in 3.7% paraformaldehyde at 4°C for 1 hour, rinsed in PBS, sunk in 30% sucrose overnight and embedded into OCT. For information regarding antibodies and dilutions, please refer to **Table 4-1**. In some cases, fluorescent images were processed using the auto-blend feature of Adobe Photoshop to sharpen images across multiple focal planes.

4.3.4 Tamoxifen

Tamoxifen was dissolved in corn oil by vortexing for a minimum of 1 hour at room temperature. A volume of 200 μL tamoxifen solution was injected intraperitoneally per 20 grams mouse body weight.

4.3.5 Antibodies

Table 4-1: Antibodies used in Chapter 4

Antibody	Species	Catalogue #	Source	Dilution	Notes
CD8	Rabbit	98941	Cell Signaling	1:400	Used frozen sections
CD45	Rat	553076	BD Biosciences	1:100	Used frozen sections
F4/80	Rabbit	70076	Cell Signaling	1:200	Used frozen sections
Foxp3	Rabbit	12653	BD Biosciences	1:400	Used frozen sections
CD200	Rat	BE0299	Bio X Cell	-	See notes from Owen & Sunny regarding antibody concentration

4.3.6 Quantification

For tumor area measurement, H&E images using identical magnification (20x) were taken spanning the entire biopsy (~1 cm) and quantitated using ImageJ software. The average tumor area per field (total sum of all tumors) was then calculated for each animal/biopsy. For each mouse, 3 random fields were assessed, and a single average tumor area sum was calculated for each field, followed by an overall average. These values were expressed relative to the tumors at 5-weeks tumors, which was set to '1'.

4.4 Results

4.4.1 Inhibiting CD200 does not suppress tumor size during initiation

To examine whether inhibiting CD200 suppresses tumor size during initiation, we turned to our established tamoxifen-inducible mouse model of BCC that targets deletion of *Ptch1* to hair follicle stem cells (*Gli1-CreERT2;Ptch1$^{fl/fl}$*, **GP mice**). At 3 weeks post-tamoxifen injection, we treated GP mice either with anti-CD200 or control IgG antibodies every 2-3 days (total of 6 injections). To examine long-term fates of these microscopic lesions, we collected serial biopsies up to 17 weeks post-tamoxifen (**Figure 4-1A**). At 5 weeks post-tamoxifen, we observed similar tumor size and observed hair follicle-associated lesions regress over time (**Figure 4-1B-C**). Early nascent GP tumors that possess anti-CD200 antibodies likely does not influence tumor regression because GP tumors spontaneously regress (see **Figure 2-1** and **Figure 2-2**). Altogether, these preliminary findings suggest inhibiting CD200 does not suppress tumor size during initiation.

4.4.2 Neutralizing rat monoclonal antibody against CD200 fail to persist

We also asked if CD200 antibodies persist in tumors throughout the duration of our experimental timeline. Although we detected anti-CD200$^+$ staining in early 5-week nascent tumors, anti-CD200 antibodies failed to persist in 12-17 week tumors (**Figure 4-1D** and see **Figure 4-1A** for experimental timeline of antibody injections). This may suggest that the antibodies we injected in GP mice are short lived.

4.4.3 Inhibiting CD200 does not promote immune cells

Finally, we characterized a subset of immune markers in 5-week anti-CD200$^+$ tumors. Regulatory T cells (Tregs) are a specialized subpopulation of T cells that suppress immune response [34]. We hypothesized CD200 neutralization might reduce immunosuppressive Tregs; however, we observed similar levels of Foxp3$^+$ Treg cells between control and anti-CD200$^+$ treated tumors (**Figure 4-2A**). We further evaluated additional immune markers and observed no changes in CD8$^+$ T cells, F4/80$^+$ macrophages, and CD45$^+$ leukocytes (**Figure 4-2A**). These data suggest inhibiting of CD200 does not promote immune cell numbers.

4.5 Discussion

Our preliminary data suggests inhibiting CD200 does not suppress tumor size or promote immune cell numbers during initiation. Since we observed CD200 antibodies unable to persist, additional experiments are needed to resolve this limitation. Because we treated GP mice at ~3

weeks post-tamoxifen induction during tumor initiation, it remains to be determined if repeated injections of CD200 at later timepoints alters immune cell activity. Previous and more recent studies have demonstrated that epithelial stem cells in the skin can retain an epigenetic memory upon imiquimod treatment [35, 36]. Imiquimod is a synthetic immune-response modifier and is known to have potent anti-viral and anti-tumor properties [37]. At the epigenetic level, Larson et al. reveal a two-step mechanism for memory establishment. Step one involves opening of chromatin memory and step two depends upon FOS-JUN/STAT3 to recall inflammatory memory [36].

While our BCC mouse model provides an excellent system to address immune privilege, we plan to suppress CD200 in our more aggressive mouse model of BCC. Performing experiments in this system will allow us to address if inhibiting CD200 suppresses pre-existing or advanced BCC tumors. While it remains to be determined, I hypothesize inhibiting CD200 in pre-existing tumors may potentially promote tumor regression. As an initial pilot experiment, I would treat GPP53 mice with anti-CD200 neutralizing antibodies and assess for tumor regression. If I observe tumor regression, then I would stain for immune cell numbers by immunofluorescence.

Reports have also shown *Notch1*-deficient skin activates inflammatory infiltrates in the stroma due to a breach in the skin barrier [38]. More recently, our lab has observed an upregulation in thymic stromal lymphopoietin (TSLP) when Notch signaling is ablated in hair follicle stem cells and the epidermis [39]. TSLP is a cytokine that normally skews towards a T helper 2 (Th2) allergic immune response in the skin and lung [40-42]. It is tempting to speculate if suppression of CD200 modulates TSLP cytokine activity in our system. Finally, it is possible that inflammation may serve a promoting role in BCC and hair follicle growth. Indeed, we have started initial experiments to evaluate if suppressing inflammation affects BCC initiation or pre-existing tumors. Early reports have utilized dexamethasone (anti-inflammatory drug) in BCC, and we have started initial treatment of dexamethasone in GPP53 mice as a pilot study [43, 44].

Altogether, we have provided initial results that inhibiting CD200 does not suppress tumor size during BCC initiation. Our data also suggest suppression of CD200 does not promote immune cell numbers in tumor-containing skin. Additional studies are needed to optimize antibody persistence in our BCC mouse model system. Overcoming this limitation should provide us the rationale to screen additional anti-tumor candidates. Ultimately, understanding

the mechanistic communication between immune and tumor cells is critical for the development of novel immunotherapies.

4.6 Acknowledgements

We are grateful to Dr. Yaqing Zhang at the University of Michigan (Marina Pasca di Magliano's Lab) for sharing antibody reagents. We are also grateful to our UROP student, Owen Doane, for performing the CD200 injections. S.Y.W. acknowledges the support of the University of Michigan Skin Biology and Diseases Resourced-based Center (UM-SBDRC) pilot program. K.G.T. was supported by the National Institute of Health Ruth L. Kirschstein Predoctoral Individual National Research Service Award (NRSA F31 CA254080).

4.7 Figures

Figure 4-1: Suppression of CD200 does not impact tumor initiation

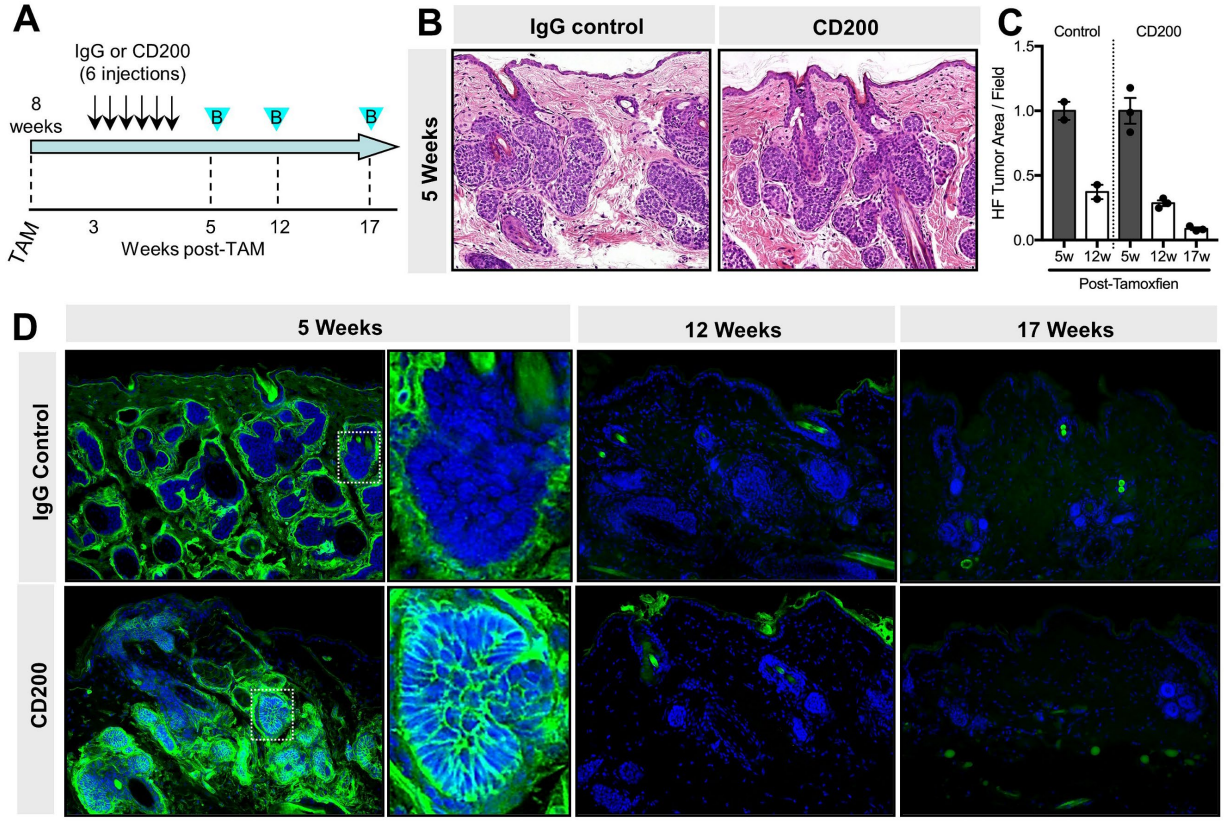

A. Experimental timeline for CD200 treatment. GP mice are injected with tamoxifen at 8 weeks of age and then treated with 200 µg of a neutralizing rat monoclonal antibody against CD200 or isotype control 3 weeks post-tamoxifen injection. Skin biopsies are then collected 5-17 weeks post-tamoxifen induction.

B. Histology of control and CD200 treated GP tumors 5-weeks post-tamoxifen induction.

C. Quantification of tumor size 5-17 weeks post-tamoxifen. Note: 17-week control IgG samples were not collected.

D. IF for anti-rat IgG (green) in 5, 12, and 17-week control and CD200 treated GP tumors.

Figure 4-2: Suppression of CD200 does not promote immune cell numbers

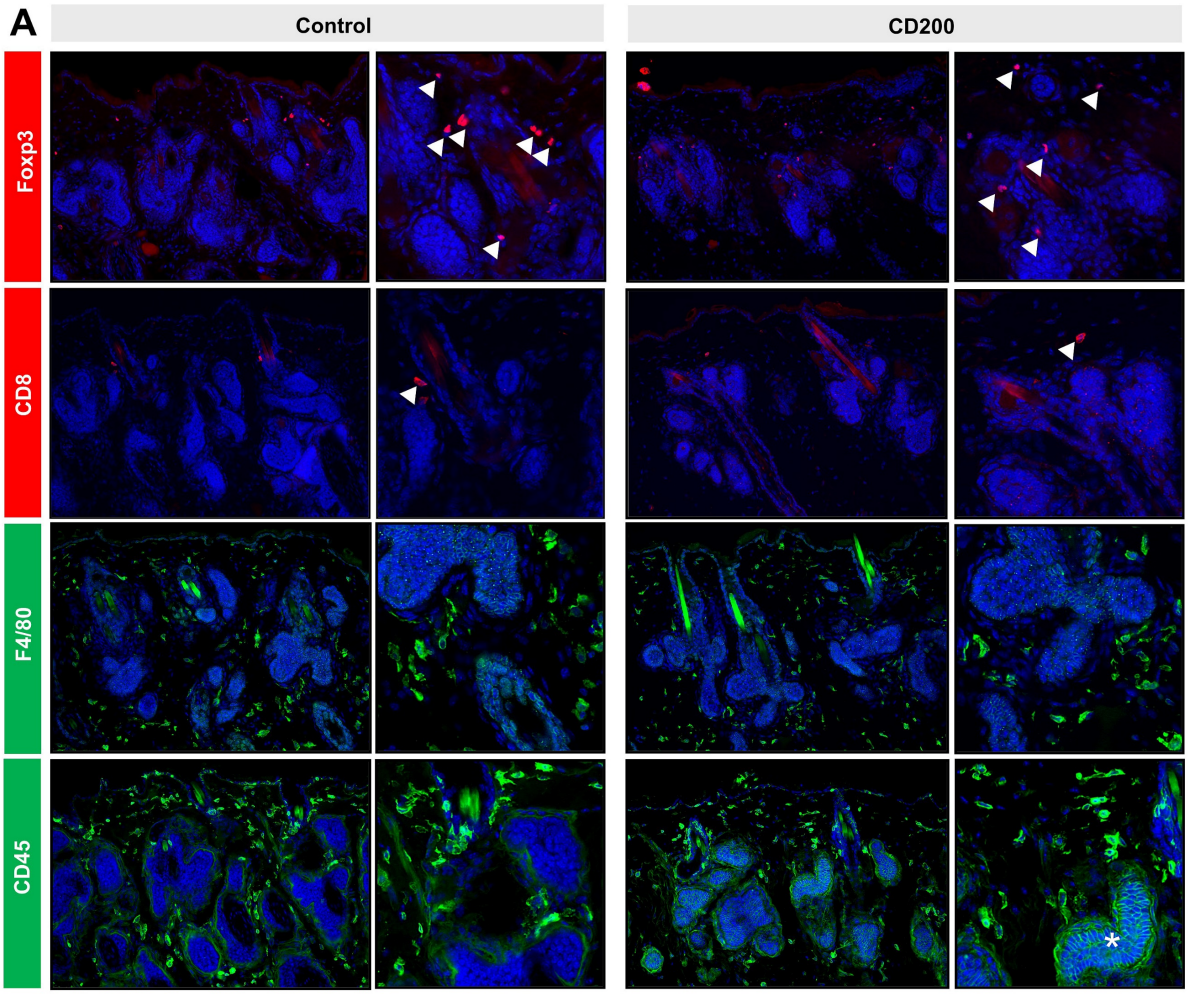

A. IF for Foxp3 (red), CD8 (red), F4/80 (green), and CD45 (green) in 5-week control and CD200 treated GP tumors. The denoted asterisk (*) is non-specific specific staining.

4.8 References

1. Tang, J.Y., et al., *Inhibiting the Hedgehog Pathway in Patients with the Basal-Cell Nevus Syndrome.* New England Journal of Medicine, 2012. **366**(23): p. 2180-2188.

2. Atwood, S.X., et al., *Smoothened variants explain the majority of drug resistance in basal cell carcinoma.* Cancer Cell, 2015. **27**(3): p. 342-53.

3. Sharpe, H.J., et al., *Genomic analysis of smoothened inhibitor resistance in basal cell carcinoma.* Cancer Cell, 2015. **27**(3): p. 327-41.

4. Eberl, M., et al., *Tumor Architecture and Notch Signaling Modulate Drug Response in Basal Cell Carcinoma.* Cancer Cell, 2018. **33**(2): p. 229-243 e4.

5. Sánchez-Danés, A., et al., *A slow-cycling LGR5 tumour population mediates basal cell carcinoma relapse after therapy.* Nature, 2018.

6. Biehs, B., et al., *A cell identity switch allows residual BCC to survive Hedgehog pathway inhibition.* Nature, 2018.

7. Kuonen, F., et al., *Loss of Primary Cilia Drives Switching from Hedgehog to Ras/MAPK Pathway in Resistant Basal Cell Carcinoma.* J Invest Dermatol, 2019. **139**(7): p. 1439-1448.

8. Kuonen, F., et al., *c-FOS drives reversible basal to squamous cell carcinoma transition.* Cell Reports, 2021. **37**(1): p. 109774.

9. Migden, M.R., et al., *PD-1 Blockade with Cemiplimab in Advanced Cutaneous Squamous-Cell Carcinoma.* N Engl J Med, 2018. **379**(4): p. 341-351.

10. Topalian, S.L., et al., *Safety, activity, and immune correlates of anti-PD-1 antibody in cancer.* N Engl J Med, 2012. **366**(26): p. 2443-54.

11. Chan, I.S., et al., *Immunotherapy for Merkel cell carcinoma: a turning point in patient care.* J Immunother Cancer, 2018. **6**(1): p. 23.

12. Lipson, E.J., et al., *PD-L1 expression in the Merkel cell carcinoma microenvironment: association with inflammation, Merkel cell polyomavirus and overall survival.* Cancer Immunol Res, 2013. **1**(1): p. 54-63.

13. Hodi, F.S., et al., *Improved Survival with Ipilimumab in Patients with Metastatic Melanoma.* New England Journal of Medicine, 2010. **363**(8): p. 711-723.

14. Moujaess, E., et al., *The emerging use of immune checkpoint blockade in the adjuvant setting for solid tumors: a review.* Immunotherapy, 2019. **11**(16): p. 1409-1422.

15. Sharpe, A.H. and K.E. Pauken, *The diverse functions of the PD1 inhibitory pathway.* Nature Reviews Immunology, 2018. **18**(3): p. 153-167.

16. Lipson, E.J., et al., *Basal cell carcinoma: PD-L1/PD-1 checkpoint expression and tumor regression after PD-1 blockade.* J Immunother Cancer, 2017. **5**: p. 23.

17. Ikeda, S., et al., *Metastatic basal cell carcinoma with amplification of PD-L1: exceptional response to anti-PD1 therapy.* npj Genomic Medicine, 2016. **1**(1): p. 16037.

18. Chang, A.L.S., et al., *Pembrolizumab for advanced basal cell carcinoma: An investigator-initiated, proof-of-concept study.* J Am Acad Dermatol, 2019. **80**(2): p. 564-566.

19. Tonks, A., et al., *CD200 as a prognostic factor in acute myeloid leukaemia.* Leukemia, 2007. **21**(3): p. 566-8.

20. Gorczynski, R.M., et al., *Breast cancer cell CD200 expression regulates immune response to EMT6 tumor cells in mice.* Breast Cancer Res Treat, 2010. **123**(2): p. 405-15.

21. Kawasaki, B.T., et al., *Co-expression of the toleragenic glycoprotein, CD200, with markers for cancer stem cells.* Biochem Biophys Res Commun, 2007. **364**(4): p. 778-82.

22. Bohling, S.D., et al., *Flow cytometric analysis of CD200 expression by pulmonary small cell carcinoma.* Cytometry B Clin Cytom, 2016. **90**(6): p. 493-498.

23. Jung, Y.S., et al., *CD200: association with cancer stem cell features and response to chemoradiation in head and neck squamous cell carcinoma.* Head Neck, 2015. **37**(3): p. 327-35.

24. Moertel, C.L., et al., *CD200 in CNS tumor-induced immunosuppression: the role for CD200 pathway blockade in targeted immunotherapy.* Journal for ImmunoTherapy of Cancer, 2014. **2**(1): p. 46.

25. Kretz-Rommel, A., et al., *CD200 Expression on Tumor Cells Suppresses Antitumor Immunity: New Approaches to Cancer Immunotherapy.* The Journal of Immunology, 2007. **178**(9): p. 5595.

26. Hoek, R.M., et al., *Down-regulation of the macrophage lineage through interaction with OX2 (CD200).* Science, 2000. **290**(5497): p. 1768-71.

27. Peterson, S.C., et al., *Basal cell carcinoma preferentially arises from stem cells within hair follicle and mechanosensory niches.* Cell Stem Cell, 2015. **16**(4): p. 400-12.

28. Rosenblum, M.D., et al., *Expression of CD200 on Epithelial Cells of the Murine Hair Follicle: A Role in Tissue-Specific Immune Tolerance?* Journal of Investigative Dermatology, 2004. **123**(5): p. 880-887.

29. Rosenblum, M.D., et al., *Characterization of CD200-Receptor Expression in the Murine Epidermis.* Journal of Investigative Dermatology, 2005. **125**(6): p. 1130-1138.

30. Cherwinski, H.M., et al., *The CD200 Receptor Is a Novel and Potent Regulator of Murine and Human Mast Cell Function.* The Journal of Immunology, 2005. **174**(3): p. 1348.

31. Rosenblum, M.D., et al., *CD200, a "no danger" signal for hair follicles.* J Dermatol Sci, 2006. **41**(3): p. 165-74.

32. Ahn, S. and A.L. Joyner, *Dynamic changes in the response of cells to positive hedgehog signaling during mouse limb patterning.* Cell, 2004. **118**(4): p. 505-16.

33. Uhmann, A., et al., *The Hedgehog receptor Patched controls lymphoid lineage commitment.* Blood, 2007. **110**(6): p. 1814-1823.

34. Rosenblum, M.D., S.S. Way, and A.K. Abbas, *Regulatory T cell memory.* Nature Reviews Immunology, 2016. **16**(2): p. 90-101.

35. Naik, S., et al., *Inflammatory memory sensitizes skin epithelial stem cells to tissue damage.* Nature, 2017. **550**(7677): p. 475-480.

36. Larsen, S.B., et al., *Establishment, maintenance, and recall of inflammatory memory.* Cell Stem Cell, 2021. **28**(10): p. 1758-1774.e8.

37. Hemmi, H., et al., *Small anti-viral compounds activate immune cells via the TLR7 MyD88-dependent signaling pathway.* Nat Immunol, 2002. **3**(2): p. 196-200.

38. Demehri, S., A. Turkoz, and R. Kopan, *Epidermal Notch1 loss promotes skin tumorigenesis by impacting the stromal microenvironment.* Cancer Cell, 2009. **16**(1): p. 55-66.

39. Veniaminova, N.A., et al., *Niche-Specific Factors Dynamically Regulate Sebaceous Gland Stem Cells in the Skin.* Dev Cell, 2019. **51**(3): p. 326-340.e4.

40. Dumortier, A., et al., *Atopic dermatitis-like disease and associated lethal myeloproliferative disorder arise from loss of Notch signaling in the murine skin.* PLoS One, 2010. **5**(2): p. e9258.

41. Demehri, S., et al., *Notch-deficient skin induces a lethal systemic B-lymphoproliferative disorder by secreting TSLP, a sentinel for epidermal integrity.* PLoS Biol, 2008. **6**(5): p. e123.

42. Wang, W., et al., *Age-Related Dopaminergic Innervation Augments T Helper 2-Type Allergic Inflammation in the Postnatal Lung.* Immunity, 2019. **51**(6): p. 1102-1118.e7.

43. Troche, J.R., et al., *Systemic glucocorticoid use and early-onset basal cell carcinoma.* Annals of epidemiology, 2014. **24**(8): p. 625-627.

44. Karagas, M.R., et al., *Non-melanoma skin cancers and glucocorticoid therapy.* Br J Cancer, 2001. **85**(5): p. 683-6.

Chapter 5: Detecting *GLI1*, *GLI2,* and *MYCN* Amplification in Human BCC

5.1 Summary

Gene amplification is a common genetic alteration in cancer, and may cause tumor cells to divide or become resistant to drug treatment [1]. As previously mentioned in chapter 2, acquired gene amplification of *Gli1* or *Gli2* enables tumors to expand indefinitely. Our observations and others collectively support the concept that hyperactive downstream Hh signaling promotes tumor progression in BCCs [2-5]. While genomic sequencing and bioinformatic algorithms can identify copy number gains or losses, DNA *in situ* is an alternative approach to visually detect copy number changes. By acquiring human BCC samples from the Mohs/Cutaneous Surgery and Oncology Clinic, I used the new DNAscope® duplex assay to detect and visualize *GLI1*, *GLI2*, and *MYCN* copy number [6]. Although I was efficiently able to detect positive signal using the DNAScope® duplex assay, I was unable to observe major copy number gains in *GLI1*, *GLI2* and *MYCN* from 16 human BCC samples. Nonetheless, the DNAscope® duplex assay is a useful system to identify any gene candidate for gene copy number.

5.2 Methods

The following protocol described below has been modified from the DNAscope® HD Duplex Detection Kit protocol (Document Number UM 324700). The entire procedure can typically be completed within 2 days.

5.2.1 DNAscope® day 1

Prepare FFPE tissue sections

- Trim paraffin blocks as needed and cut embedded tissue into 5 μm sections using a microtome.
- Air dry slides **OVERNIGHT** at **RT**.
- Bake slides in a dry oven for **1 Hour** at **60°**.

Deparaffinize FFPE sections

- Histoclear – **10 mins** (agitate slides ~halfway through incubation)
- 100% ethanol – **4 mins** (agitate halfway)
- Remove the slides from the rack, and with the section face-up. Dry slides in a drying oven for **5 mins** at **60°C** (or until completely dry)**.**

Create a barrier

- Use Pap pen to draw a circle around each specimen and let dry **~10 min** at **RT.**

Apply DNAscope RNA Removal Solution

- Add ~2-3 drops of DNAscope RNA removal solution to each slide. Incubate for **30 min** at **40° C**.
- Remove slides from oven, tap off solution and wash briefly in MilliQ water (x2).

Apply Hydrogen Peroxide

- Add ~2-3 drops of Hydrogen Peroxide to cover each section. Incubate for **10 min** at **RT**.
- Tap off solution and wash briefly in MilliQ water (x2).

Apply Protease Plus

- Add ~2-3 drops of Protease Plus to entirely cover each section. Incubate for **15 min** at **40° C**.
- Remove slides from oven, tap off solution and wash briefly in MilliQ water (x2).

Prepare 1X Wash Buffer

- Prepare 1X Wash Buffer (1:50 dilution).
    - (Warm 50X Wash Buffer up to **40°C** for **10–20 MIN** before preparation.)

Prepare 1X DNAscope target retrieval

- Prepare 1X DNAscope target retrieval buffer (1:10 dilution)

Perform target retrieval

- Preheat 1x Target Retrieval Reagent *AND* water in for 2 min @ high power.
- Put slides into slide rack and slowly submerge **into the boiling water** for **10 seconds.**
- Immediately transfer into **boiling 1X DNA scope retrieval buffer.**
- Reheat solution until boiling – stop microwave – continue to heat samples for **30 min** at the lowest setting (10% power); the solution should simmer, but not boil over.
    - During retrieval step, prepare probes (*see below*)
- Remove slides from target retrieval buffer and transfer to hot water. Rinse for **5-10 seconds**.
- Transfer slides to *1X Wash buffer* and keep slides immersed at RT.
- Pipette the probe mixture to tissue. Incubate for **OVERNIGHT (~15-18 hrs)** at **40° C.**

Preparing the probes

- Warm probes for at least **10 MIN** at **40°C** in a water bath or incubator.
- Briefly spin the C2 probe (*skinny tube*) to collect the liquid at the bottom of the tubes.
- Mix 1:50 ratio of C2 probe (*skinny tube*) to C1 probe (pipette 1 volume of C2 probe to 50 volumes of C1 probe into a tube. Invert the tube several times.

5.2.2 DNAScope® day 2

- Remove Amp1-10 reagents from cold room and equilibrate at RT.

- Use made 1x wash buffer from the day before (can be stored at RT for 1 month).
- Remove slides from oven, flick off excess liquid and place slides in 1x Wash Buffer. Incubate for **4 min** and agitate by moving slide up/down in between.

Hybridize AMP1

- Tap off excess liquid from slide, add **~2 drops of AMP1** to entirely cover each section.
- Close tray and insert into the oven for **30 min at 40° C.**
- Remove from oven; tap off liquid; put in 1x Wash Buffer for **4 min** at RT with occasional agitation (use new wash buffer).

Hybridize AMP2

- Tap off excess liquid from slide, add **~2 drops of AMP2** to entirely cover each section.
- Close tray and insert into the oven for **30 min at 40° C.**
- Remove from oven; tap off liquid; put in 1x Wash Buffer for **4 min** at RT with occasional agitation (use new wash buffer).

Hybridize AMP3

- Tap off excess liquid from slide, add **~2 drops of AMP3** to entirely cover each section.
- Close tray and insert into the oven for **15 min at 40° C.**
- Remove from oven; tap off liquid; put in 1x Wash Buffer for **4 min** at RT with occasional agitation (use new wash buffer).

Hybridize AMP4

- Tap off excess liquid from slide, add **~2 drops of AMP4** to entirely cover each section.
- Close tray and insert into the oven for **30 min at ROOM TEMP***
- Tap off liquid; put in 1x Wash Buffer for **4 min** at RT with occasional agitation (use new wash buffer).

Hybridize AMP5

- Tap off excess liquid from slide, add **~2 drops of AMP5** to entirely cover each section.
- Close tray and insert into the oven for **15 min at ROOM TEMP***
- Tap off liquid; put in 1x Wash Buffer for **4 min** at RT with occasional agitation (use new wash buffer).

Detect the red signal

- Make RED working solution per section by using a 1:50 ratio of Red-B to Red -A.
- Tap off excess liquid from slide, add **~150 µL RED solution** to entirely cover each section.
- Close tray and insert into the oven for **10 min at ROOM TEMP*.**

- Tap off liquid; put in 1x Wash Buffer for **4 min** at RT with occasional agitation (use new wash buffer).

Hybridize AMP6

- Tap off excess liquid from slide, add **~2 drops of AMP6** to entirely cover each section.
- Close tray and insert into the oven for **15 min at 40° C.**
- Remove from oven; tap off liquid; put in 1x Wash Buffer for **4 min** at RT with occasional agitation (use new wash buffer).

Hybridize AMP7

- Tap off excess liquid from slide, add **~2 drops of AMP7** to entirely cover each section.
- Close tray and insert into the oven for **15 min at 40° C.**
- Remove from oven; tap off liquid; put in 1x Wash Buffer for **4 min** at RT with occasional agitation (use new wash buffer).

Hybridize AMP8

- Tap off excess liquid from slide, add **~2 drops of AMP8** to entirely cover each section.
- Close tray and insert into the oven for **30 min at ROOM TEMP° C.**
- Tap off liquid; put in 1x Wash Buffer for **4 min** at RT with occasional agitation (use new wash buffer).

Hybridize AMP9

- Tap off excess liquid from slide, add **~2 drops of AMP9** to entirely cover each section.
- Close tray and insert into the oven for **15 min at ROOM TEMP° C.**
- Tap off liquid; put in 1x Wash Buffer for **4 min** at RT with occasional agitation (use new wash buffer).

Hybridize AMP10

- Tap off excess liquid from slide, add **~2 drops of AMP10** to entirely cover each section.
- Close tray and insert into the oven for **15 min at ROOM TEMP° C.**
- Tap off liquid; put in 1x Wash Buffer for **4 min** at RT with occasional agitation (use new wash buffer).

Detect the blue signal

- Make BLUE working solution per section by using a 1:50 ratio of Blue-B to Blue -A.
- Tap off excess liquid from slide, add **~150 µL BLUE solution** to entirely cover each section.
- Close tray and insert into the oven for **10 min at ROOM TEMP*.**
- Tap off liquid; put in 1x Wash Buffer for **5 min** at RT with occasional agitation (use new wash buffer).

- Rinse slides quickly in water to remove excess wash buffer

Counterstain the slides

- Dip slide into 1:8 diluted Hematoxylin solution (purple, diluted into water) for 1.5 min.
    - Use beaker for slide dipping
- Put slides in tap water and wash by moving up and down 3-5 times.
- Put slides in 1x PBS. Sections should turn blue.
- Repeat wash step with fresh tap water (2 changes total).

Dehydrate slides and mount samples.

- Remove the slide rack from the staining dish and dry slides in a **60°C** dry oven for **10–15 MIN**.
    - Avoid prolonged dehydration.
    - Note: Protocol DOES NOT recommend dehydrating in alcohol.
- Cool the slides for **5 MIN** at **RT**.
- Briefly dip one slide into fresh pure xylene and immediately place 1–2 drops of VectaMount on the slide before the xylene dries.
- Carefully place coverslip over the tissue section. Avoid trapping air bubbles.
- Air dry slides for ≥**5 MIN**.

5.3 Results and Discussion

By acquiring designed DNAscope human probes to human *GLI1*, *GLI2* and *MYCN*, I was indeed able to detect positive signal (**Figure 5-1A-B**). However, I am unable to detect and visualize copy number gain. See **Table 5-1** for a summary of the stained human BCC samples.

Results from this assay can be visually scored by comparing the ratio between red dots (gene of interest) and blue dots (control probe to gene of interest). For example, wild type cells should possess 2 red dots and 2 control blue dots (ratio = 1). Cells that possess copy number gain should have >3 red dots to 2 blue dots (ratio > 1). To determine the relative red to blue ratio, I would capture 3 representative fields per sample and quantitate cells with blue control positive staining. I would then obtain the relative ratio value by taking the total sum of red to blue dots.

In addition, 4 out of 16 human samples possess good "acceptable" staining (see **Table 5-1**). My definition of acceptable staining is when both red and blue dots are visible in tumor cells. I have suspected and have verified that the blue chromagen reagent can go bad when performing this assay. While I was unable to observe copy number gains, it is important to note

that ~8% and ~12% of human BCC possess *GLI1/GLI2* and *MYCN* amplification, respectively [7, 8]. This could be a reason why I was unable to detect copy number gain. However, these preliminary results provide the rationale to evaluate additional human BCC samples when acquired in the future. Collectively, the technique described here may offer an efficient approach to identify gene copy number on any tissue of interest and can be reliably performed with experience.

5.4 Acknowledgements

We are grateful to the staff at the Mohs/Cutaneous Surgery and Oncology Clinic at the U-M Rogel Cancer Center for providing us human BCC samples. S.Y.W. acknowledges the support of the Leo Foundation (LF18017); the American Cancer Society; the Donald & Patricia Roof Fund for Skin Cancer Research; and the NIH (R21CA209166 and R56AR075638). S.Y.W. also acknowledges the support from the UM Skin Biology and Disease Resource-based Center (P30AR075043) and NCI Cancer Center Support Grant (P30CA046592). K.G.T. was supported by the National Institute of Health Ruth L. Kirschstein Predoctoral Individual National Research Service Award (NRSA F31 CA254080).

5.5 Figures

Figure 5-1: DNA *in situ* hybridization of *GLI1/GLI2* and *MYCN* in human BCC

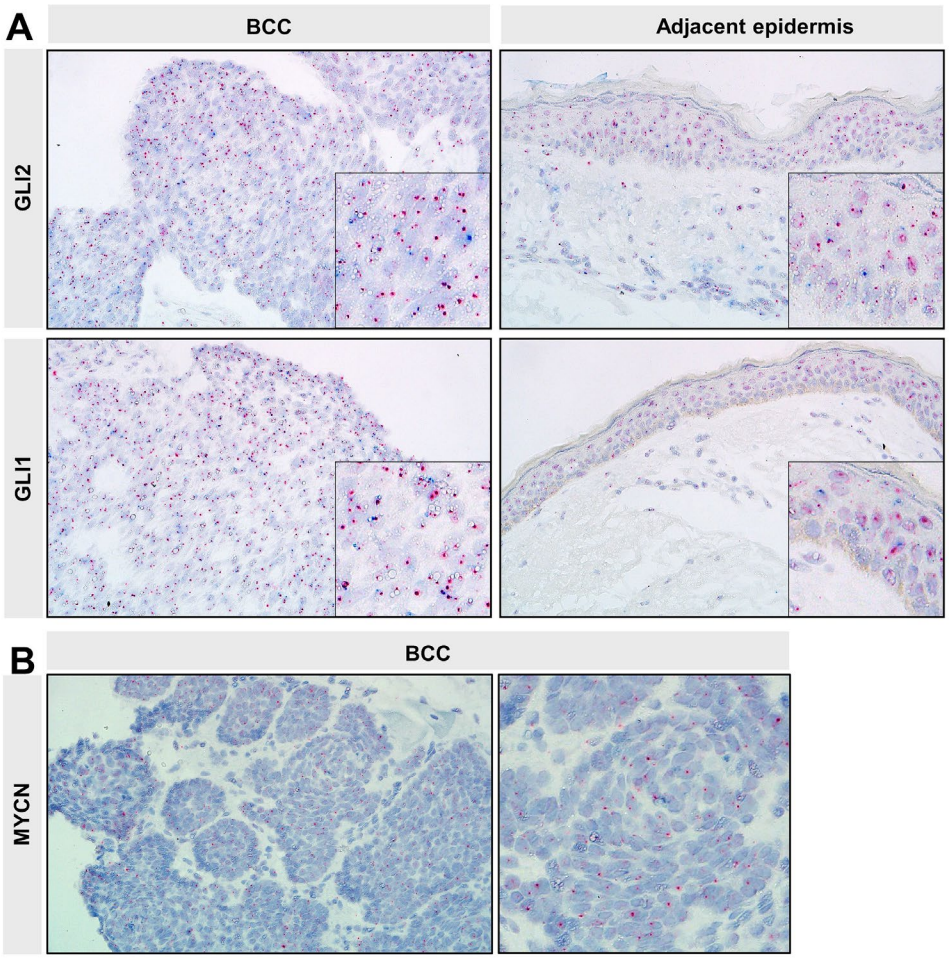

A. Top panels, *GLI2* (red) staining with respect to chromosome 2 (blue) in BCC and adjacent epidermis. Bottom panels are similar as above, but for *GLI1* (red) staining with respect to chromosome 12 (blue).

B. *MYCN* (red) staining with respect to chromosome 2 (blue) in BCC. Note: the control blue probe did not work due to a reagent going bad.

Table 5-1: Summary of DNAScope staining for *GLI1/2* and *MYCN*

Human tumor ID	**Date stained**	***GLI1***	***GLI2***	***MYCN***	**Notes**	**Before or after new chromagen reagent**	**Stained by**
21-11783	6.16.21	-	Yes	-	No amplification for *GLI2*	Before (Yes, blue dots working)	KT
21-6677	6.16.21	-	Yes	-	No amplification for *GLI2*	Before (Yes, blue dots working)	KT
4-29-T1	7.26.21	Yes	Yes	-	No amplification for *GLI1/2*	Before (NO blue dots)	KT
6-9-T2	7.26.21	Yes	Yes	-	No amplification for *GLI1/2.*	Before (NO blue dots)	KT
6-17-T1	7.26.21	Yes	Yes	-	No amplification for *GLI1/2.*	Before (NO blue dots)	KT
6-17-T2	7.26.21	Yes	Yes	-	No amplification for *GLI1/2.*	Before (NO blue dots)	KT
4-26-T1	7.26.21	Yes	Yes	-	No amplification for *GLI1/2.*	Before (NO blue dots)	KT
7-12-T1	8.18.21	Yes	Yes	-	**Good staining, but no amplification for *GLI1/2***	Before (Yes, blue dots working)*	KT
7-28-T1	9.7.21 (GLI1/2) 1/27/22 (MYCN)	Yes	Yes	Yes	**Good staining, for *GLI1/2***. Overall, no amplification	Before (Yes, blue dots working for GLI1/2 on 9/7/21)* Before (NO blue dots for MYCN on 1/27/22)	KT
7-28-T2	9.7.21 (GLI1/2) 1/27/22 (MYCN)	Yes	Yes	Yes	**Good staining, for *GLI1/2.*** Overall, no amplification	Before (Yes, blue dots working for GLI1/2 on 9/7/21)* Before (NO blue dots for MYCN on 1/27/22)	KT
10-14-T	1.27.22	-	-	Yes	No amplification for *MYCN*	Before (NO blue dots)	KT
7-12-T1	3.18.22	Yes	Yes	Yes	**Good staining, but no amplification for *GLI1/2* and *MYCN***	After (Yes, blue dots working)	KT
4-29-T1	4.21.22	-	-	Yes	No amplification for *MYCN*	After (Yes, blue dots working)	KT
4-21-T1	4.21.22	-	-	Yes	No amplification for *MYCN*	After (Yes, blue dots working)	KT
4-26-T1	4.21.22	-	-	Yes	No amplification for *MYCN*	After (Yes, blue dots working)	KT
10-7D-T	7.1.22	Yes	Yes	Yes	No amplification for *GLI1/2* and *MYCN*	After (NO blue dots)	TH
10-7A-T	7.1.22	Yes	Yes	Yes	No amplification for *GLI1/2* and *MYCN*	After (NO blue dots)	TH

Note:

- Information for human BCC collection is located on the "Human BCCs – MOHS" Dropbox spreadsheet.
- Also see "DNAscope summary spreadsheet"

5.6 References

1. Albertson, D.G., *Gene amplification in cancer.* Trends in Genetics, 2006. **22**(8): p. 447-455.

2. Nilsson, M., et al., *Induction of basal cell carcinomas and trichoepitheliomas in mice overexpressing Gli-1.* Proc Natl Acad Sci USA, 2000. **97**: p. 3438-3443.

3. Hutchin, M.E., et al., *Sustained Hedgehog signaling is required for basal cell carcinoma proliferation and survival: conditional skin tumorigenesis recapitulates the hair growth cycle.* Genes Dev, 2005. **19**(2): p. 214-23.

4. Grachtchouk, V., et al., *The magnitude of hedgehog signaling activity defines skin tumor phenotype.* Embo j, 2003. **22**(11): p. 2741-51.

5. Grachtchouk, M., et al., *Basal cell carcinomas in mice overexpressing Gli2 in skin.* Nature Genetics, 2000. **24**(3): p. 216-217.

6. Murlidhar, V.W., L; Tondnevis, F; Todorov, C; Gaspar, J; Sahajan, A; Zhang, B; Ma, X. *DNAScope™: A novel chromogenic in-situ hybridization technology for high-resolution detection of SNA copy number and structural variations* 2020; Available from: https://acdbio.com/dnascope-assay.

7. Bonilla, X., et al., *Genomic analysis identifies new drivers and progression pathways in skin basal cell carcinoma.* Nat Genet, 2016. **48**(4): p. 398-406.

8. Freier, K., et al., *Recurrent NMYC copy number gain and high protein expression in basal cell carcinoma.* Oncology Reports, 2006. **15**(5): p. 1141-45.

Chapter 6: Future Directions

6.1 Summary

My thesis examined genetic factors that modulate basal cell carcinoma, a Hedgehog-driven skin cancer. Using our lab's established BCC mouse model system, I was able to identify the acquisition of somatic secondary mutations that promote tumor progression. Here, I discuss lingering questions, propose future experiments, and reflect on key lessons I have learned.

6.2 Lingering questions

6.2.1 Will suppressing downstream Hh activity inhibit macroscopic tumor progression?

In chapter 2, I sought to define how BCC-like tumors that are driven by mutations that activate upstream Hh signaling (loss of *Ptch1*) overcome tumor dormancy and progress [(1)]. As mentioned already, we conclude hyperactive Hh activity is essential for tumor progression. If amplification of *Gli1*/*Gli2* or upregulation of *MYCN* is critical for tumor progression, will suppressing these factors inhibit tumor growth? To address these questions, I would perform the following experiments discussed below.

An immediate experiment to perform is to genetically ablate *Mycn* in our system. Indeed, we are in the process of incorporating *Mycn* floxed alleles into *Gli1;Ptch1;p53* mice (**GPP-Mycn mice**). Because we already confirmed GPP53 macroscopic tumors possess elevated Mycn expression (**Figure 2-6**), I hypothesize that deletion of *Mycn* should result in the development of fewer macroscopic tumors. However, it is likely that *Cre* recombination will not be 100% efficient in GPP-Mycn mice and macroscopic tumors may still develop. To overcome this issue, GPP-Mycn mice that develop macroscopic tumors can be retreated with tamoxifen (intraperitoneal or by tamoxifen chow), and I would expect macroscopic tumor regression. In line with ablating *Mycn*, we are also in the processing of incorporating the doxycycline inducible *TRE-MYCN/Luciferase* overexpression allele into GPP53 mice (**GPP53-TRE-MYCN/Luc, GPPT mice**). If GPPT mice develop macroscopic tumors that express this transgene, then I would remove GPPT mice from doxycycline to turn off *MYCN* expression and would expect tumor regression. Indeed, we have observed GPT tumors regress when *MYCN* transgene is

turned off (**Figure 6-1A**). Furthermore, when GPT mice are placed back on doxycycline chow, we observe tumor recurrence (**Figure 6-1A**). Collectively, these experiments described here should further support the importance of Mycn in BCC biology.

Our data also suggest microscopic BCCs can "breakthrough" into macroscopic disease by amplifying *Gli* activity. I hypothesize deletion of *Gli1* and/or *Gli2* in GPP53 mice should result reduced macroscopic tumors. To my knowledge, I am unable to find reports of readily available $Gli1^{flox}$ conditional alleles. To circumvent this issue, I would incorporate *Gli1-β-galactosidase* (LacZ) alleles into GPP53 mice [2-4]. An advantage of this system will allow us to transiently assess LacZ activity and serve as a readout for *Gli1* deletion. To ablate *Gli2*, I would incorporate the $Gli2^{flox}$ conditional alleles into GPP53 mice [5]. For all mouse experiments, I would perform similar experiments as discussed above and expect a reduction in macroscopic tumor development.

While the above proposed experiments will provide functional roles for *Mycn* and *Gli1*/*Gli2* in BCC biology, what are the mechanisms that can suppress these critical downstream Hh factors? There is an expanding rationale for using bromodomain (BRD) protein inhibitors to suppress MYC activity [6, 7]. BRDs bind onto acetylated lysines in histone tails and then recruit various chromatin factors and transcriptional machinery for the regulation of gene transcription. Indeed, Puissant et al. identified JQ1 as a bromodomain candidate that confers an inhibitory effect in neuroblastoma [8]. Shahbazi et al. further observed synergistic inhibition of JQ1 and Panobinostat (histone deacetylase inhibitor), reduce MYCN protein expression [9]. Finally, Tang et al. demonstrated JQ1 inhibits Hh activity in *Ptch*-deficient medulloblastoma and basal cell carcinoma [10]. Based off these data, will JQ1 reduce Mycn levels in our system? As a pilot experiment, I would perform JQ1 drug treatment using our established GPP53 BCC cell line (or ASZ cell line) for 1 week and expect a reduction in Mycn protein levels by western blot. Because our lab is familiar with drug oral gavage treatment [11], future studies may also involve JQ1 oral gavage treatment in GPP53 mice.

There are also additional indirect mechanisms that regulate MYCN. Aurora-A is also suggested to modulates MYCN protein stability [12, 13]. Aurora-A is normally associated with mitotic spindles poles and can interact with the N-terminus of MYCN. This interaction interferes with FBXW7-mediated degradation, which subsequently promotes MYCN protein stabilization (reviewed in [14]). Indeed, it has been demonstrated that allosteric Aurora-A

inhibitors induces rapid cell death in neuroblastoma [15, 16]. Mechanistically, Aurora-A inhibitors alter the conformation of Aurora-A kinase, which subsequently degrades MYCN and may provide therapeutic benefit to patients. In addition, Polo-like kinase 1 (PLK1) can be an alternative mechanism in stabilizing MYCN activity [17]. Normally, PLK1 enhances MYCN protein by phosphorylating and antagonizing FBXW7-mediated MYCN degradation. I therefore hypothesize Aurora-A or PLK1 inhibitors would reduce Mycn activity and promote tumor regression in our system. Collectively, the experiments described in this section will evaluate whether suppressing downstream *Mycn*, *Gli1*, or *Gli2* activity inhibits tumor progression.

6.2.2 What is the role of telomerase in BCCs?

Previous reports have identified telomerase reverse transcriptase (*TERT*) promoter mutations in >50% of human BCC, SCC, and melanoma [18-22]. Telomeres are unique structures at the end of chromosome and serve to protect the chromosomal ends from DNA degrading activities [23]. A minimum length of TTAGGG repeats and complex known as shelterin is required for telomere protection. The shelterin complex is comprised of 3 shelterin subunits (TRF1, TRF2, and POT1) and interconnected by 3 shelterin proteins (TIN2, TPP1, and Rap1) [24]. TERT is responsible for the extension of telomeres by adding specific short repetitive DNA sequences. Indeed, Bodnar et al. demonstrated telomerase overexpression is sufficient to extend cell lifespan [25]. In addition, *Tert*-transgenic mouse models that possess aberrant telomerase expression results in spontaneous tumors [26-29]. Chiba et al. suggest *TERT* promoter mutations first delay replicative senescence (phase 1), which subsequently causes increased telomeres and telomerase activity to promote telomere-driven genomic instability (phase 2) [30].

Preliminary observations from our lab have confirmed upregulation of *Tert* mRNA expression in GPP53 macroscopic tumors when compared to microscopic tumors (**Figure 6-2A**). These observations could indicate that *Tert* upregulation is an additional genetic factor that modulates tumor progression. We also confirmed *Tert* mRNA expression in anagen hair follicles (**Figure 6-2B**). These data might suggest a potential link between Hh, Mycn, and Tert activity. Indeed, MYCN is reported to activate *TERT* (reviewed in [31]). This raises the question if genetically ablating *Tert* in our system yields fewer macroscopic tumors. I therefore would incorporate $Tert^{flox}$ conditional alleles into GPP53 mice [32]. As discussed above, if there are any macroscopic tumors that escape *Cre* recombination, I would re-treat mice with tamoxifen to fully

ablate *Tert*. These experiments may provide the rationale to identify therapeutic mechanisms to control Tert activity in BCCs.

In chapter 4, I discussed the concepts for immunotherapy and immune privilege. While there are phase III trials for TERT vaccines (GV1001), results from clinical trials have not been promising [33, 34]. Duperret et al. observed synergistic blockade of CTLA-4 and DNA vaccine targeting the tumor antigen TERT causes robust anti-tumor activity [35]. Will a synergistic immune-promotion and TERT vaccine suppress BCC progression? Because we have verified our technique for injecting neutralizing antibodies in chapter 4, I would utilize either α-mouse PD-1 (clone RMP1-14, Bio X Cell) or α-mouse CTLA-4 (clone 9D9, Bio X Cell) in combination with the synthetic consensus mouse TERT DNA vaccine (mTERT) generated by Duperret et al. As a pilot experiment, I would inject GP mice with α-CTLA-4 and mTERT for 2 weeks, and harvest skin biopsies 5-17 weeks post-tamoxifen. I will then characterize GP tumors by IHC staining for proliferation (Ki67); quiescence (p21, p16, β-galactosidase); and apoptosis (cCasp3, TUNEL). Similar experiments may be performed in GPP53 mice and I would expect a reduction in macroscopic tumor formation. These experiments described in this section may potentially open a new avenue for the role of telomerase in BCC biology.

6.2.3 What are potential transcriptional mechanisms in BCCs?

As mentioned already, our lab has successfully established BCC cell lines derived from GPP53 macroscopic tumors. To date, our lab has generated over 17 cell lines and profiled 5 cell lines by RNA-seq. With these ongoing efforts, our RNA-seq analysis should identify additional candidates and provide us the rationale to perform functional experiments in our *Gli1-Cre^{ERT2};Ptch1$^{flox/flox}$* system. Given the importance of GLI transcription factors in Hh signaling, we are in the early phases of performing Gli1 chromatin immunoprecipitation followed by sequencing (ChIP-Seq) [36]. The expectation of these experiments is to identify chromosomal profiles that are enriched at GLI1 target genes. If unique GLI1 target genes are identified, I would refer to our RNA-seq data and confirm the changes in gene expression. Together, the proposed ChIP- and RNA-seq experiments described here may further identify existing or novel transcriptional mechanisms in BCC biology.

6.3 Lessons learned and concluding remarks

In this thesis, I sought to understand the genetic factors that modulate BCC tumorigenesis. There are many key lessons that I have learned based off the questions I hypothesized throughout

my PhD thesis research. While there are >50,000 genes in the mouse genome [37], it is reassuring that macroscopic BCC tumors in our system can "find a way" to amplify *Gli* activity for tumor progression. For the first time, we functionally show upregulation of *MYCN*, a downstream effector of Hh signaling, is a critical driver for BCC progression. While BCCs are addicted to high level Hh pathway activity, we now demonstrate that collaborating oncogenic pathways and secondary mutations may also facilitate BCC progression. The quest to distinguish functional driver mutations versus passenger mutations remains open-ended. In summary, my thesis unlocked a portion of the complex mutational network for BCC and may open new avenues for therapeutic targeting strategies.

6.4 Figures

Figure 6-1: GPT macroscopic tumors regress when *MYCN* transgene is turned off

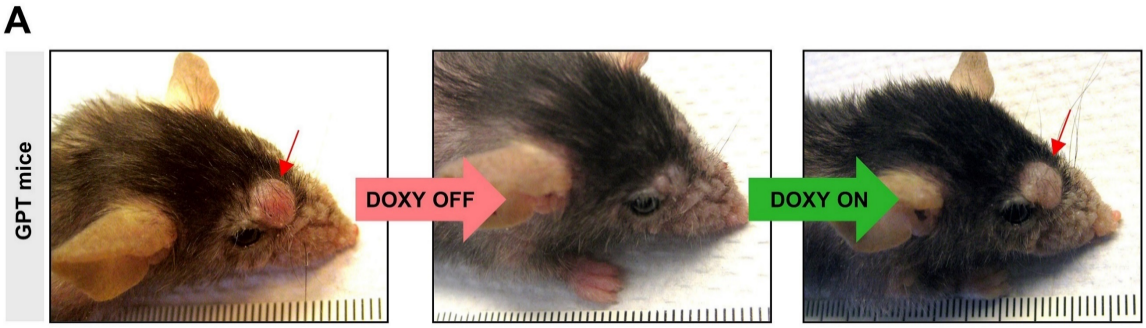

A. GPT macroscopic tumors can regress and recur when *MYCN* transgene is removed (middle photo) or turned back on (right photo).

Figure 6-2: *Tert* mRNA expression is upregulated in macroscopic tumors and is expressed in anagen hair follicles

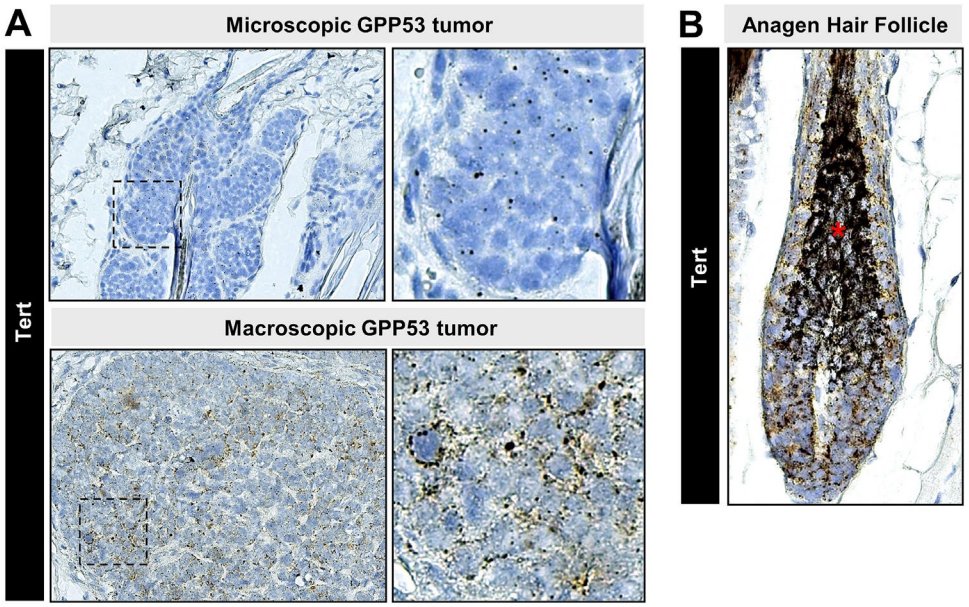

A. mRNA *in situ* staining for *Tert* in microscopic (top panels) and macroscopic (bottom panels) GPP53 tumors.
B. mRNA *in situ* staining for *Tert* in anagen hair follicle. The red asterisk (*) indicates background staining for hair shaft and melanocytes.

6.5 References

1. Trieu, K.G., et al., *Basal cell carcinomas acquire secondary mutations to overcome dormancy and progress from microscopic to macroscopic disease.* Cell Rep, 2022. **39**(5): p. 110779.

2. Bai, C.B., et al., *Gli2, but not Gli1, is required for initial Shh signaling and ectopic activation of the Shh pathway.* Development, 2002. **129**(20): p. 4753-61.

3. Xiao, Y., et al., *Neural Hedgehog signaling maintains stem cell renewal in the sensory touch dome epithelium.* Proc Natl Acad Sci U S A, 2015. **112**(23): p. 7195-200.

4. Brownell, I., et al., *Nerve-derived sonic hedgehog defines a niche for hair follicle stem cells capable of becoming epidermal stem cells.* Cell Stem Cell, 2011. **8**(5): p. 552-65.

5. Corrales, J.D., et al., *The level of sonic hedgehog signaling regulates the complexity of cerebellar foliation.* Development, 2006. **133**(9): p. 1811-21.

6. Pérez-Salvia, M. and M. Esteller, *Bromodomain inhibitors and cancer therapy: From structures to applications.* Epigenetics, 2017. **12**(5): p. 323-339.

7. Shorstova, T., W.D. Foulkes, and M. Witcher, *Achieving clinical success with BET inhibitors as anti-cancer agents.* British Journal of Cancer, 2021. **124**(9): p. 1478-1490.

8. Puissant, A., et al., *Targeting MYCN in neuroblastoma by BET bromodomain inhibition.* Cancer Discov, 2013. **3**(3): p. 308-23.

9. Shahbazi, J., et al., *The Bromodomain Inhibitor JQ1 and the Histone Deacetylase Inhibitor Panobinostat Synergistically Reduce N-Myc Expression and Induce Anticancer Effects.* Clin Cancer Res, 2016. **22**(10): p. 2534-44.

10. Tang, Y., et al., *Epigenetic targeting of Hedgehog pathway transcriptional output through BET bromodomain inhibition.* Nat Med, 2014. **20**(7): p. 732-40.

11. Eberl, M., et al., *Tumor Architecture and Notch Signaling Modulate Drug Response in Basal Cell Carcinoma.* Cancer Cell, 2018. **33**(2): p. 229-243 e4.

12. Otto, T., et al., *Stabilization of N-Myc is a critical function of Aurora A in human neuroblastoma.* Cancer Cell, 2009. **15**(1): p. 67-78.

13. Rickman, D.S., J.H. Schulte, and M. Eilers, *The Expanding World of N-MYC-Driven Tumors.* Cancer Discov, 2018. **8**(2): p. 150-163.

14. Liu, Z., et al., *Targeting MYCN in Pediatric and Adult Cancers.* Frontiers in Oncology, 2021. **10**.

15. Brockmann, M., et al., *Small molecule inhibitors of aurora-a induce proteasomal degradation of N-myc in childhood neuroblastoma.* Cancer Cell, 2013. **24**(1): p. 75-89.

16. Gustafson, W.C., et al., *Drugging MYCN through an allosteric transition in Aurora kinase A.* Cancer Cell, 2014. **26**(3): p. 414-427.

17. Xiao, D., et al., *Polo-like Kinase-1 Regulates Myc Stabilization and Activates a Feedforward Circuit Promoting Tumor Cell Survival.* Mol Cell, 2016. **64**(3): p. 493-506.

18. Maturo, M.G., et al., *Coding and noncoding somatic mutations in candidate genes in basal cell carcinoma.* Scientific Reports, 2020. **10**(1): p. 8005.

19. Griewank, K.G., et al., *TERT promoter mutations are frequent in cutaneous basal cell carcinoma and squamous cell carcinoma.* PLoS One, 2013. **8**(11): p. e80354.

20. Huang, F.W., et al., *Highly recurrent TERT promoter mutations in human melanoma.* Science, 2013. **339**(6122): p. 957-9.

21. Horn, S., et al., *TERT promoter mutations in familial and sporadic melanoma.* Science, 2013. **339**(6122): p. 959-61.

22. Pópulo, H., et al., *TERT promoter mutations in skin cancer: the effects of sun exposure and X-irradiation.* J Invest Dermatol, 2014. **134**(8): p. 2251-2257.

23. Blackburn, E.H., *Switching and signaling at the telomere.* Cell, 2001. **106**(6): p. 661-73.

24. de Lange, T., *Shelterin: the protein complex that shapes and safeguards human telomeres.* Genes Dev, 2005. **19**(18): p. 2100-10.

25. Bodnar, A.G., et al., *Extension of life-span by introduction of telomerase into normal human cells.* Science, 1998. **279**(5349): p. 349-52.

26. González-Suárez, E., et al., *Increased epidermal tumors and increased skin wound healing in transgenic mice overexpressing the catalytic subunit of telomerase, mTERT, in basal keratinocytes.* Embo j, 2001. **20**(11): p. 2619-30.

27. González-Suárez, E., J.M. Flores, and M.A. Blasco, *Cooperation between p53 mutation and high telomerase transgenic expression in spontaneous cancer development.* Mol Cell Biol, 2002. **22**(20): p. 7291-301.

28. Artandi, S.E., et al., *Constitutive telomerase expression promotes mammary carcinomas in aging mice.* Proc Natl Acad Sci U S A, 2002. **99**(12): p. 8191-6.

29. Canela, A., et al., *Constitutive expression of tert in thymocytes leads to increased incidence and dissemination of T-cell lymphoma in Lck-Tert mice.* Mol Cell Biol, 2004. **24**(10): p. 4275-93.

30. Chiba, K., et al., *Mutations in the promoter of the telomerase gene TERT contribute to tumorigenesis by a two-step mechanism.* Science, 2017. **357**(6358): p. 1416-1420.

31. Yuan, X., C. Larsson, and D. Xu, *Mechanisms underlying the activation of TERT transcription and telomerase activity in human cancer: old actors and new players.* Oncogene, 2019. **38**(34): p. 6172-6183.

32. Liu, T., et al., *Conditional Knockout of Telomerase Reverse Transcriptase in Mesenchymal Cells Impairs Mouse Pulmonary Fibrosis.* PLoS One, 2015. **10**(11): p. e0142547.

33. Guterres, A.N. and J. Villanueva, *Targeting telomerase for cancer therapy.* Oncogene, 2020. **39**(36): p. 5811-5824.

34. Zanetti, M., *A second chance for telomerase reverse transcriptase in anticancer immunotherapy.* Nat Rev Clin Oncol, 2017. **14**(2): p. 115-128.

35. Duperret, E.K., et al., *Synergy of Immune Checkpoint Blockade with a Novel Synthetic Consensus DNA Vaccine Targeting TERT.* Mol Ther, 2018. **26**(2): p. 435-445.

36. Park, P.J., *ChIP–seq: advantages and challenges of a maturing technology.* Nature Reviews Genetics, 2009. **10**(10): p. 669-680.

37. Bult, C.J., et al., *Mouse genome database 2016.* Nucleic Acids Research, 2016. **44**(D1): p. D840-D847.